BUBBLE DYNAMICS IN COMBINED CONSTANT-FLOW AND CONSTANT-PRESSURE BARBOTAGE

by

PING YUEN JOSEPH CHAN

A Thesis

Presented to

The Faculty of Graduate Studies

The University of Manitoba

In Partial Fulfillment

of the Requirements for the Degree of

Master of Science

 September, 1985

ISBN Ø-315-33546-7

BUBBLE DYNAMICS IN COMBINED CONSTANT-FLOW AND CONSTANT-PRESSURE BARBOTAGE

BY

PING YUEN JOSEPH CHAN

A thesis submitted to the Faculty of Graduate Studies of the University of Manitoba in partial fulfillment of the requirements of the degree of

MASTER OF SCIENCE

ABSTRACT

Due to the similarities between boiling heat transfer and barbotage systems, there has been an increased interest in simulating boiling by barbotage. The author believes this is the first time that in pool barbotage, bubble growth under the combined effects of constant pressure and constant flow in parallel has been investigated. Using high-speed cine photography, bubble radii as a function of time were obtained with water as the liquid, air as the gas and over a range of plenum-chamber pressures and constant-flow rates. This type of apparatus appears to give additional scope, compared with pure constant-pressure or pure constant-flow barbotage, in obtaining control over the shape of the bubble growth curves.

A simple theoretical analysis of the problem was performed; key relations were the Rayleigh equation and the orifice equation. The theoretically predicted bubble growth curves were found to be in good agreement with the experimental data.

ACKNOWLEDGEMENTS

The author wishes to express his gratitude to Professor G.E. Sims for his advice and guidance; to the staff of University of Manitoba Mechanical Engineering Department, especially Mr. J. Finken, for their co-operation during the investigation.

Special gratitude to my friend Mr. S.L. Ursel for his encouragement and financial support have led to the finish of this study; to Mrs. L. Isbister for the typing of the manuscript of this work.

The author is also grateful to University of Manitoba and to the National Research Council of Canada for the financial assistance during the study.

TABLE OF CONTENTS

LIST OF FIGURES

LIST OF TABLES

NOMENCLATURE

A	Area	m^2 or cm^2
C_d	Coefficient of discharge	
D	Diameter	m or cm
E	Dimensionless parameter (Eqn. 2.6)	
E'	Dimensionless parameter (Eqn. 5.7)	
F	Dimensionless constant flow rate	
g	Gravitational acceleration	m/sec^2 or cm/sec^2
H_{fg}	Latent heat of vaporization	J/kg
Ja	Jacob number (Eqn. 2.7)	
K	Flow coefficient	
$\dot{m}$	Mass flow rate	kg/sec
N_C	Plenum chamber parameter (Eqn. 2.4)	
P	Pressure	N/m^2
ΔP^*	Dimensionless pressure drop (Eqn. 5.7)	
Q	Volumetric air flow rate	m^3/sec or cm^3/sec
R	Radius	m or cm
R_o	Outer radius of annular orifice	m or cm
R_*	Dimensionless radius (Eqn. 5.7)	
Re_o	Orifice Reynolds number (Eqn. A.4)	
t	Time	sec
t_*	Dimensionless time (Eqn. 5.7)	
T	Temperature	°C or K
V	Volume of bubble	m^3 or cm^3

Greek Symbols

ρ	Density	kg/m^3
σ	Surface tension	N/m or dynes/cm
∞	At a large distance	
α	Thermal diffusivity of liquid	m^2/sec
μ	Dynamic visosity	kg/m sec

Subscript

a	Annular
act	Actual
b	Bubble
d	Departure
c	Constant-flow rate condition
I	Indicated air flow rate
l	Liquid
m	Metering conditions
o	Orifice
p	Constant-pressure conditions
t	Ante-chamber
tot	Total
sat	Saturation temperature of liquid
v,vap	Vapor
w	Wall or surface

CHAPTER 1

INTRODUCTION

1.1 Background

Boiling heat transfer is a mode of heat transfer that occurs with a change in phase from liquid to vapour. Since the heat transfer rate in boiling is usually high, boiling has been used to cool devices requiring high heat-transfer rates such as rocket motors and nuclear reactors. However, boiling is a complex phenomenon. The complexity arises out of the fact that boiling is a process in which several inter-dependent phenomena occur simultaneously. Thus, bubble growth depends on heat transfer, while the heat transfer depends among other things, on agitation due to bubble growth and motion. In addition, the process depends on such stochastic factors as nucleation, distribution of bubbling sites, and their condition at the start of boiling.

In order to improve the understanding of the boiling process, "barbotage" systems are used to simulate the boiling process. The term "barbotage" as used here is defined as the bubbling of a gas through a drilled or porous surface into a liquid in which the gas is essentially insoluble. It is important itself in many operations involving the transfer of heat or mass in chemical processes. In addition, it is attractive for the study of bubble-

stirred boundary layers as the bubble generation rate is independent of the rate of heat transfer and can be accurately controlled and measured.

When considering barbotage as an analog of boiling, various aspects may be examined. These may be purely hydrodynamic or may include heat transfer. Some investigators [e.g. 2, 45] have concentrated on heat-transfer coefficients, comparing these coefficients in boiling and barbotage. As regards the hydrodynamics, the similarities in appearance of the bubbling flow regimes in barbotage and saturated nucleated boiling have been noted [54, 55, 60]; the similarities of initiation and of growth rate and growth times have been pointed out [e.g. 48, 54]. In Ref. [48], the constant-pressure barbotage data was used to obtain the growth exponent n in an equation of the form R vs. t^n; they suggested the time exponent n of nucleate boiling data was 'sandwiched' between the constant-flow and constant-pressure conditions. Cheung [7] simulated the bubble growth of nucleate boiling bubbles using constant-flow barbotage and of course, by the nature of constant-flow barbotage, was limited to a growth exponent of 1/3.

Because of this very considerable interest shown in the simulation of boiling by barbotage systems, one of the goals of the present work was to investigate whether improvements could be made in the simulation process. The study concen-

trated exclusively on 'pool' barbotage.

1.2 Purpose and Scope

The present investigation can be grouped into four main parts:

(1) As mentioned earlier, barbotage systems can be used to simulate boiling bubbles. For constant-pressure barbotage, Subash and Sims [48] indicated that, over the life of the bubbles, the growth exponents were larger than the $\frac{1}{2}$ associated with the classic boiling case. Cheung [7] indicated the constant-flow barbotage generally agreed well with boiling bubbles. But, due to the nature of constant-flow barbotage, the time exponent is fixed at 1/3. In the present work combined constant-flow and constant-pressure barbotage was investigated to try to determine whether some additional control could be gained over the growth exponent, with special attention being paid to an exponent of $\frac{1}{2}$.

(2) Much barbotage literature [4, 7, 12, 13, 26, 48] indicated that two extreme cases of pool barbotage, namely the "constant-flow-rate case" and "constant-pressure case" had already been examined, but the "combined" case of constant-flow and constant-pressure had not been investigated (neither experimentally nor theoretically). Therefore, it was decided to conduct experiments for this case to determine the bubble growth curves. Distilled water with air as the injected gas were the fluids used. Experiments were con-

ducted with different combinations of pressure inside an ante-chamber and constant-flow rate to determine the bubble growth.

(3) A simple theoretical analysis was performed to predict the bubble growth for the aforesaid "combined" constant-flow and constant-pressure case.

(4) The experimental data were compared with the theoretical values. The flow coefficient which appears in the formulation of the theory was determined experimentally for the present annular orifice.

1.3 Layout of Thesis

Chapter 2 includes a literature review on barbotage dynamics and nucleate boiling dynamics. A detailed description of the experimental apparatus and photographic equipment is given in Chapter 3, while Chapter 4 covers the experimental procedures and conditions. Chapter 5 outlines a theoretical approach to solve the present problem of bubble growth. Results and discussion are presented in Chapter 6 which includes the comparison between experimental and theoretical results. Bubble behaviour and discussion of the time exponent of bubble growth in barbotage are also presented in this chapter. Figures 5.2 through 5.13 show the theoretical results of bubble growth. Figures 6.3 through 6.13 show the experimental results while Figures 6.14 through 6.24 give

the comparison between experimental and theoretical results. Table 6.3 indicates the time exponent of present bubble growth. The summary and conclusion are presented in Chapter 7. The appendices include:

(A) Determination of flow coefficient for the annular orifice in the present work.

(B) Calculation of actual constant-flow rate at the orifice.

(C) Calculation of bubble volume.

(D) Computer program for calculation of R_* vs. t_*.

(E) Bubble identification and tabulated data.

(F) Bubble growth data for 0.3-cm diameter orifice plate.

CHAPTER 2

REVIEW OF THE LITERATURE

2.1 Barbotage Dynamics

The injection of gas into a liquid through a submerged orifice is an important phenomenon in connection with distillation, absorption, and mass and energy transfer processes. The formation of such bubbles under certain conditions has been studied extensively. If there is a high pressure-drop restriction between the orifice and gas chamber (such as a long thin capillary tube), the pressure fluctuations due to the forming bubbles are much smaller than the pressure drop between the orifice and the gas chamber. In this case, the gas flow rate can be treated as a constant; this is referred to as the "constant-flow-rate" condition. If the volume of the gas chamber upstream of the orifice is very large by comparison with the volume of the bubble being formed, and if the pressure drop across the orifice is small, the situation corresponds to the "constant-pressure" condition. For conditions intermediate between these two limits, the chamber volume must be taken into account. The phenomenon of bubble formation* under various conditions was reported in an early paper by Hughes et al.[23], then a theory for the mechanism of bubble formation was proposed by Davidson and

*Of the extensive literature, only the most important papers related to this study are mentioned here and elsewhere.

Schüler [12, 13]. McCann and Prince [31] used potential-flow theory to describe the flow of gas from an ante-chamber into a spherical bubble growing at the orifice; they also estimated the weeping rate after the bubble detachment. A full review was done later by Park [34] and by Kumar and Kuloor [26]. The following review on the bubble growth rate keeps emphasis on the two limiting cases, that is constant flow and constant pressure.

Bubble growth rate

Bubble formation, can, in general, be considered to be governed by the fluid dynamics and interfacial forces [48] due to:

1. Momentum of the injected gas stream,
2. Inertia of the displaced liquid,
3. Drag on the interface associated with the motion of the liquid relative to the bubble,
4. Buoyancy, and
5. Surface tension.

Davidson et al. [12, 13] and Kumar and Kuloor [26] proposed their theories of bubble formation to determine the break-off diameter based on the various forces acting on the bubble which related to the liquid and gas physical properties and the gas flow rate. Aspects of the bubble-forming device such as geometry, material of construction,

chamber volume and depth of the liquid above the orifice also affect the bubble sizes. The thickness of orifice plate may also affect the bubble size. The effect has been reported to become significant if the thickness is equal to or greater than 100 times the value of orifice diameter [23].

Constant-flow-rate case

As mentioned earlier, bubble formation at the tip of a long capillary tube can be treated as the constant-flow condition. Since the gas flow is constant, the bubble growth is simply expressed as

$$\frac{dV}{dt} = Q \qquad (2.1)$$

where

V = volume of the bubble,

t = time,

Q = gas flow rate.

If the bubble volume is assumed to be of a spherical shape, then Eqn. 2.1 can be written as

$$\frac{d}{dt}\left(\frac{4}{3}\pi R^3\right) = Q \qquad (2.2)$$

where R is the radius of the bubble. Rearranging and integrating Eqn. 2.2 with the initial condition as $R = 0$ at $t = 0$ gives

$$R = \left(\frac{3}{4\pi}\right)^{1/3} Q^{1/3} t^{1/3} \qquad (2.3)$$

Equations 2.1 and 2.2 are to be used as part of the theoretical derivation given in Chapter 5.

Constant-pressure case

The bubble formation at an orifice which is supplied with gas from an ante-chamber at constant pressure, is referred to as the constant-pressure condition. The rate of gas flow for such a system has been found to vary throughout the formation period as the result of a variation of the pressure drop across the orifice which is a result of the varying pressure within the bubble. The system is approximated in practice when an orifice is supplied with gas by a large ante-chamber. Hughes et al. [23] have derived a dimensionless group which characterizes the effect of the ante-chamber on bubble formation as follows:

$$N_C = \frac{g\ (\rho_l - \rho_g) V_t}{A_o\ \rho_g\ c^2} \qquad (2.4)$$

where

g = acceleration due to gravity,

ρ_l = liquid density,

ρ_g = gas density,

V_t = the ante-chamber volume,

A_o = orifice cross-sectional area,

c = the velocity of sound in the gas.

Values of the ante-chamber volume which make $N_c \ll 1$ approximate the condition of the constant-flow-rate case whereas those which make $N_c \gg 1$ approximate the condition of constant pressure. Equation 2.4 was used to determine the size of the ante-chamber volume in the present work ($N_c \simeq 100$).

Subash and Sims [48] formulated a bubble growth equation under the constant-pressure condition by combining the Rayleigh equation and the orifice equation. The result of the formulation is given in the following dimensionless relation:

$$R_* \ddot{R}_* + 1.5 \dot{R}_*^2 + 8E R_*^4 \dot{R}_*^2 + \frac{2}{R_*} = 2\Delta P^* \qquad (2.5)$$

where

$$\left.\begin{aligned} R_* &\equiv \frac{R}{R_o}, \\ \dot{R}_* &\equiv \frac{dR_*}{dt_*}, \\ \ddot{R}_* &\equiv \frac{d}{dt_*}\left[\frac{dR_*}{dt_*}\right], \\ t_* &\equiv t\left[\frac{\sigma}{\rho_l R_o^3}\right]^{\frac{1}{2}}, \\ \Delta P^* &\equiv \frac{P_t - P_\infty}{\frac{2\sigma}{R_o}}, \\ E &\equiv \frac{1}{K^2}\frac{\rho_g}{\rho_l}, \end{aligned}\right\} \qquad (2.6)$$

R = Radius of the bubble,

R_o = Radius of the circular orifice,

K = Flow coefficient,

P_t = Pressure in the plenum chamber,

P_∞ = Pressure at a large distance from the bubble at the level of the orifice,

t = time,

σ = Surface tension,

ρ_g = Gas density,

ρ_l = Liquid density.

The solution of Eqn. 2.5 can be carried out by numerical integration, using fourth-order Runge-Kutta formula with the initial condition at time t = 0 as

$$R_* (0) = 1$$

$$\dot{R}_* (0) = 0$$

The bubble growth rates predicted by Eqn. 2.5 have been found to be in good agreement with the experimental data for water, acetone, and hexane by Subash and Sims [48]. In this thesis a theoretical analysis is presented for the bubble formation under the combined effects of constant-flow and constant-pressure conditions; this is in Chapter 5.

2.2 Nucleate Boiling Dynamics

The phenomenon of nucleate boiling has attracted great attention because of its unusually high heat-transfer rates.

It is especially bubble growth which interests here. Bubble growth is a combined problem of dynamics and heat transfer. Dynamic considerations control the early part of bubble growth while heat transfer controls the later part; generally, the heat-transfer-controlled portion is of a much longer duration compared with the dynamically controlled portion. The classical analyses [e.g. 14, 16, 35] have as a result in the thermally controlled region and for growth in a uniformly superheated liquid, that the radius varies as the square root of time. Of special interest, because of its use in an earlier study of boiling simulation, is the work of Cole and Shulman [8] which involved bubble growth at a heat transfer surface in saturated nucleate pool boiling using a number of liquids. The empirical equation describing their extensive results is

$$R = 2.5\ J_a^{3/4}\ \sqrt{\alpha t} \qquad (2.7)$$

where

$$J_a \equiv \frac{C_p\ \rho_l\ (T_w - T_{sat})}{H_{fg}\ \rho_v}\ ,$$

α = thermal diffusivity of the liquid,

C_p = specific heat at constant pressure,

T_w = wall temperature at superheated conditions,

T_{sat} = saturation temperature of the liquid,

H_{fg} = latent heat of vaporization of the liquid.

Concerning other experimental data for bubble growth at a heating surface, besides the time exponent ½ discussed above, one see other values. A discussion appears in Cheung [7], where the quoted range of the exponent of time varies from approximately 0.1 to 1.0.

Good reviews of boiling bubble dynamics can be found in Refs. [22, 51, 53].

2.3 Analogy Between Barbotage and Nucleate Boiling

Much research concerning nucleate boiling [8, 9, 19, 35] has been conducted during the past several years in order to determine the heat-transfer mechanisms. Broadly speaking, the mechanisms can be grouped into two main categories: (i) convective or agitation effects characterized by heat transfer associated with the movement of, and molecular diffusion through the liquid phase; (ii) latent-heat effect, characterized by heat transfer due to the formation and transport of the vapour phase. In order to establish the importance of the bubble-induced agitation mechanism, an examination of the bubble behaviour is essential. Zuber [60] was among the first to note the similarity in appearance of the bubbling flow regimes in barbotage and saturated nucleate pool boiling. He considered Davidson and Amick's [11] description of the appearance of barbotage bubbles forming under constant-flow-rate conditions and noted that the description fitted well the bubble formation in Yamagata and Nishikawa's [59] experiments in nucleate boiling. Wallis [54] compared

Staniszewski's [47] data for bubble growth rate in boiling to Siemes and Kauffmann's [43] constant-flow barbotage and pointed out that the equations they derived had the same basic form.

Barakat [4] compared constant-pressure and constant-flow barbotage bubbles with the boiling bubble from Han and Griffith [18] for water and illustrated that the bubble growth rates showed more similarity between boiling and the constant-flow barbotage bubbles rather than the constant-pressure bubble. Barakat and Sims [6] compared the toluene boiling results of Cooper and Lloyd [9] with constant-flow barbotage bubbles which revealed some similarities in the heat-transfer coefficient between them. They also compared [5] the flow pattern about their own barbotage bubbles and the boiling bubbles reported by Kutateladze and Mamontova [27].

Subash and Sims [48] showed the boiling growth rate results fell between the results of the two extreme cases of barbotage systems, namely constant-flow-rate and constant-pressure conditions. They pointed out the bubble departure sizes in barbotage and boiling were comparable in magnitude in the static regime. They also compared the dependence of frequency of breakoff diameter in boiling and barbotage and showed the trend of lowering frequency as the bubble departure diameter increased.

Recently Cheung [7] compared the hydrodynamics of constant-flow barbotage bubbles with boiling results of

Cole and Shulman [8] for different liquids. He showed that the bubble growth (R vs. t) was in good agreement with the boiling results except very close to zero time. He also showed the growth rate ($\frac{dR}{dt}$ vs. t) of the barbotage was close to the lower limit of boiling results reported by Cole and Shulman [8]. He compared the departure radii in boiling and barbotage and found quite satisfactory agreement.

CHAPTER 3

APPARATUS

3.1 General Description

The schematic arrangement of the apparatus is illustrated in Fig. 3.1. Air from the air compressor which operated between 552 kPa (80 psig) and 690 kPa (100 psig) was reduced to the experimental operating condition by means of the pressure regulator. The air then passed through a filter and a gas dryer which removed the contaminants such as oil particles, dust and moisture present in the air. Then the air line branched to two flow meters. Both contained a built-in needle valve; one of them for the constant-flow stream was used to measure the flow rate, the other for the constant-pressure stream, was used to control the pressure inside the ante-chamber. Both air streams were saturated with distilled water at pool temperature by passing through the saturators. Finally, one of the saturated air streams entered the capillary tube which was situated in the centre of the orifice. (The word "orifice" with the prefix "circular" means the hole drilled in the centre of the orifice plate, while with prefix "annular" means the annular opening formed when the tube is situated at the centre of the circular orifice. In cases with no prefix, the context should make the meaning clear.)

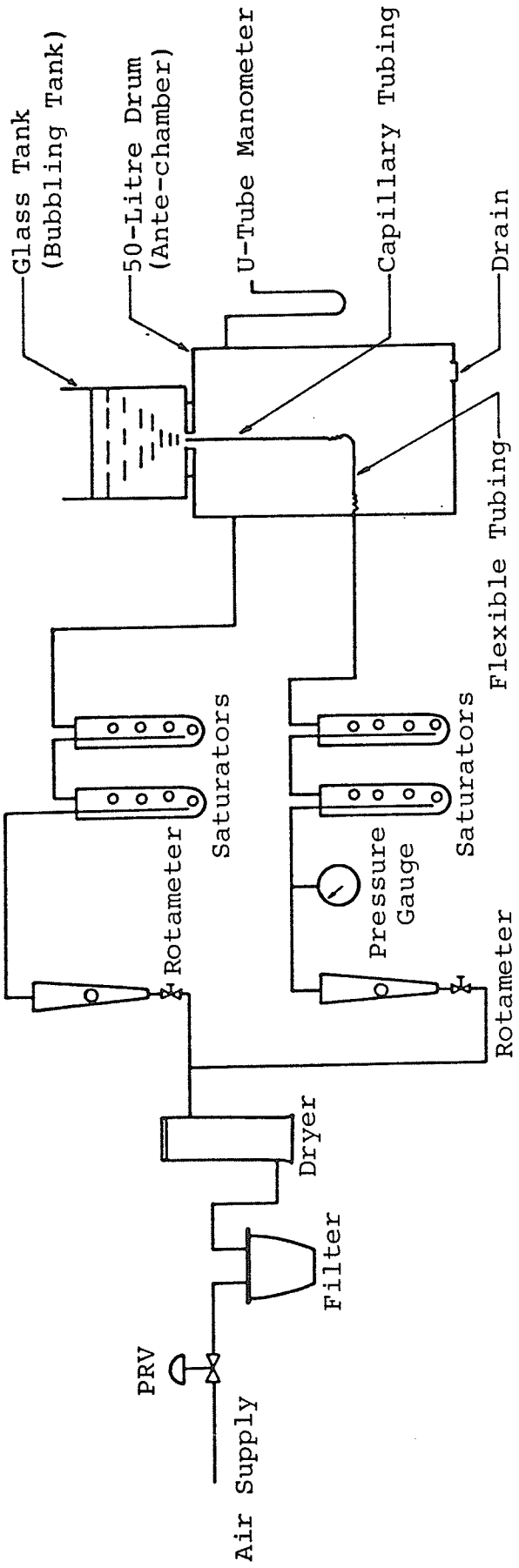

Fig. 3.1 Schematic Diagram of Apparatus

For the constant-flow stream, the line pressure between the flow meter and the saturator was measured by a pressure gauge for the calculation of constant air flow rate (Details of this calculation are presented in Appendix B.). The other air stream entered a 50-litre drum (the ante-chamber) from which it passed through the annular orifice into the bubbling tank containing the distilled water.

Details of the assembly comprising the container, the collar and the ante-chamber are shown in Fig. 3.2.

3.2 Orifice Plate

The orifice plate, as shown in Fig. 3.3, was made of stainless steel. The plate was 13.50 cm (5.32 in.) in diameter and the thickness was 1.15 cm (0.45 in.), machined as shown, and with a circular orifice drilled at the centre. The orifice was 0.502 cm (0.19 in.) in diameter. The size was chosen as most barbotage investigations fell between 0.2 cm to 0.6 cm. A long stainless steel capillary of 0.277 cm (0.11 in.) O.D. was held at the centre of the circular orifice by the "Unislide" assembly as the passage for the constant-flow stream. The constant-pressure flow passed from the ante-chamber through the annular orifice into the liquid bath.

Another combination of circular orifice and capillary tubing (smaller sizes) was used to take some, but not a complete set of data. The orifice and results are described in Appendix F together with the reasons for appearing in an

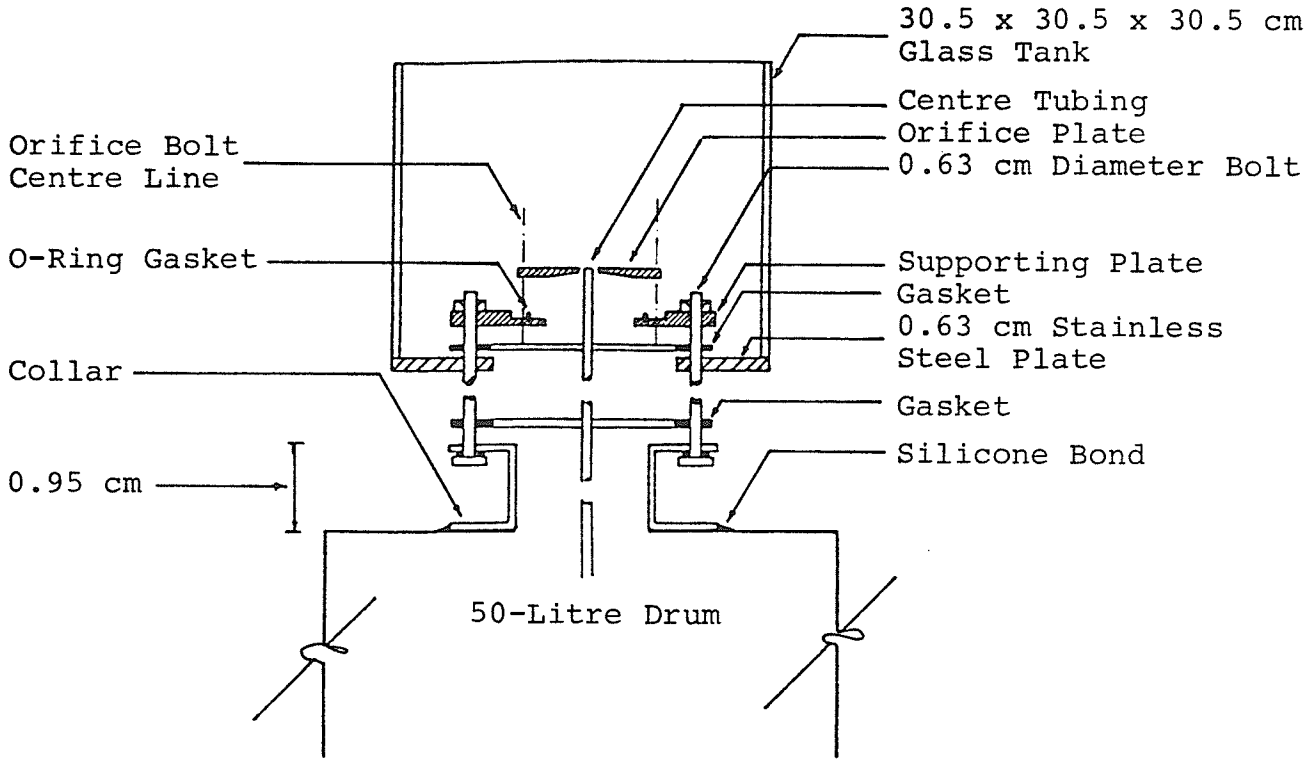

Fig. 3.2 Details of Container Assembly

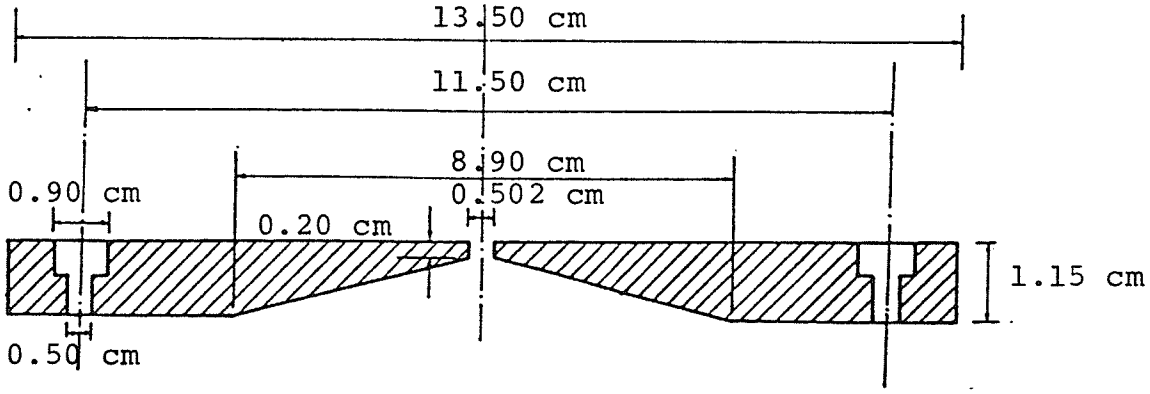

Fig. 3.3 Orifice Plate

appendix.

3.3 Ante-Chamber

The bubbling tank with the orifice plate was fastened to the ante-chamber top through a collar. Inside the 50-litre ante-chamber, the "Unislide assembly" was located beneath the orifice holding the capillary in the desired position. The capillary connected via flexible tubing to one fitting in the ante-chamber wall which in turn connected to the air supply. The pressure inside the ante-chamber was measured by using a vertical U-tube liquid manometer, containing Meriam oil (sp. gr. 0.784). Figure 3.4 shows details of the ante-chamber.

3.4 Unislide Assembly

The position of the capillary tubing inside the orifice for the constant-flow supply was controlled by a combination of three Unislide assemblies (Velmex, Inc.). The general arrangement is shown in Fig. 3.4. The component assemblies were of two Series A Model 1503D for the Y- and Z- direction and one Series A Model 2504D for the X-direction. The three components together will be called the "Unislide assembly". It allowed for accurate and quick placement of the capillary tubing by giving control of movement in three directions.

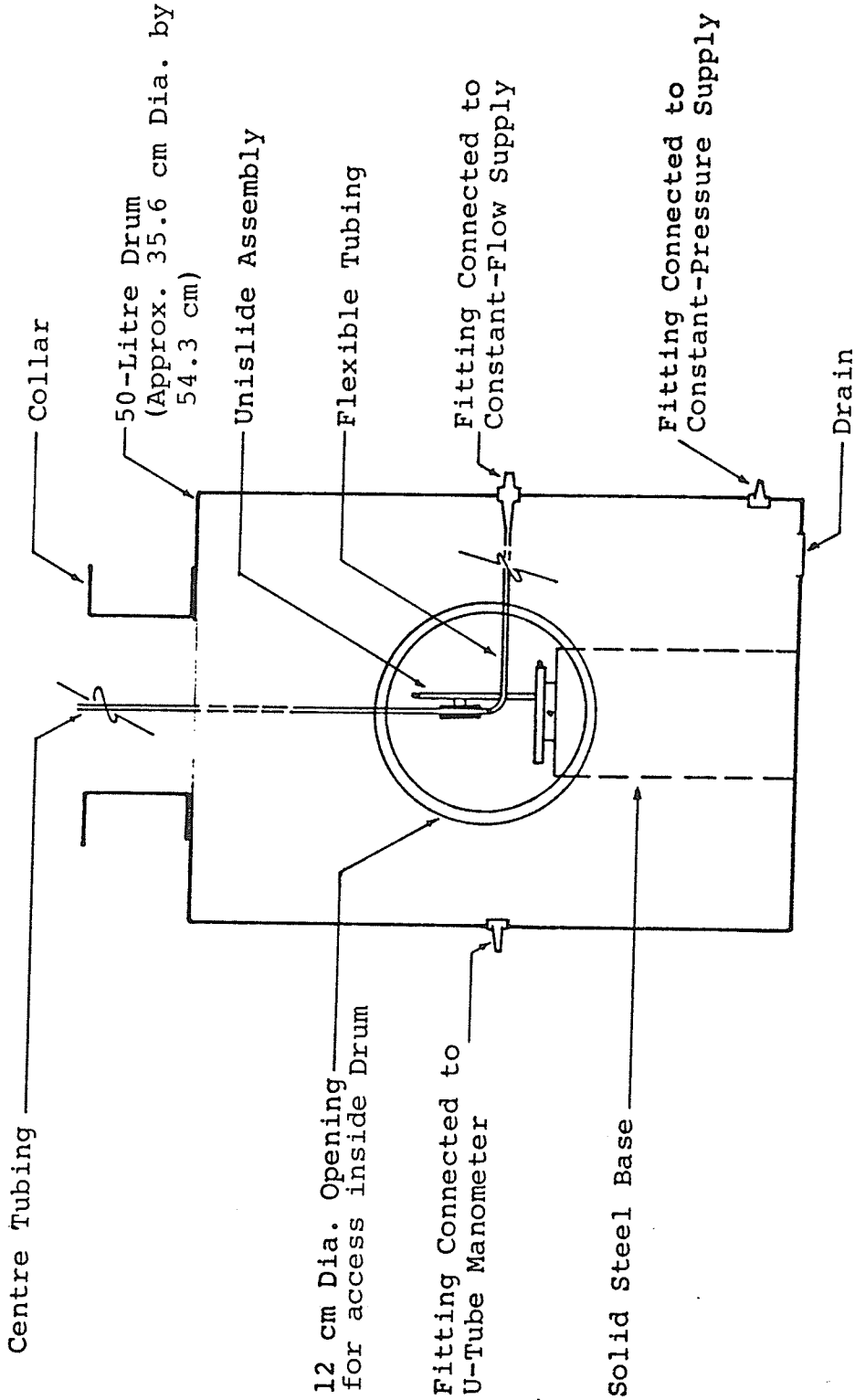

Fig. 3.4 Details of Ante-Chamber and Unislide Assembly Arrangement

3.5 Photographic Apparatus

The bubble formation process at the level of the orifice was recorded by means of a 16 mm high-speed motion picture camera; this was a Hycam Model 41-0004, camera operating for the present experiments in the range of 500 to 2500 frames per second, using Kodak 16 mm, Ektachrome, VNX 430.7250 colour film in 30.5-m (100-ft) rolls. The frame speed could be accurately obtained from a timer light arrangement (Series 100) inside the camera (LED operating at 100 hertz driven by a miniaturized crystal-controlled generator) which placed markers along the film outside the frames. The camera was placed at a distance from the orifice plane, so that the terminal bubble forming at the orifice could be completely captured on film. Two Smith-Victor 650-watt (at 115 volts) lamps were used with a glass diffusing screen to provide optimum illumination for photography. The light arrangement resulting in sharply defined bubble profiles is shown in Fig. 3.5 and was based on the experience of Cheung [7] and others [4, 48]. A Pentax Spotmeter III light meter was used to determine the correct combination of film speed (ASA 400), f-stop, and camera speed. Before photographing the bubbles, a stainless steel rod of known diameter (0.95 cm) was suspended vertically above the orifice, and its image was recorded at 500 frames/second. The ratio of the actual diameter to its image, acted as a "scale factor" so that the true volume of a bubble could be determined from

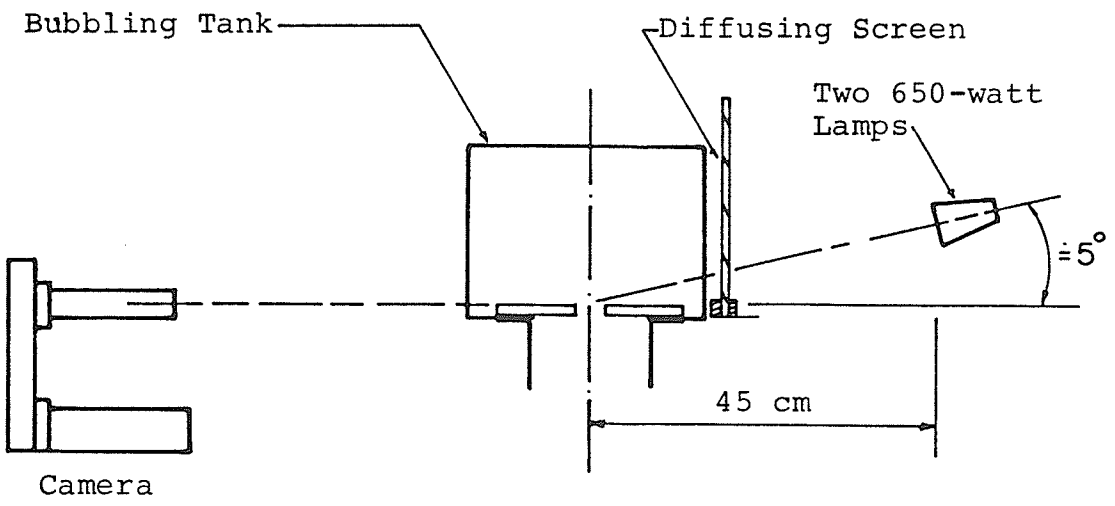

ELEVATION

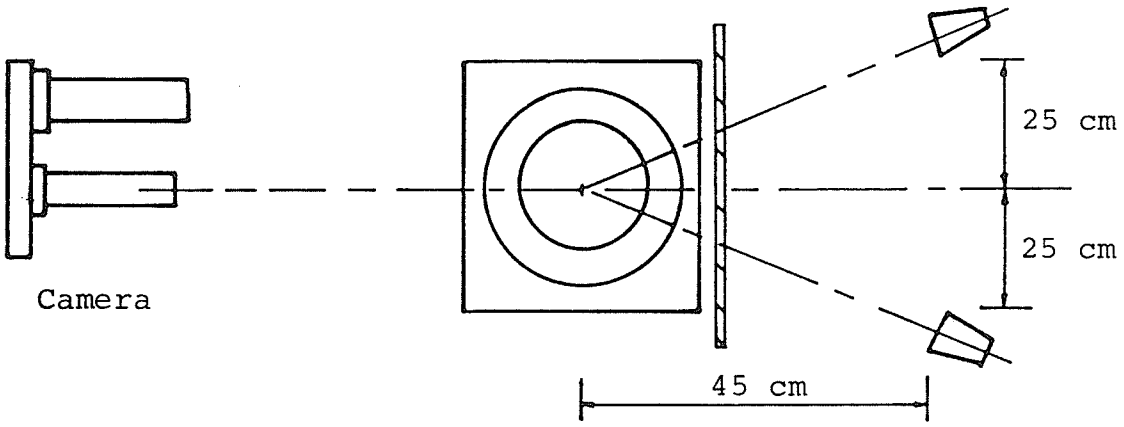

PLAN

Fig. 3.5 Arrangement of Photographic Equipment

its magnified image. A motion picture analyser (LW model 900) was used to project frame-by-frame photographs on a PCD viewer (model 2AE-3A) equipped with a digital X-Y reader. The equipment allowed for the measurement of bubble dimensions with an accuracy of approximately 0.01 cm in the actual bubble.

CHAPTER 4

PROCEDURE

4.1 Introductory Remarks

This chapter describes the procedure used in the experiments. The procedure of setting up the apparatus is presented in Section 4.2; this includes how to determine the capillary tube position relative to the centre of the circular orifice. Section 4.3 then describes the procedure of photographing the bubbles at the level of the orifice. A brief description of calculating the instantaneous volume of a bubble is presented in Section 4.4 while the computation of the bubble volume is illustrated in detail in Appendix C.

4.2 Apparatus Set Up

Prior to running the apparatus, certain preparations had to be made before starting the experiment. The procedure was as follows:

1. The bubbling tank was washed with ordinary soap and rinsed thoroughly with distilled water. It was then dried with a piece of clean cloth.

2. The four saturators were cleaned and filled to the two-thirds level with distilled water.

3. The orifice plate was put into the correct position and fastened.

4. The Unislide assembly with the capillary tube was put inside the ante-chamber through the 12 cm diameter door.

5. The capillary tube was connected to the air supply system through one of the fittings in the drum.

6. The capillary tube outlet end was first brought to the same level as the top of the orifice plate by adjusting the Z-direction of the Unislide assembly.

7. The capillary was adjusted as closely as possible to the centre of the circular orifice by eye. In order to estimate the error, this process was repeated several times in a separate test and each time a photograph of the orifice (plan view) was taken by a 35 mm camera (Nikon FE); then the error was measured from enlarged photographs. The typical error $(\frac{e}{r})$ was of the order of 4 - 5% where e and r are shown in Fig. 4.1.

8. The door of the ante-chamber was tightly closed.

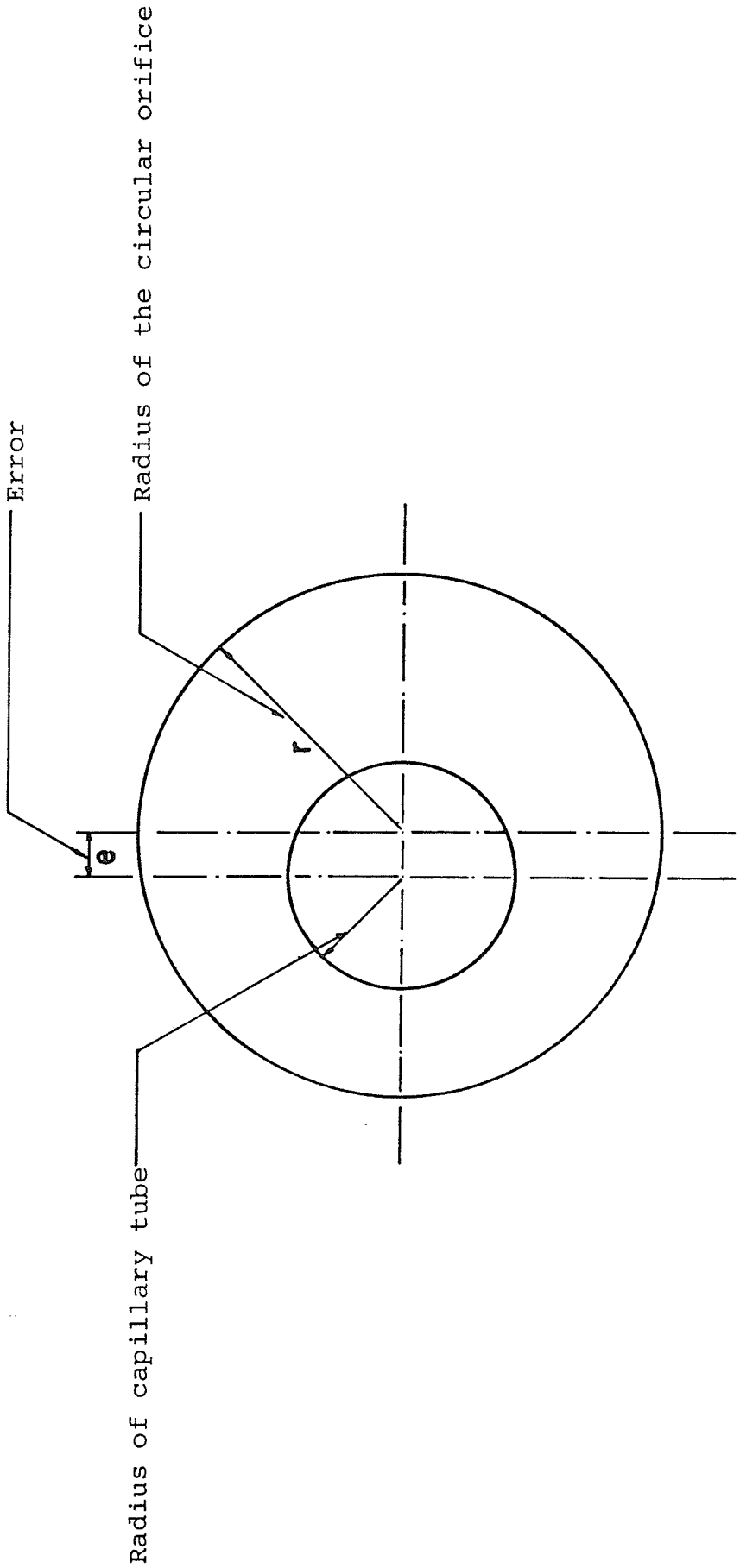

Fig. 4.1 Error between the centre lines of the circular orifice and the capillary tube

4.3 Bubble Image Photography

Photographic records of bubble growth were obtained using distilled water as the liquid and air as the injected gas. An experimental run was conducted as follows:

1. The air supply system was connected to the bubbling unit and then turned on for a while to ensure steady flow to the capillary and the ante-chamber. This precaution was necessary to prevent liquid leaking through the orifice while the container was being filled.

2. The glass tank was filled with distilled water to a depth of 12.7 cm above the orifice.

3. The constant-flow rate was measured by the flow meter.

4. The pressure inside the ante-chamber was set to any desired value by means of the needle valve.

5. Allowing some time to ensure steady-state operation, the values of the constant-flow rate, ante-chamber pressure, line pressure downstream of flow meter, the atmospheric pressure, the room temperature and the pool temperature were recorded.

6. The correct combination of frame speed and aperture was determined.

7. A stainless steel rod of 0.95 cm diameter was put in the plane of the orifice and photographed at 500 frames per second for two seconds.

8. With the rod removed, the experimental conditions were rechecked.

9. The frame speed was set at 2000 frames per second, the aperture adjusted and the bubble image was photographed.

4.4 Calculation of Instantaneous Volume of Bubble

The high speed photography provided an effective way to measure the volume of a bubble by projecting it frame-by-frame on a screen equipped with an X-Y digital reader. The volume of the bubble was calculated from the two-dimensional profile obtained by photography. The procedure for computing the volume of a bubble is illustrated in detail in Appendix C. By assuming the measured volume equal to a sphere of equal volume, the equivalent radius of the bubble R_{eq} was obtained from the following equation:

$$R_{eq} = [\frac{3\ V_{measured}}{4\ \pi}]^{1/3}$$

where

$V_{measured}$ = volume measured from the film.

4.5 Test Conditions

The conditions under which the experiments were performed are summarized in Table 4.1. The constant-flow rate through the central tubing was corrected to the orifice conditions (air saturated with vapour at the pool temperature and pressure at the level of orifice). Detailed calculations are presented in Appendix B. The values of the actual flow rates in the orifice were used to determine the F values in Table 4.1*.

---

*The symbols F, E' and ΔP^* are explained in Sec. 5.2, but are defined below for convenience:

$$F \equiv Q_c\ (\frac{\rho_l}{\sigma R_o^3})^{\frac{1}{2}},\quad E' \equiv \frac{\pi^2\ R_o^4}{A_a^2}(\frac{1}{K^2}\ \frac{\rho_g}{\rho_l}),\quad \Delta P^* = \frac{P_t - P_\infty}{\frac{2\sigma}{R_o}}$$

The flow coefficient (K) [3] through the annular orifice was determined by measurement. The procedure is described in Appendix A. An average value of 0.69 was used to determine the E' values in Table 4.1.

Pool: Open to atmosphere
Gas: Air
Liquid: Distilled Water
Depth of Liquid: 12.7 cm above the orifice
Atmospheric Pressure: 75.50 - 77.30 cm Hg (precise values in App. E)
Room and pool: 22.2 - 25.6°C (precise values in App. E)
E': 5.11×10^{-3} - 5.17×10^{-3} (precise values in App. E)
Orifice dimensions:
Circular orifice diameter = 0.502 cm
Capillary tube I.D.= 0.216 cm
O.D.= 0.277 cm

Film Identification	ΔP*	Actual Constant-Flow Rate at Orifice cm^3/sec	F
A	1.24	0.00	0.00
B		10.98	10.29
C		17.74	16.64
D		24.16	22.64
E		31.56	29.58
F		37.83	35.45
G	2.04	0.00	0.00
H		17.77	16.66
I		27.98	26.24
J	2.44	0.00	0.00
K		17.77	16.66

Table 4.1 Experimental Conditions for the Bubble Growth Experiments

CHAPTER 5

THEORETICAL ANALYSIS

5.1 Introductory Remarks

The purpose of this chapter is to formulate a theoretical analysis of the problem of bubble growth from a submerged orifice under the combined effects of the two limiting cases, namely, constant-flow and constant-supply-pressure conditions. By knowing the plenum pressure, constant-flow rate, properties of fluids, orifice and tube geometry, the problem can be formulated into a dimensionless form and solved numerically.

5.2 Theoretical Formulation of the Problem

The equation of bubble growth can be derived by beginning with the Rayleigh Eqn. [37] as follows:

$$R\ddot{R} + \frac{3}{2}\dot{R}^2 + \frac{2\sigma}{\rho_l R} = \frac{P_b - P_\infty}{\rho_l} \qquad (5.1)$$

where

R = radius of the bubble,

$\dot{R}$ = first derivative of the radius with respect to time,

$\ddot{R}$ = second derivative of the radius with respect to time,

σ = surface tension of the liquid,

ρ_l = density of liquid,

P_b = pressure in the bubble, and

P_∞ = pressure at a large distance from the bubble at the level of the orifice.

Certain assumptions are involved in the formulation and use of the above equation.

(1) The gas-liquid interface is spherical during the formation of the bubble.

(2) The fluid surrounding the interface is quiescent and incompressible and of infinite extent.

(3) The pressure inside the bubble is uniform at any instant.

(4) Liquid flow is irrotational.

(5) There is no transfer of liquid vapour into the bubble.

Examination of Eqn. 5.1 shows two unknown variables, R and P_b are involved. A second equation is therefore necessary to obtain a solution. At any instant, as the

bubble forms at the orifice (Fig. 5.1), the flow rate into the bubble is given by

$$Q_{tot} = Q_c + Q_p \tag{5.2}$$

where

Q_{tot} = the total flow rate (a function of time),

Q_c = the constant gas flow rate (independent of time), and

Q_p = the gas flow rate through the annular orifice (a function of time).

For Q_p the orifice equation can be used:

$$Q_p = K A_a \left[\frac{2 (P_t - P_b)}{\rho_g}\right]^{\frac{1}{2}} \tag{5.3}$$

wherein it is implied that the gas (air) is incompressible, and

K = the flow coefficient ($K = C_d M$ in which C_d is the coefficient of discharge and M is the velocity of approach factor [3]).

P_t = the pressure in ante-chamber,

P_b = the pressure inside the bubble,

ρ_g = gas density,

A_a = the cross-sectional area of the annular portion of the orifice.

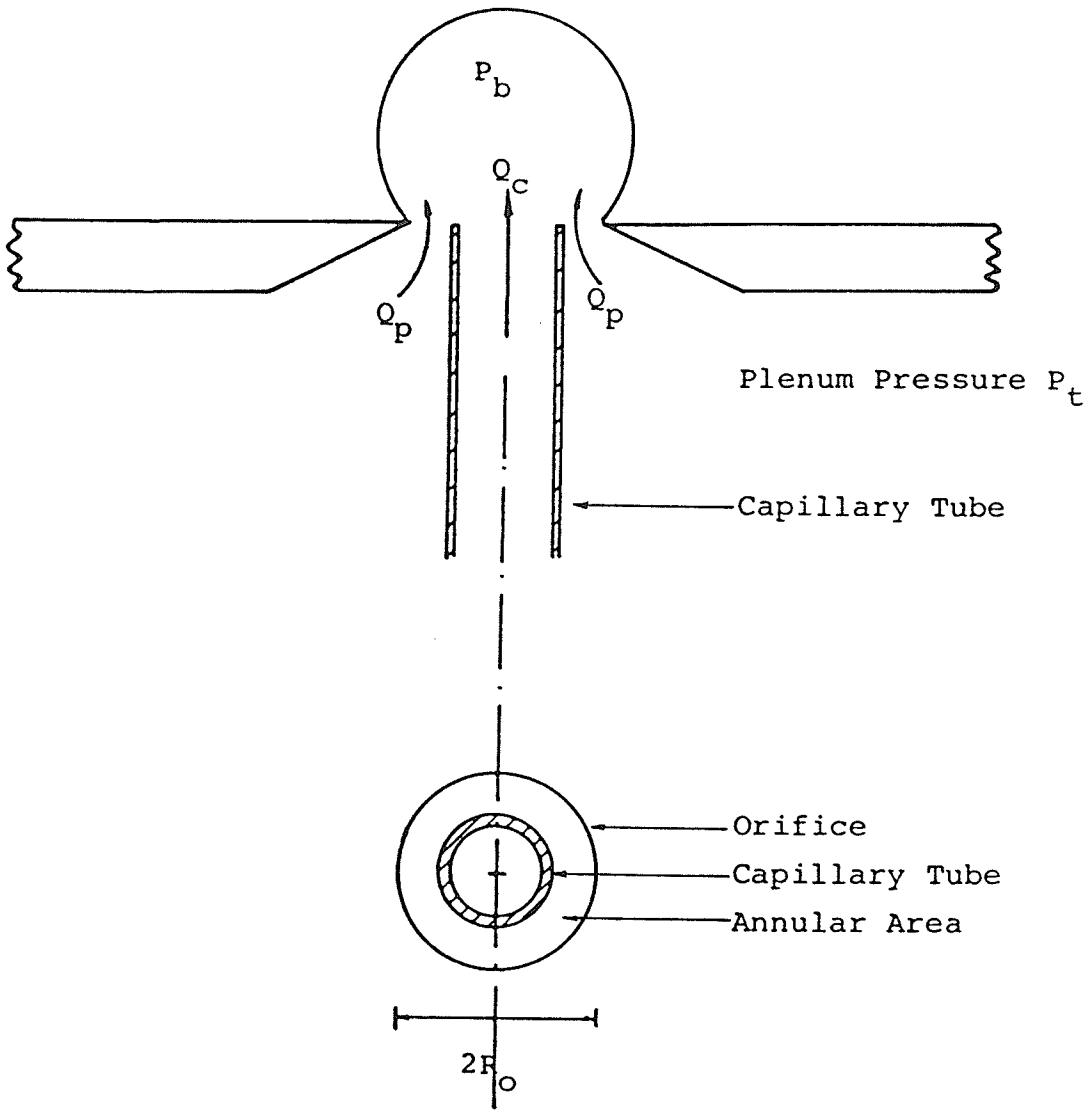

Fig. 5.1 Bubble Formation at the Orifice

For a spherical bubble, the volume V would be $\frac{4}{3}\pi R^3$, and

$$Q_{tot} = \frac{dV}{dt} = 4\pi R^2 \dot{R} \tag{5.4}$$

From (5.2) - (5.4), we have

$$4\pi R^2 \dot{R} = Q_c + K A_a \left[\frac{2(P_t - P_b)}{\rho_g}\right]^{\frac{1}{2}} \tag{5.5}$$

Solving for P_b from Eqn. 5.5 and substitution in Eqn. 5.1 yields

$$R\ddot{R} + \frac{3}{2}(\dot{R})^2 + \frac{2\sigma}{\rho_l R} = \frac{P_t - P_\infty}{\rho_l} - \frac{\rho_g}{\rho_l (K A_a)^2}\left[8\pi^2 R^4 \dot{R}^2 - 4Q_c \pi R^2 \dot{R} + \tfrac{1}{2}Q_c^2\right] \tag{5.6}$$

Equation 5.6 can be manipulated into dimensionless form by using the following definitions

$$\begin{aligned}
R_* &\equiv \frac{R}{R_o}, \\
t_* &\equiv t\left(\frac{\sigma}{\rho_l R_o^3}\right)^{\frac{1}{2}}, \\
\dot{R}_* &\equiv \frac{dR_*}{dt_*}, \\
E' &\equiv \frac{\pi^2 R_o^4}{A_a^2}\frac{\rho_g}{K^2 \rho_l}, \\
F &\equiv Q_c \left(\frac{\rho_l}{\sigma R_o^3}\right)^{\frac{1}{2}}, \\
\Delta P^* &\equiv \frac{P_t - P_\infty}{\frac{2\sigma}{R_o}}.
\end{aligned} \tag{5.7}$$

The final equation is

$$R_* \ddot{R}_* + 1.5 \dot{R}_*^2 + 8E'R_*^4 \dot{R}_*^2 - \frac{4E'F}{\pi} R_*^2 \dot{R}_* + \frac{2}{R_*} =$$

$$2 \Delta P^* - \frac{E'F^2}{2\pi^2} \qquad (5.8)$$

Equation 5.7 was solved by numerical integration, using a fourth order Runge-Kutta formula with initial conditions at time t = o as

$$R_* = 1$$

$$\frac{dV}{dt} = 4\pi R^2 \dot{R} = Q_c$$

$$\dot{R}_* = \frac{F}{4\pi R_*^2}$$

or

$$\dot{R}_* = \frac{F}{4\pi}$$

The Amdahl 5850 computer was used to solve the equation. The computer program is presented in Appendix D.

5.3 Theoretical Results

A theoretical analysis of the bubble growth rate was presented in the previous section. The final Eqn. 5.7 was solved and the results are given here.

Equation 5.7 is the theoretical equation written in dimensionless form and its solution takes the form of R_* as a function of t_* for various values of the three parameters

E', ΔP^* and F. A close examination of the E' value shows it can not be less than zero, and practically it should not be greater than 1. The ante-chamber pressure and the constant-flow rate through the centre tubing are related to ΔP^* and F respectively. These two values can be varied to obtain sets of curves for R_* vs. t_*. In the present work, the value of ΔP^* is increased from 1 to 3; this is the practical range over which one can conduct experiments. The parameter F is varied from 0 (pure constant-pressure case) to 125 (in terms of Q_c this represents a flow rate just a little less than the maximum used by Cheung [7] in his pure constant-flow experiments). The solution is generated up to $t_* \simeq 14$ which is equal to the maximum experimental value so far obtained [48]. The resulting curves are presented in Figs. 5.2 through 5.13.

Such presentation allows one to determine quickly the approximate growth curve, once E', ΔP^* and F are established for any given system. Obtaining the theoretical growth curve from the figures presented would not be as accurate as solving Eqn. 5.8 numerically (unless the values of the parameters were precisely the same as those used here), but very much more convenient. Curves representing the constant-pressure case can also be obtained simply by setting the value of F equal to zero. The results then reduce to Subash's solution [48]. This extreme case is also included in the figures.

It should be noted that in some figures, e.g. Fig. 5.2 with F = 0.001, the theoretical growth curves appear not to change from $R_* = 1$ up to some finite t_*; actually R_* is increasing but on the scale of the figure, the curves appear coincident with $R_* = 1$.

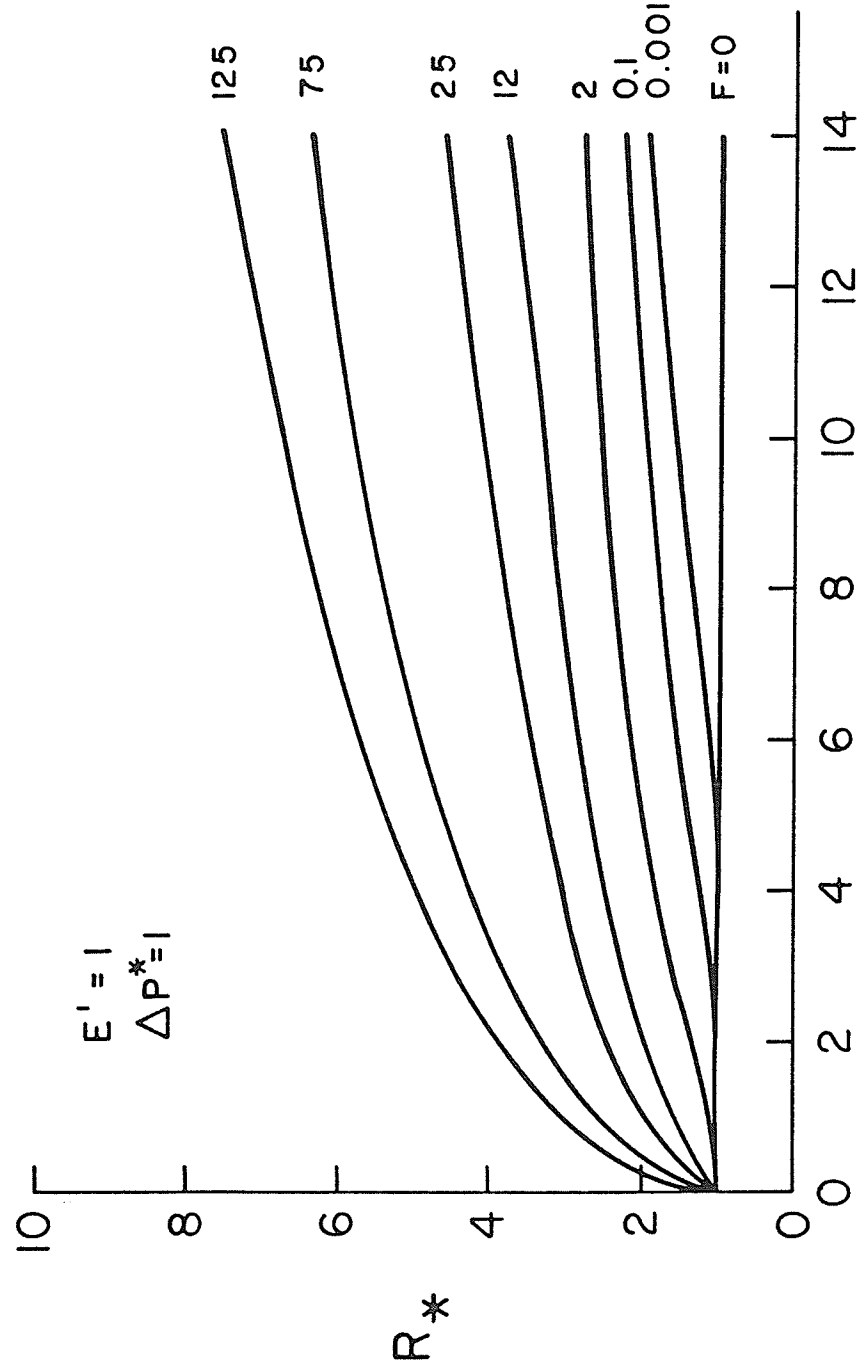

Fig. 5.2 Theoretical Bubble Growth Curves for E' = 1, $\Delta P^* = 1$

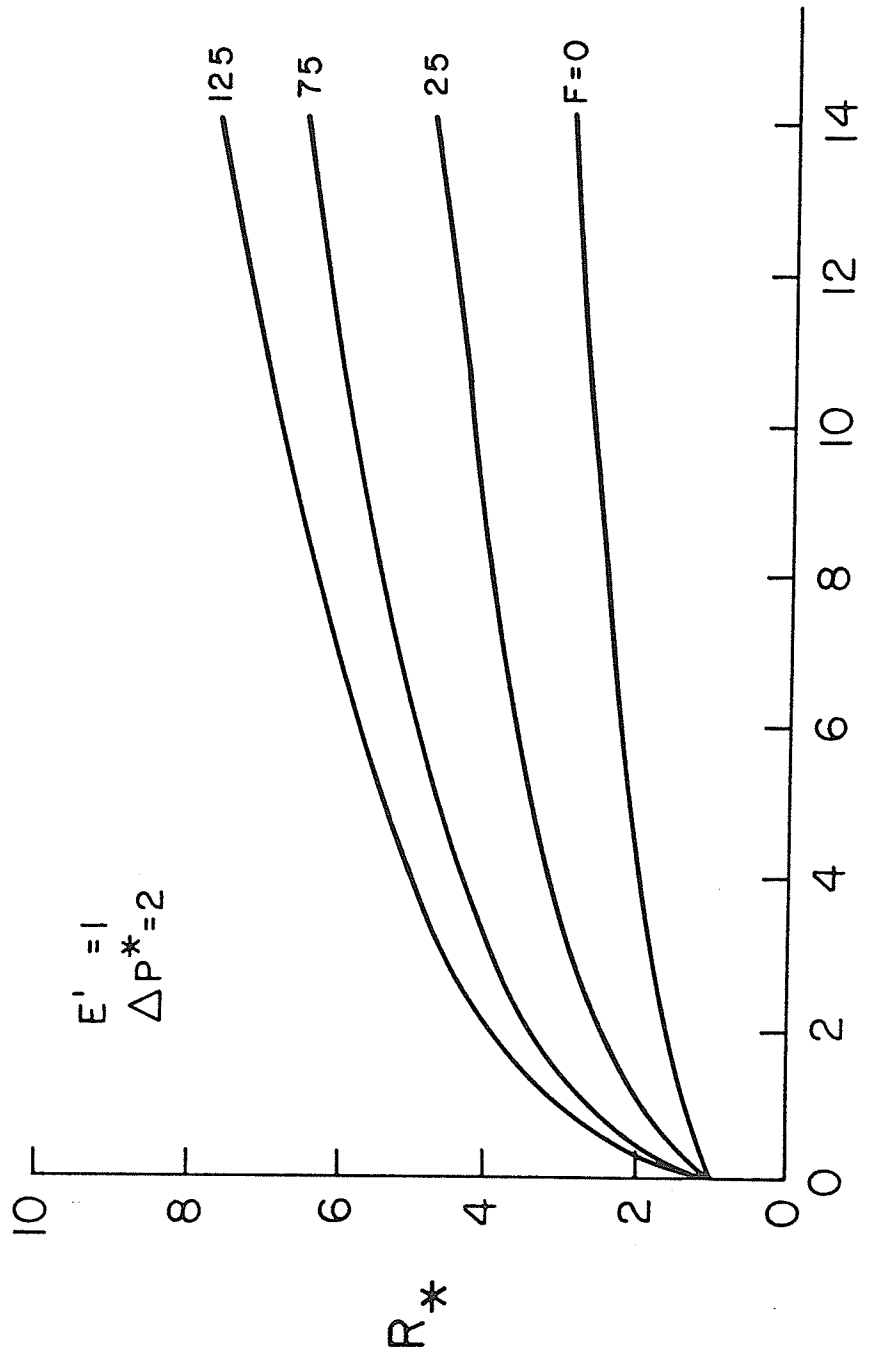

Fig. 5.3 Theoretical Bubble Growth Curves for E' = 1, $\Delta P^* = 2$

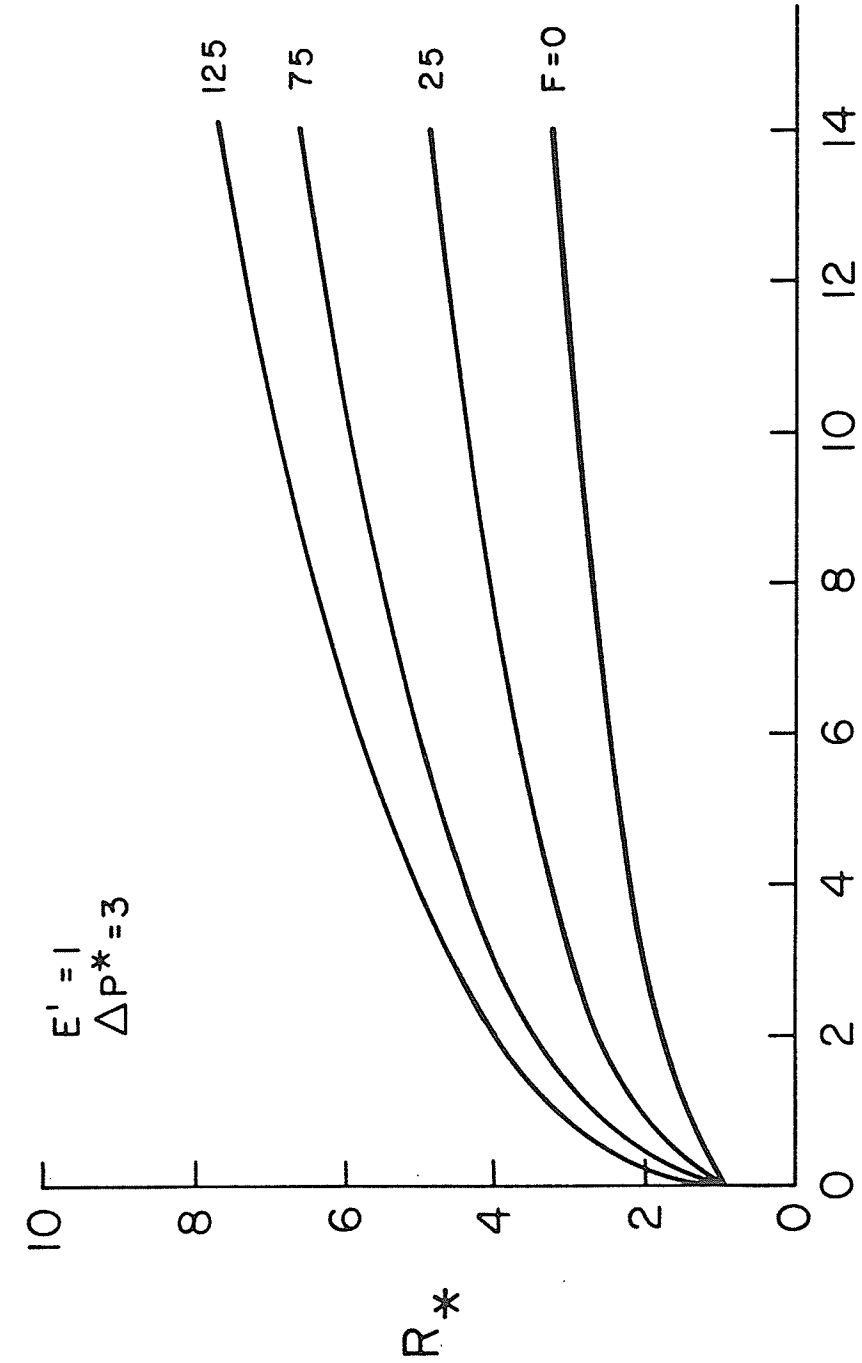

Fig. 5.4 Theoretical Bubble Growth Curves for E' = 1, $\Delta P^* = 3$

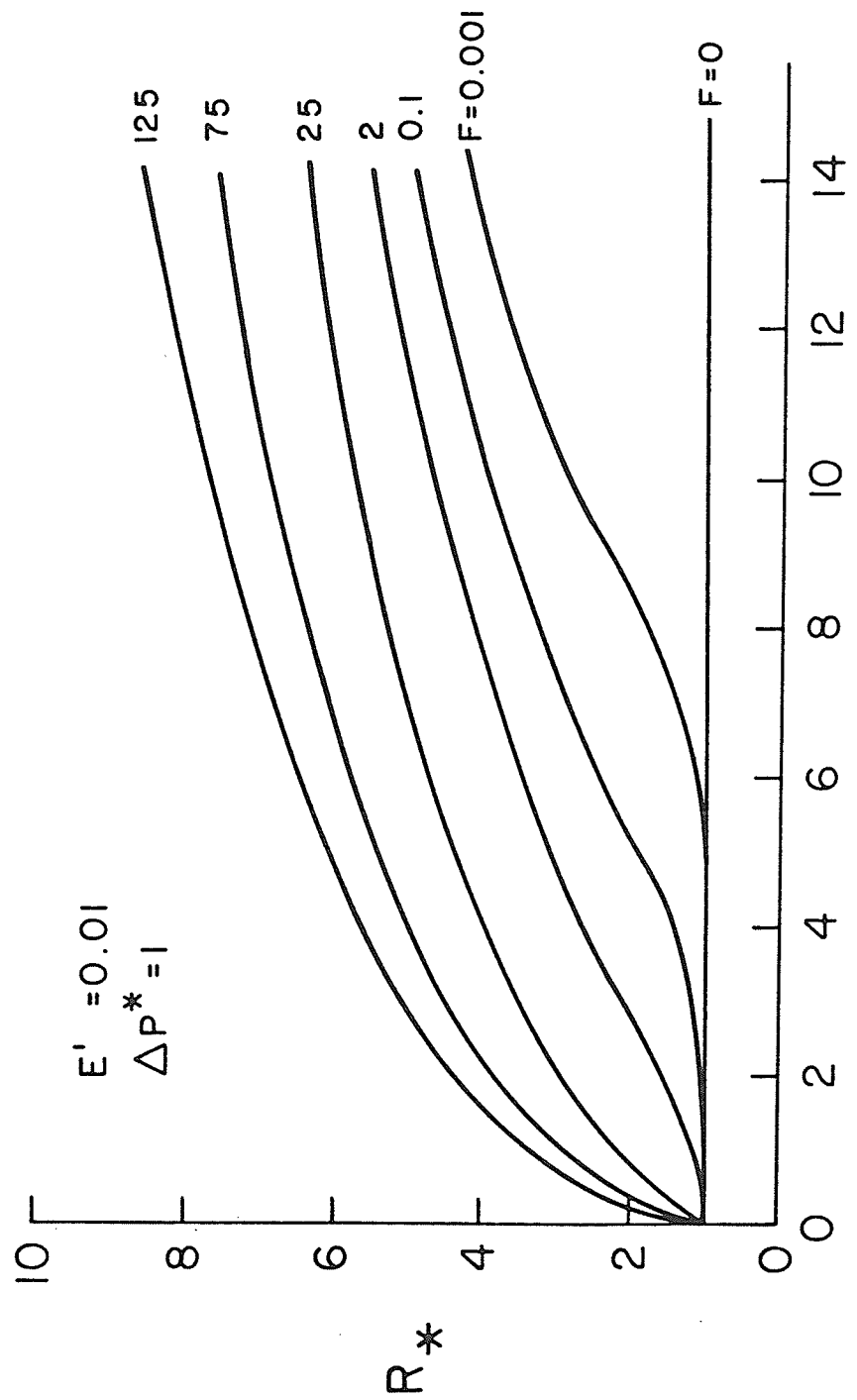

Fig. 5.5 Theoretical Bubble Growth Curves for E' = 0.01, $\Delta P^* = 1$

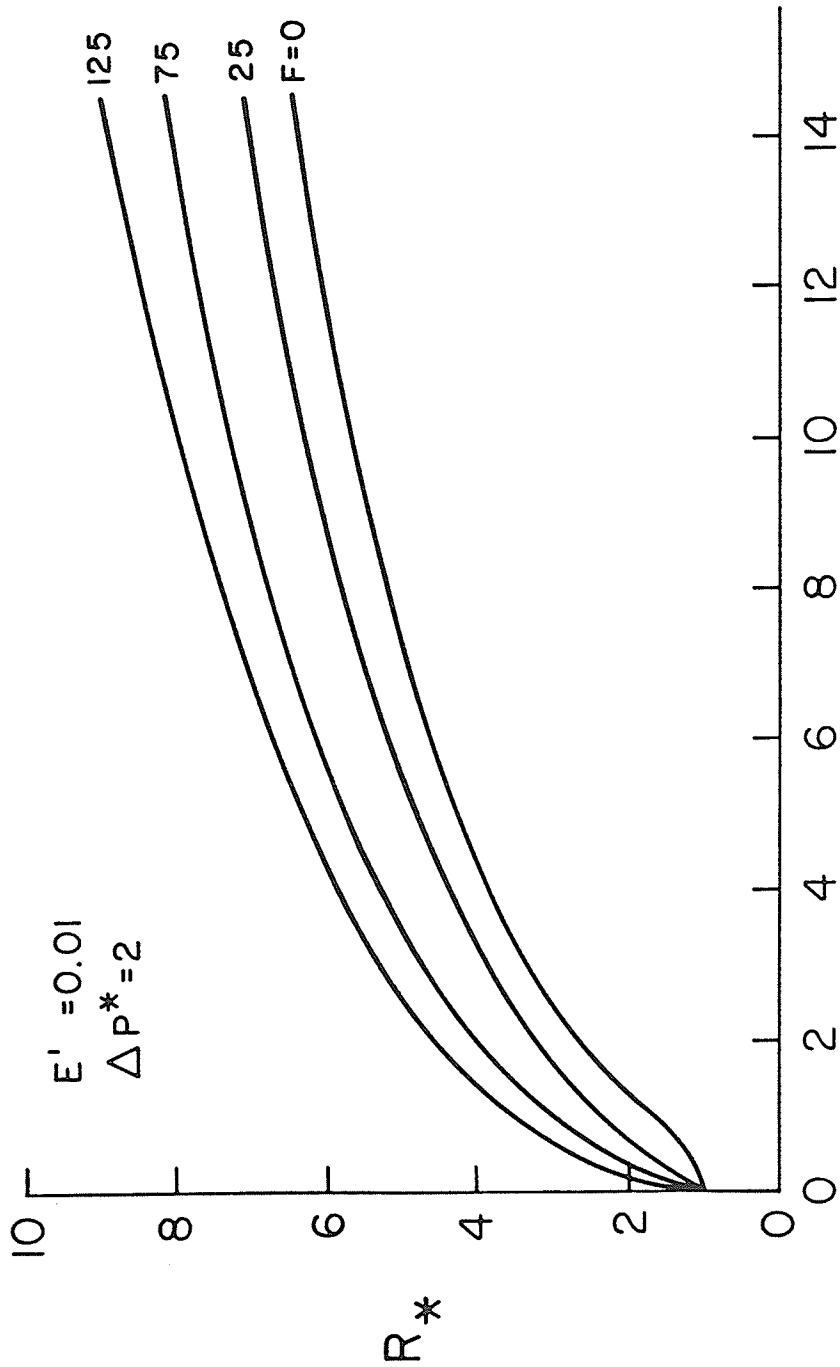

Fig. 5.6 Theoretical Bubble Growth Curves for E' = 0.01, $\Delta P^* = 2$

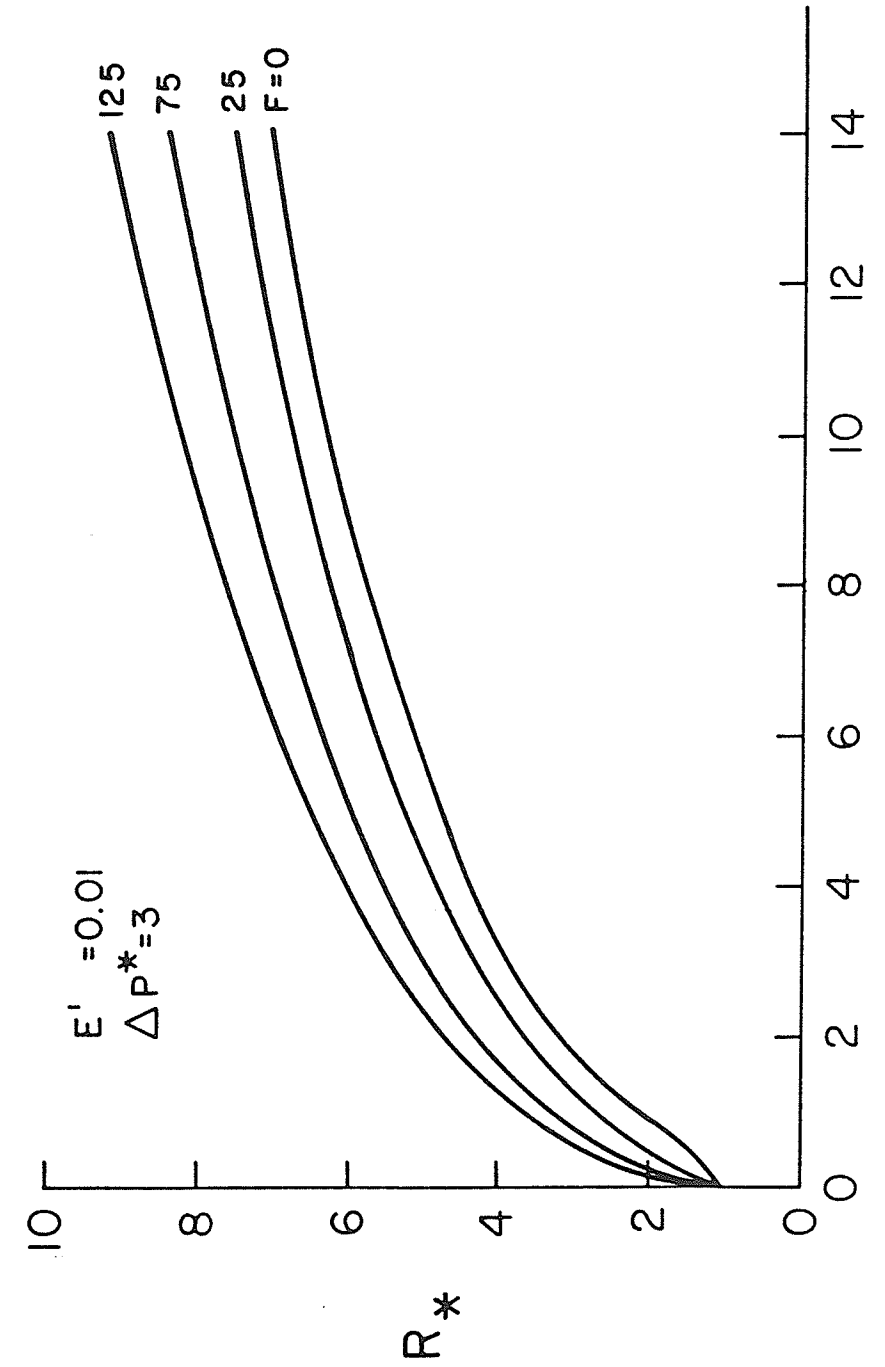

Fig. 5.7 Theoretical Bubble Growth Curves for E' = 0.01, $\Delta P^* = 3$

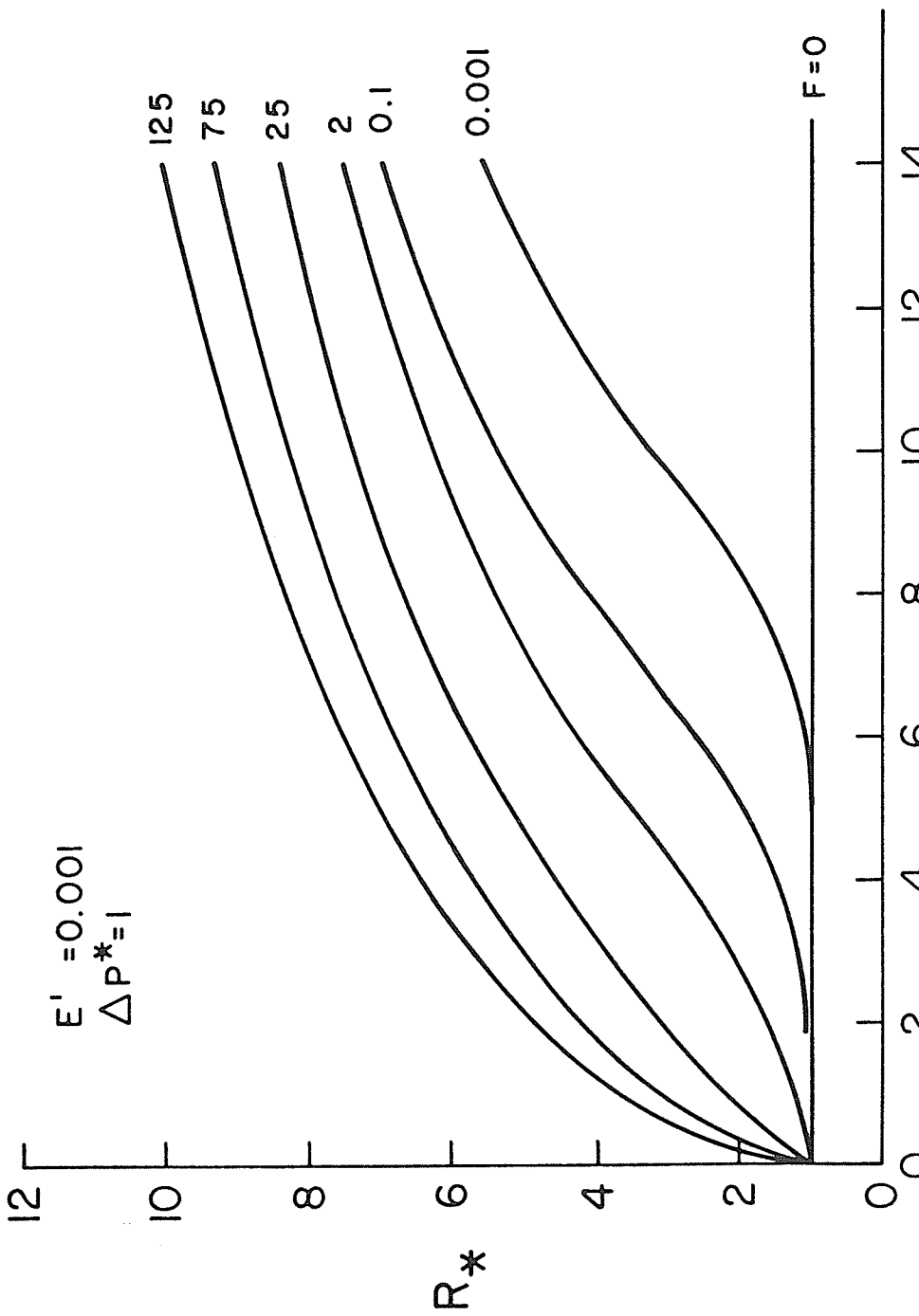

Fig. 5.8 Theoretical Bubble Growth Curves for E' = 0.001, $\Delta P^* = 1$

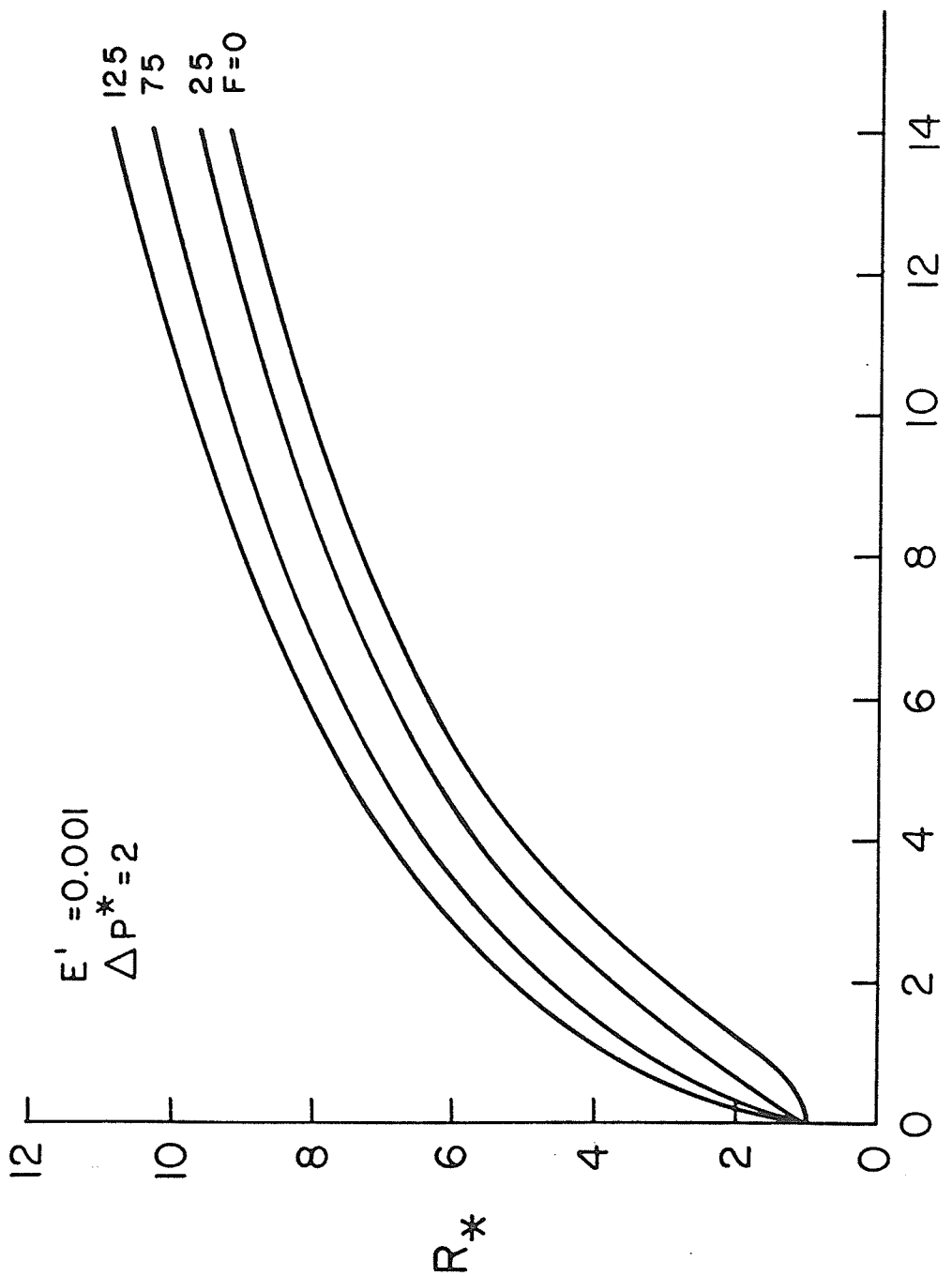

Fig. 5.9 Theoretical Bubble Growth Curves for E' = 0.001, $\Delta P^* = 2$

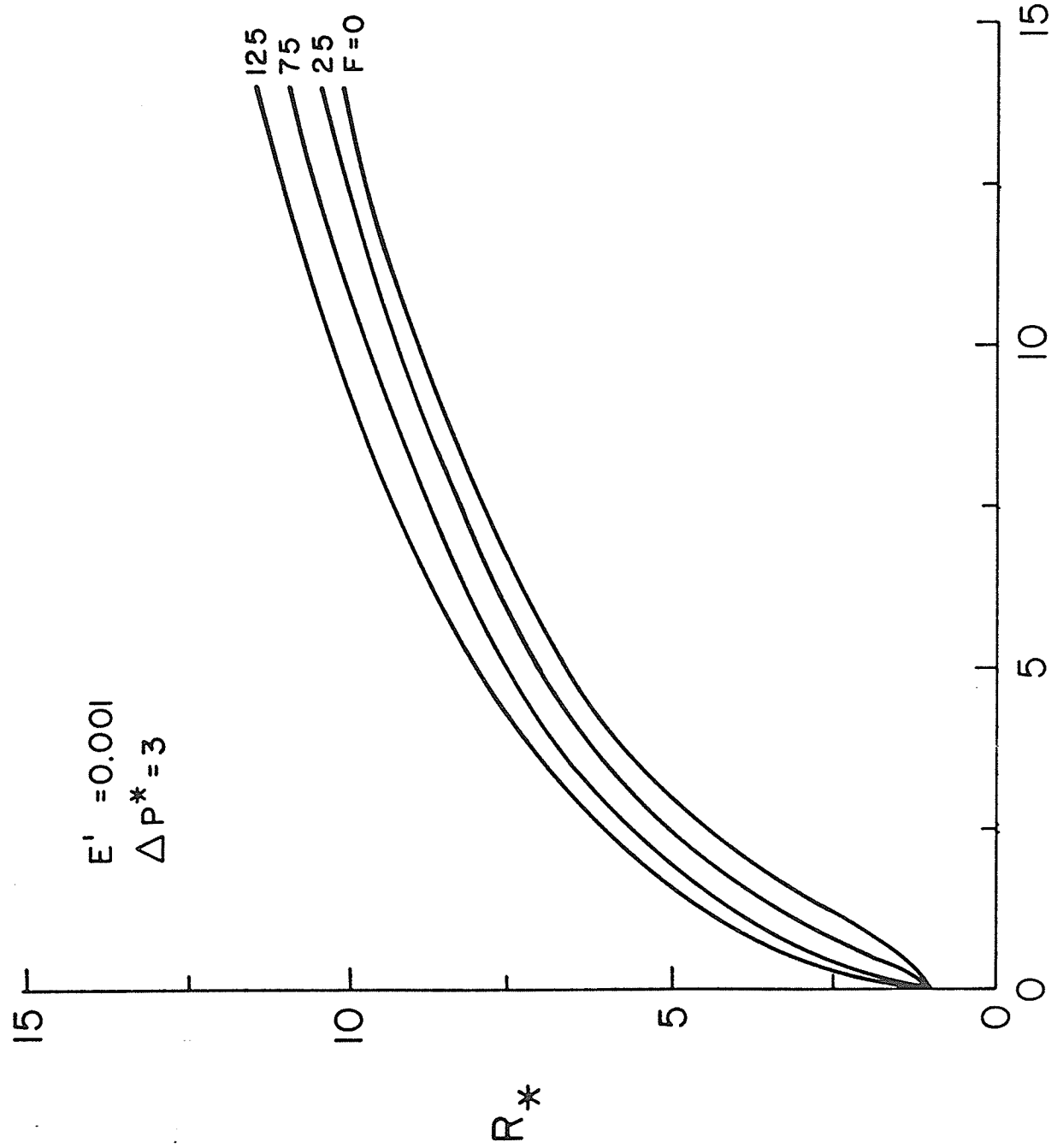

Fig. 5.10 Theoretical Bubble Growth Curves for E' = 0.001, $\Delta P^* = 3$

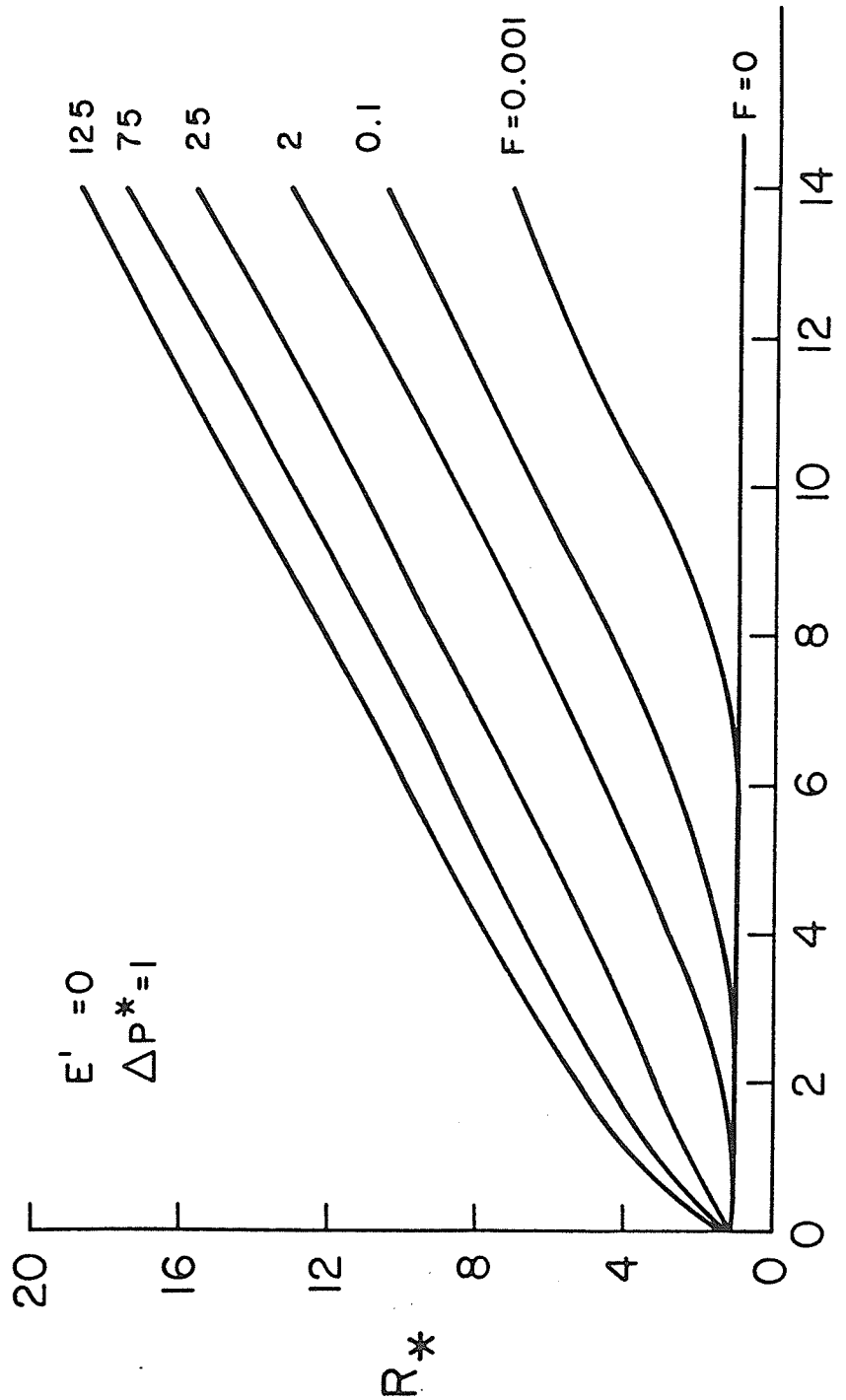

Fig. 5.11 Theoretical Bubble Growth Curves for E' = 0, $\Delta p^* = 1$

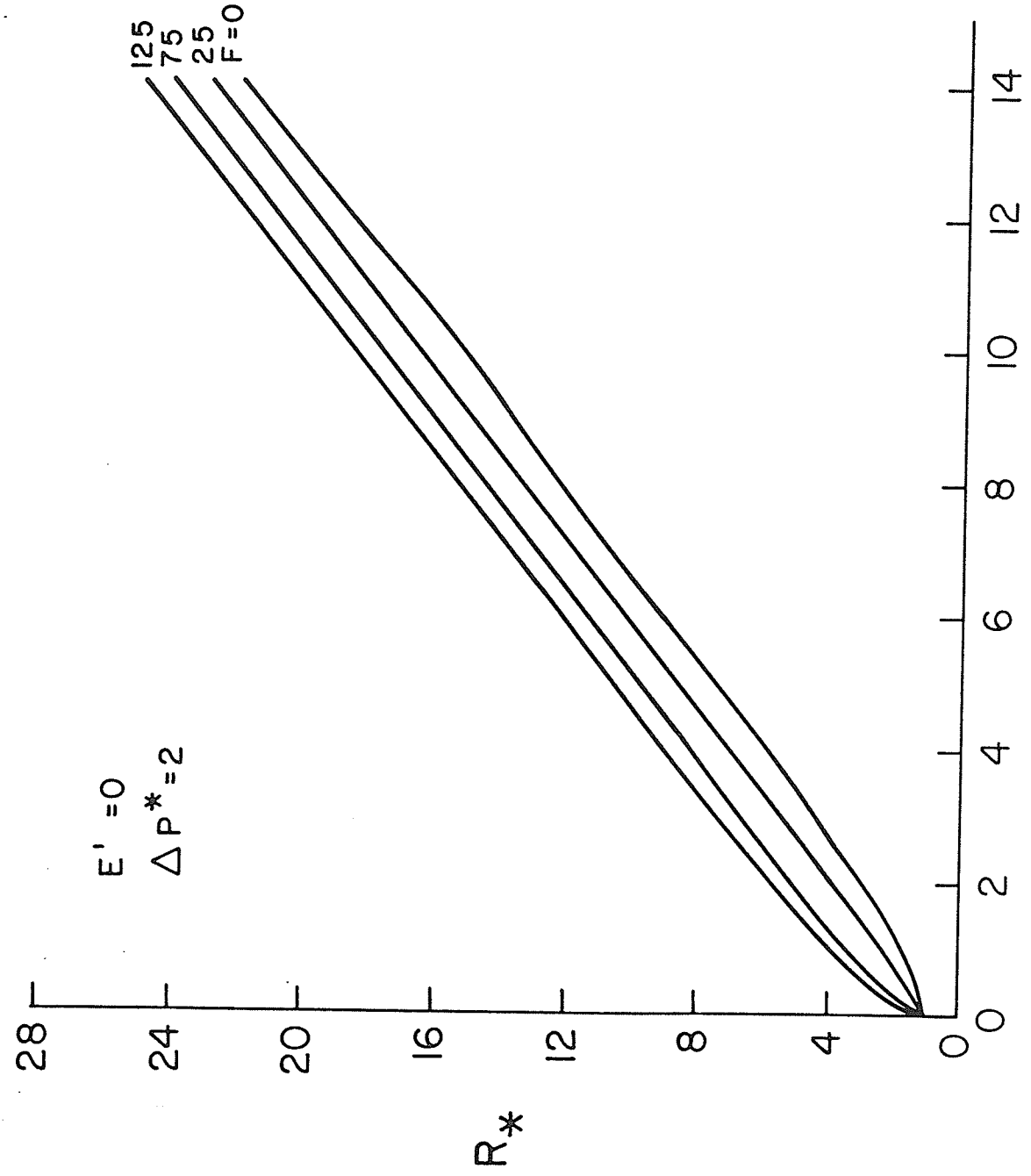

Fig. 5.12 Theoretical Bubble Growth Curves for E' = 0, $\Delta P^* = 2$

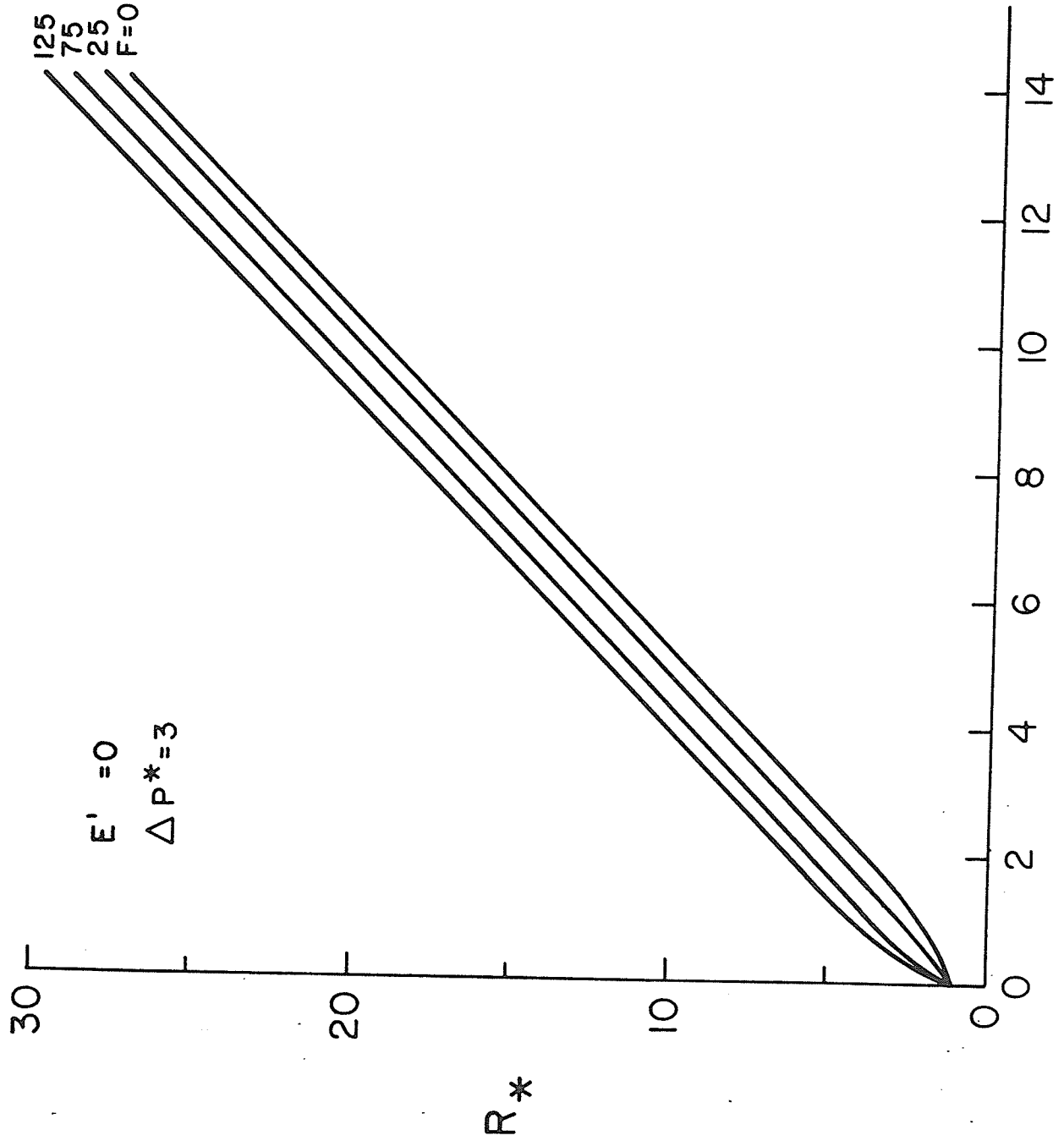

Fig. 5.13 Theoretical Bubble Growth Curves for E' = 0, $\Delta P^* = 3$

CHAPTER 6

RESULTS AND DISCUSSIONS

6.1 Bubble Observations

Bubble formation at the orifice was observed and could be generally categorized as follows:

(1) Double bubbles,

(2) Series of three bubbles,

(3) Series of more than three bubbles.

Figure 6.1 shows the typical behaviour of double-bubble formation. A typical sequence started generally with a small interface left behind by a departed bubble or a small meniscus appearing at the orifice after a time interval. (There were only a few bubbles of this latter type, and these were with the pure constant-pressure case, i.e. $F = 0$.) Due to the mass flow rate into the bubble, it began to grow and assumed a somewhat pear-shape. As the size of the first bubble increased further, a short stem started forming and connected the first bubble to the orifice. As the bubble moved up further, this stem began to form the second bubble, the two parts developing a neck between them (this neck was not so sharp or did not have a clean break as was the case with Cheung's [7] constant-volume bubbles) so marking the end of the life of the first bubble at the orifice. The secondary bubble started rising and penetrating

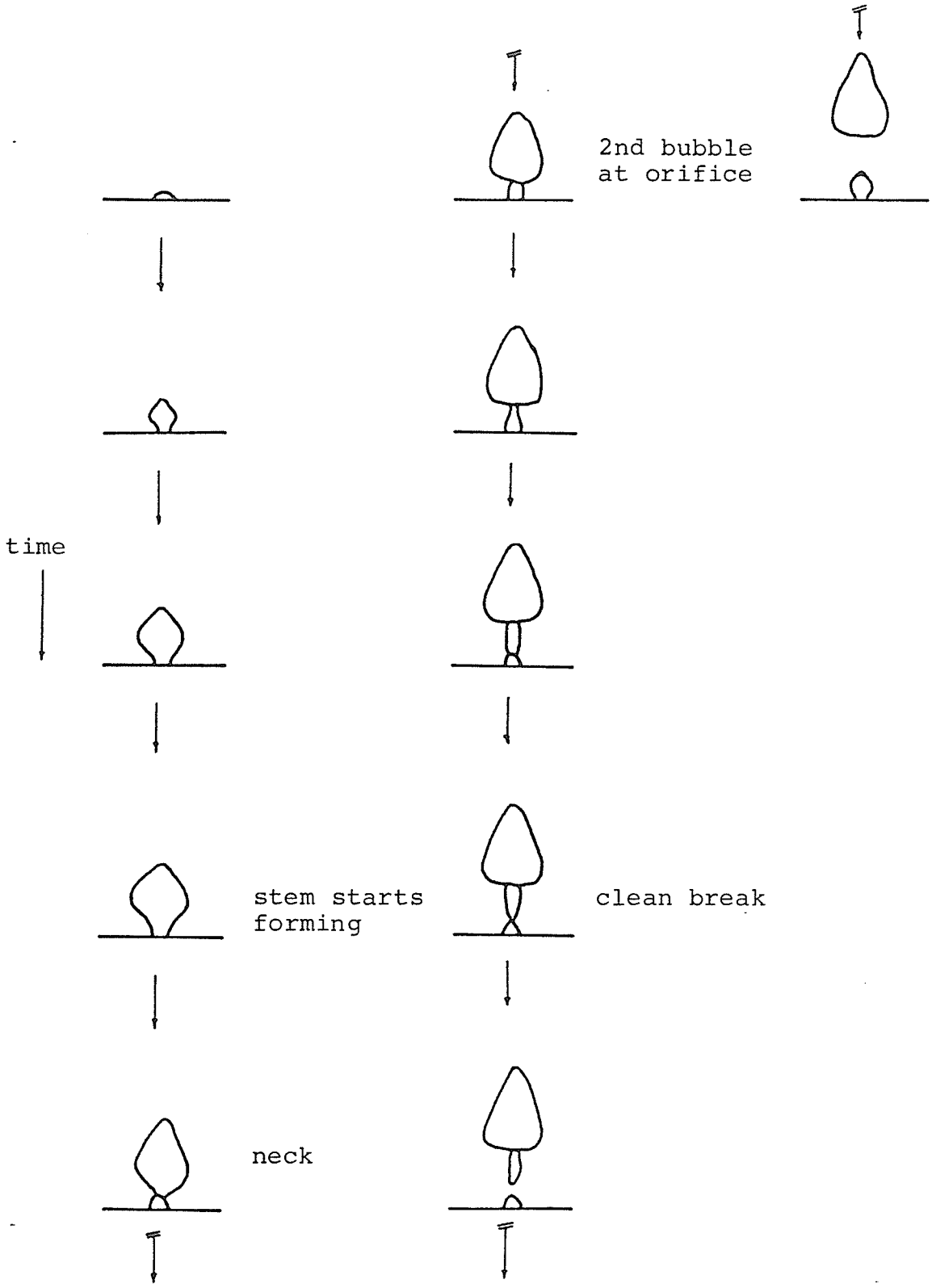

Fig. 6.1 Typical Behaviour of Double Bubbles

through the first bubble as they moved upwards and later integrated as a single unit. Finally the second bubble was severed from the orifice leaving behind a hemispherical interface.

The sequence of formation of a three-bubble series is shown in Fig. 6.2. The first two bubbles of the series behaved similarly to the double bubble as described above. The third bubble in the series started completely free after the second bubble broke free at the orifice. It grew fast enough to catch up to the combination of the first and second bubbles. During the later part of growth period, the third bubble fed the preceding bubble (combination of first and second bubbles) causing it to enlarge in size. The third bubble usually ended in a stem and then broke away from the orifice giving a shape like that of a mushroom for the three combined bubbles.

For series of more than three bubbles, the bubble series of this type could be broken down into: a number of double bubbles, a number of three-bubble series or some combination of double bubbles and three-bubble series. The bubble connecting these double bubbles and/or three-bubble series together acted as a "first-like" bubble except it contacted the previous bubble for part of its growth period during which its volume could not be measured.

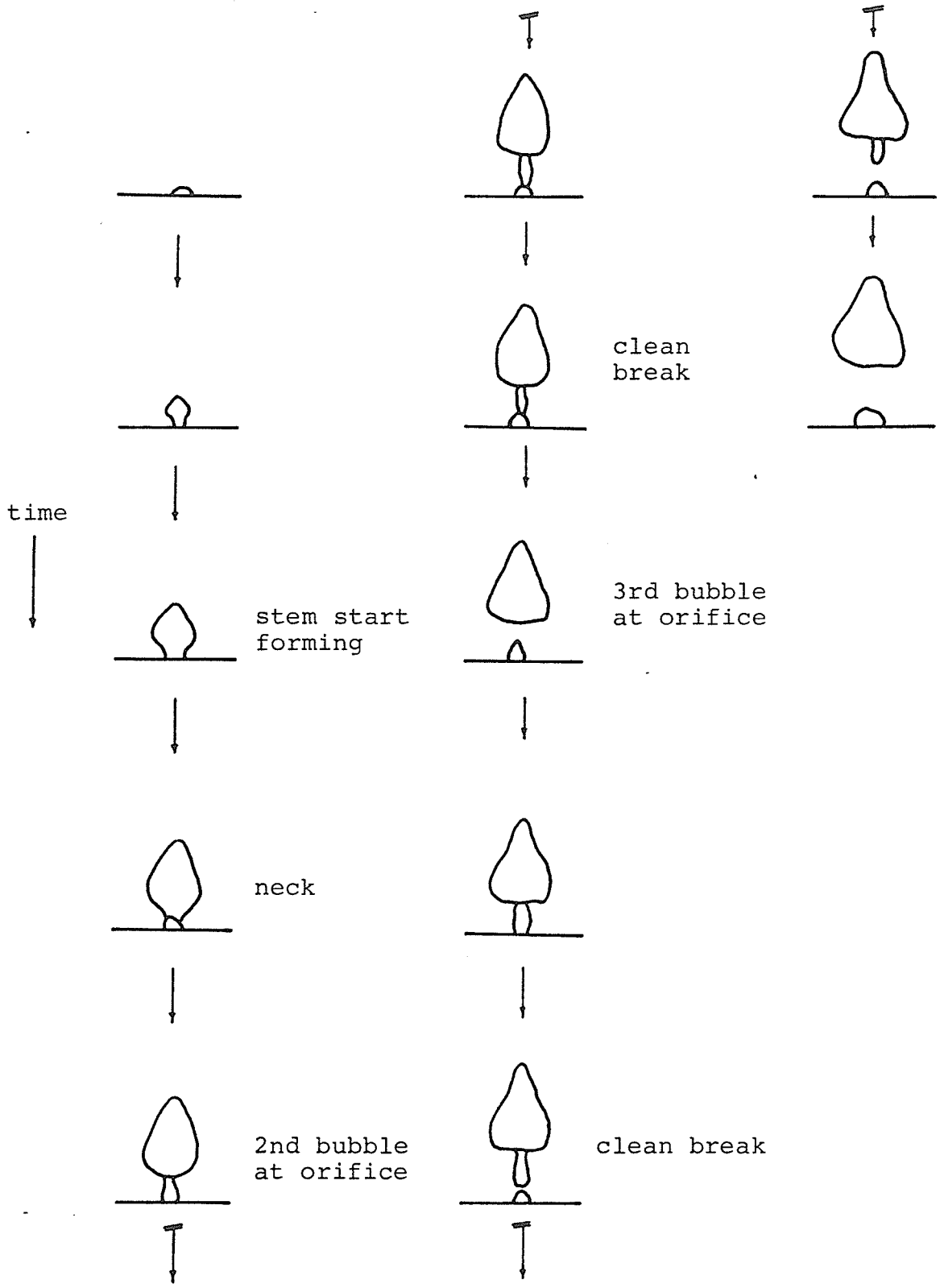

Fig. 6.2 Typical Behaviour of 3-Bubble Series

Film No.	ΔP*	F	Frame Nos. Analyzed	Bubble Type Observed
A	1.24	0.0	2-1482	7 Double Bubbles
B		10.29	58-1490	2 Double Bubbles 4 3-Bubble Series
C		16.64	145-1635	2 Double Bubbles 3 3-Bubble Series 1 4-Bubble Series
D		22.64	63-1500	3 Double Bubbles 4 3-Bubble Series
E		29.58	58-1341	1 Double Bubble 4 3-Bubble Series 1 4-Bubble Series
F		35.45	49-1542	3 3-Bubble Series 1 5-Bubble Series 1 6-Bubble Series
G	2.04	0.0	0-1581	6 Double Bubbles 1 4-Bubble Series
H		17.75	26-1545	4 Double Bubbles 3 3-Bubble Series
I		27.38	54-1586	7 Double Bubbles 1 3-Bubble Series
J	2.44	0.0	4-1529	6 Double Bubbles 2 3-Bubble Series
K		17.78	251-1581	1 Double Bubble 5 3-Bubble Series

Table 6.1 Summary of Bubble Type Observed

Table 6.1 summarizes the bubble types for different experimental conditions on analyzing the first approximately 1500 frames of each film from the first blank frame (see Appendix E for explanation of the term "blank frame").

It was always a "first bubble" which was analyzed to obtain R vs. t.

6.2 Bubble Growth

6.2.1 Experimental Results

Figures 6.3 to 6.13 show the bubble growth in terms of equivalent radius (cm) against time (ms). The curves corresponding to various conditions are summarized in Table 6.2. For each film, three "first bubbles" were chosen at random for analysis.

Zero time

"Zero time" was taken to correspond to the frame when there was a finite volume left behind at the orifice as the departing bubble just severed its connection from it or the frame prior to the one where the bubble first appeared as a meniscus (a few for $F = 0$, low ΔP^* conditions, but none analyzed here). There is an uncertainty in time which is equal to the time between two successive pictures. The error is less than 0.5 ms, in a total growth time of about 55 ms.

Liquid = Distilled water
Orifice Diameter = 0.502 cm
Capillary tube
I.D. = 0.216 cm
O.D. = 0.277 cm

Film Identification	Fig. No. for Data	Fig. No. for Comparison with Theory	ΔP^*	F	E'
A	6.3	6.14	1.24	0.0	0.00511
B	6.4	6.15		10.3	0.00517
C	6.5	6.16		16.6	0.00517
D	6.6	6.17		22.6	0.00517
E	6.7	6.18		29.6	0.00512
F	6.8	6.19		35.5	0.00512
G	6.9	6.20	2.04	0.0	0.00511
H	6.10	6.21		16.7	0.00512
I	6.11	6.22		26.2	0.00511
J	6.12	6.23	2.44	0.0	0.00511
K	6.13	6.24		16.7	0.00512

Table 6.2 Experimental Conditions for the Bubble Growth Results

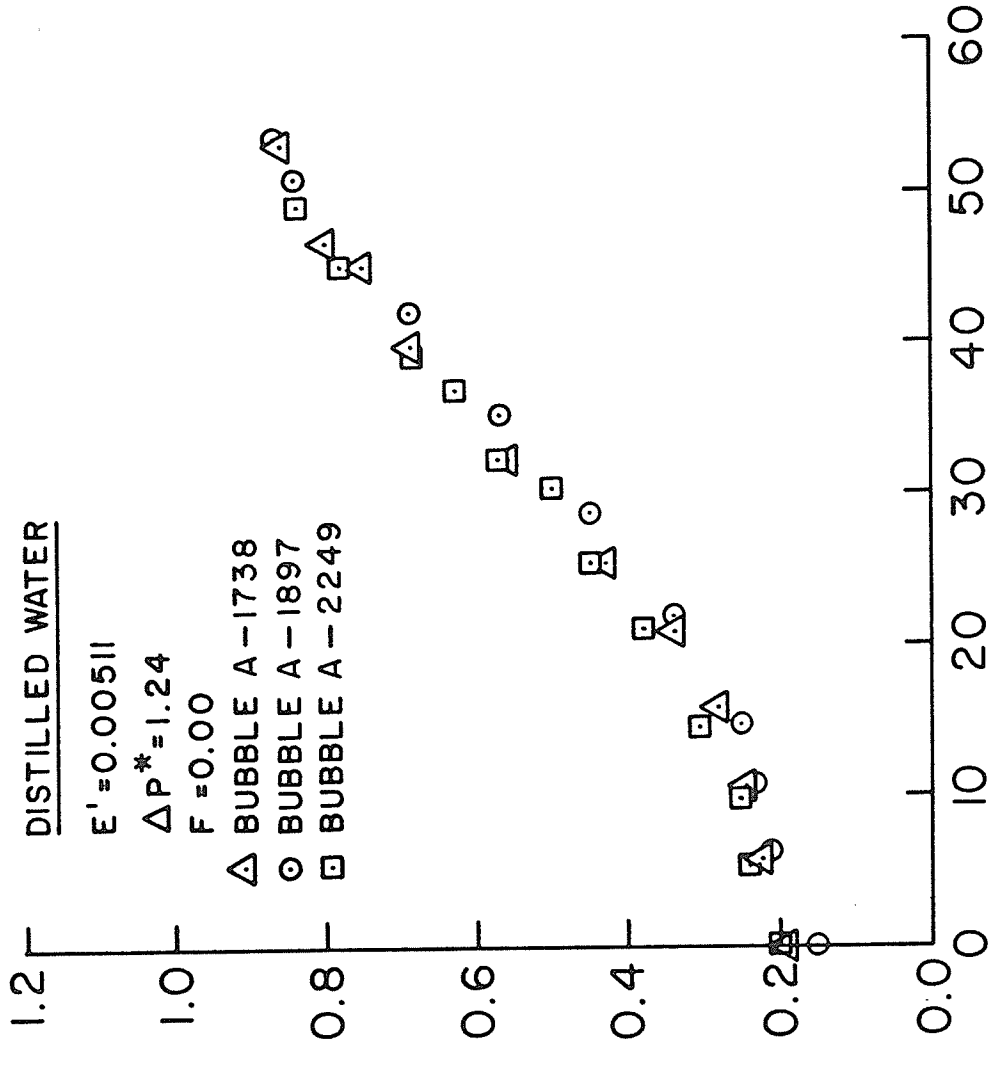

Fig. 6.3 Bubble Growth Data in Distilled Water
(E' = 0.00511, ΔP* = 1.24, F = 0.00)

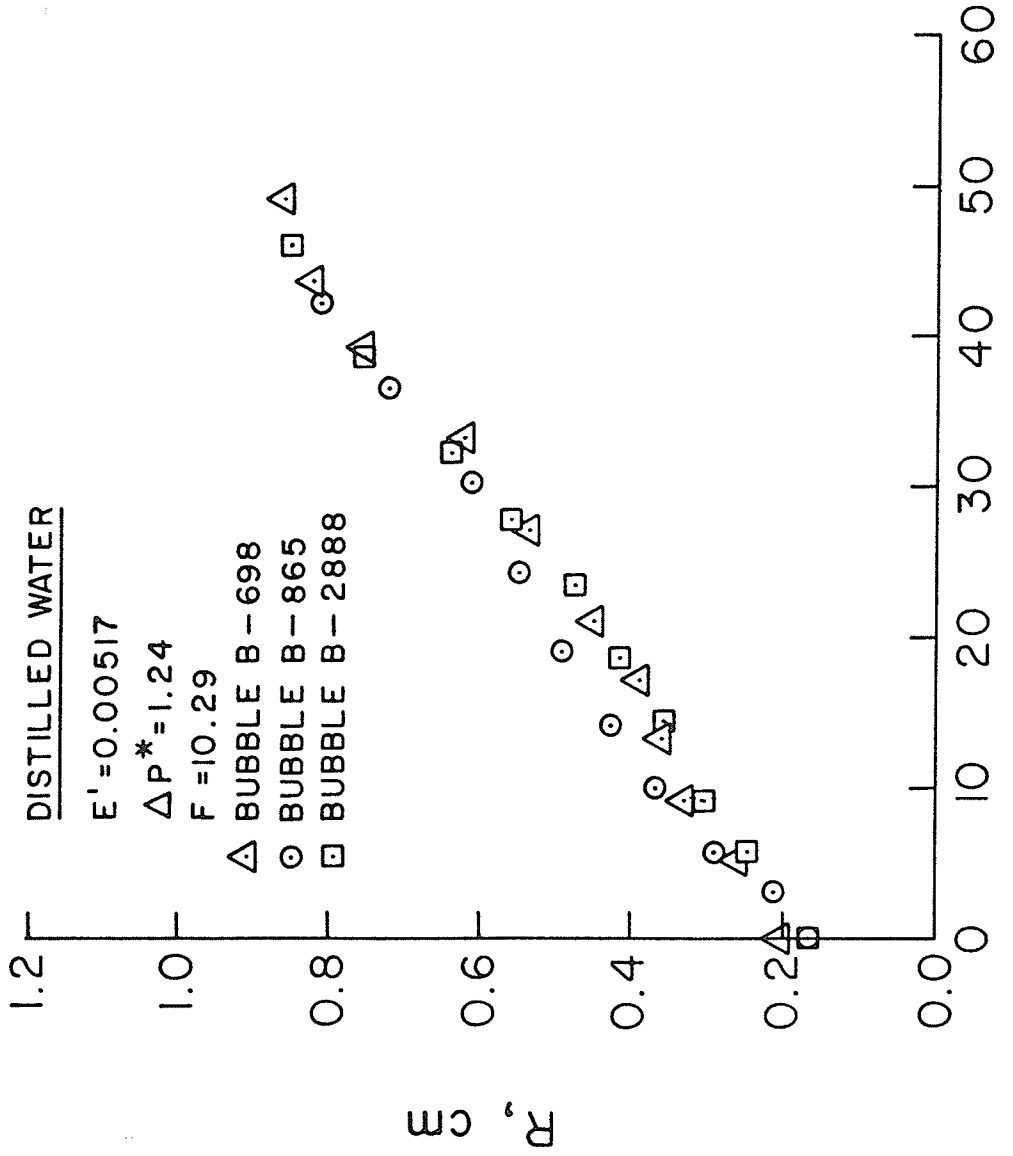

Fig. 6.4 Bubble Growth Data in Distilled Water
(E' = 0.00517, ΔP* = 1.24, F = 10.29)

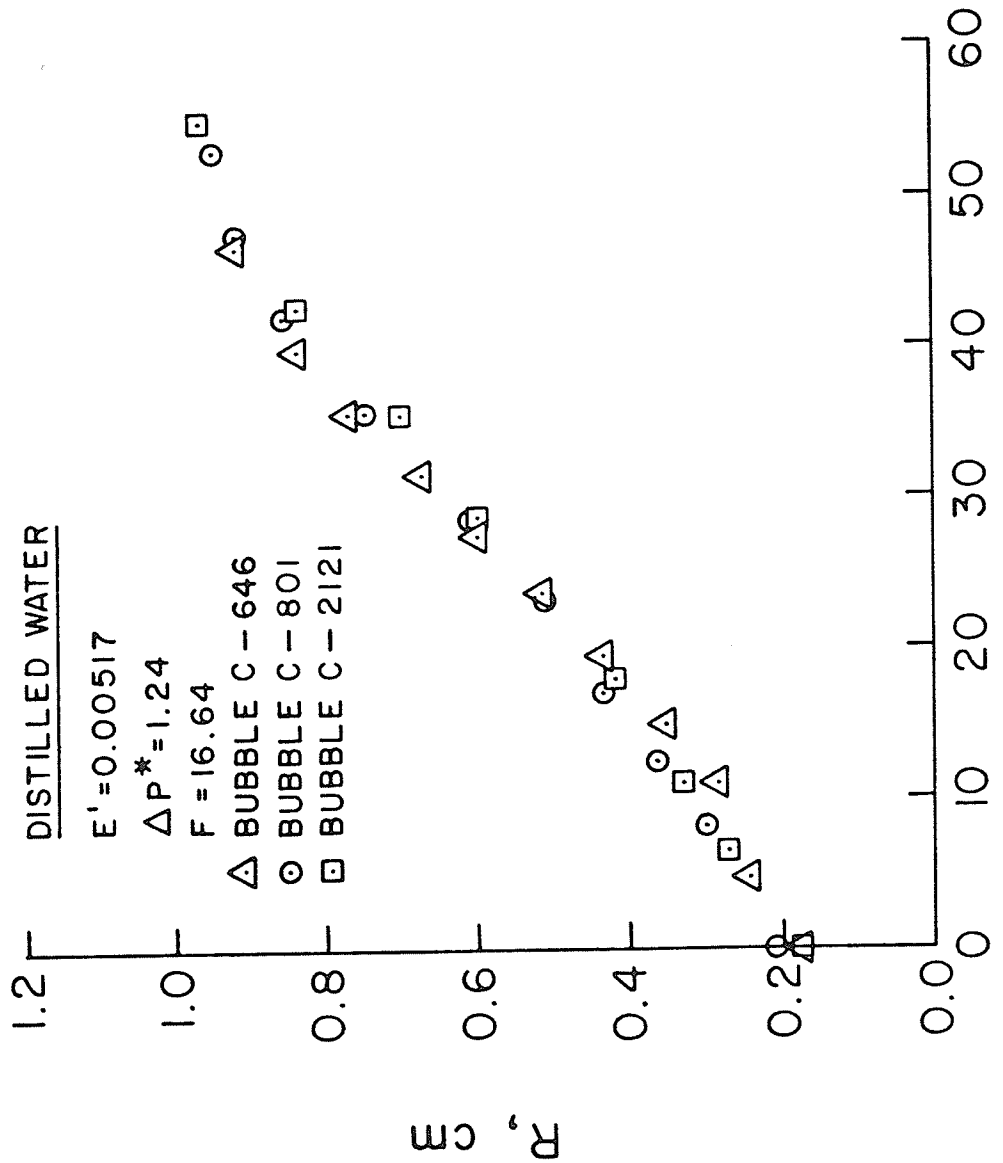

Fig. 6.5 Bubble Growth Data in Distilled Water
($E' = 0.00517$, $\Delta P^* = 1.24$, $F = 16.64$)

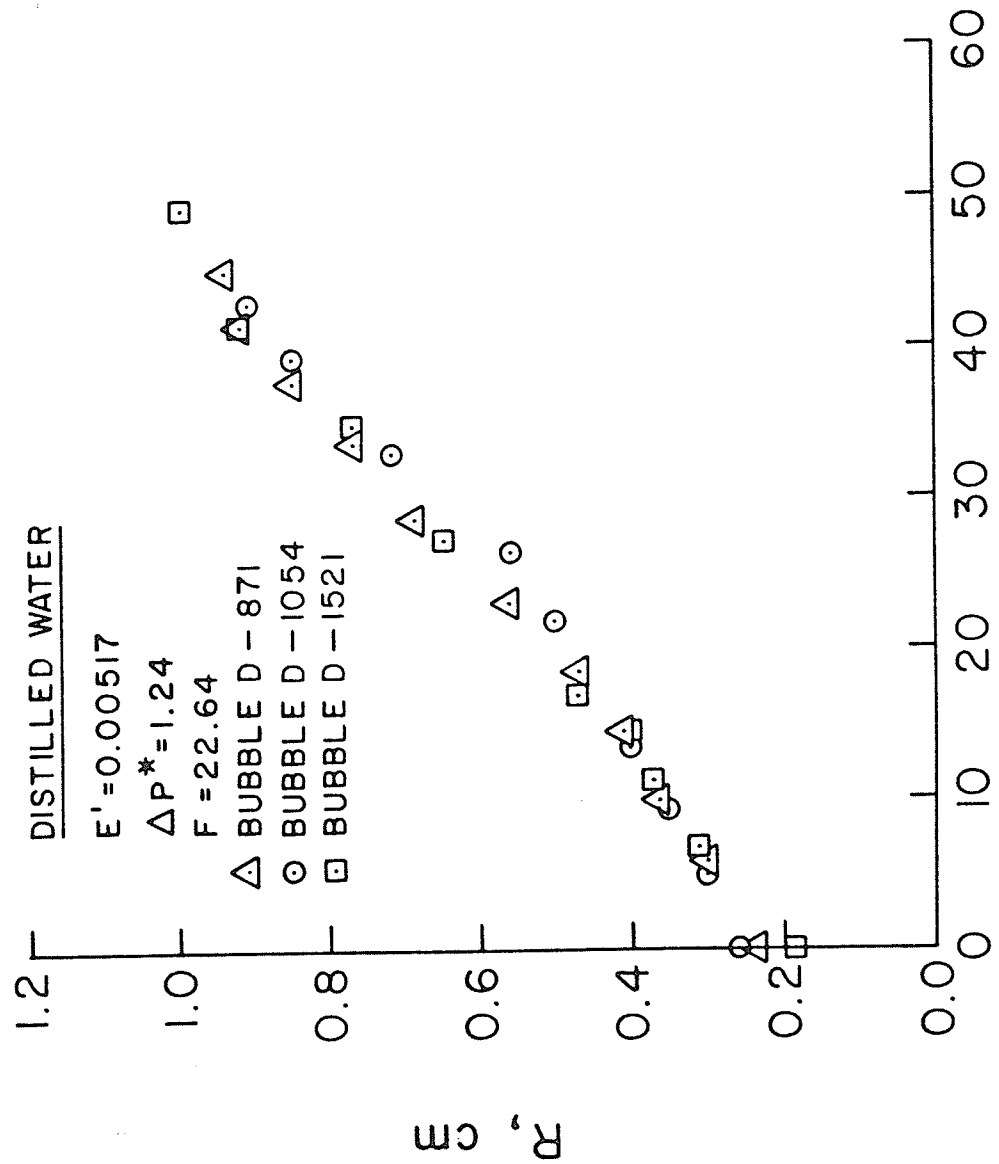

Fig. 6.6 Bubble Growth Data for Distilled Water
(E' = 0.00517, ΔP* = 1.24, F = 22.64)

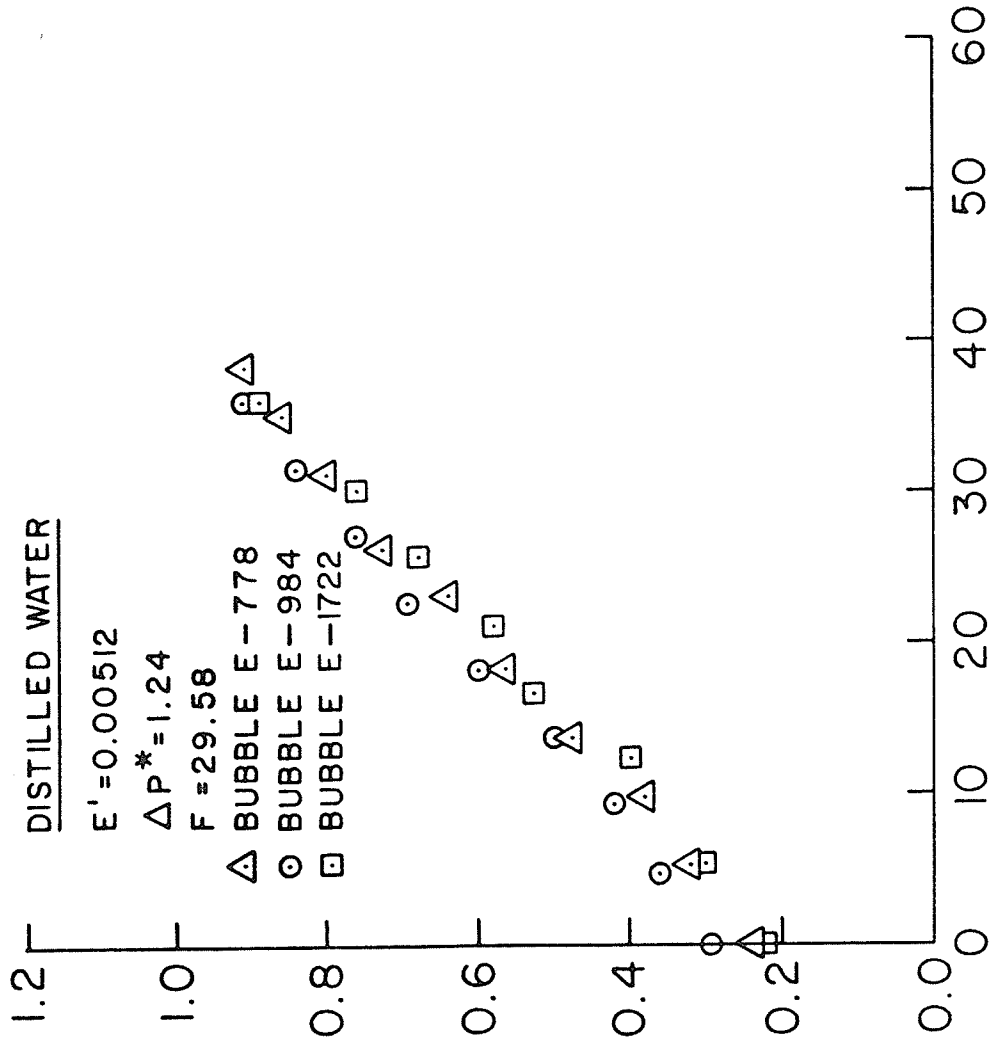

Fig. 6.7 Bubble Growth Data in Distilled Water
(E' = 0.00512, ΔP^* = 1.24, F = 29.58)

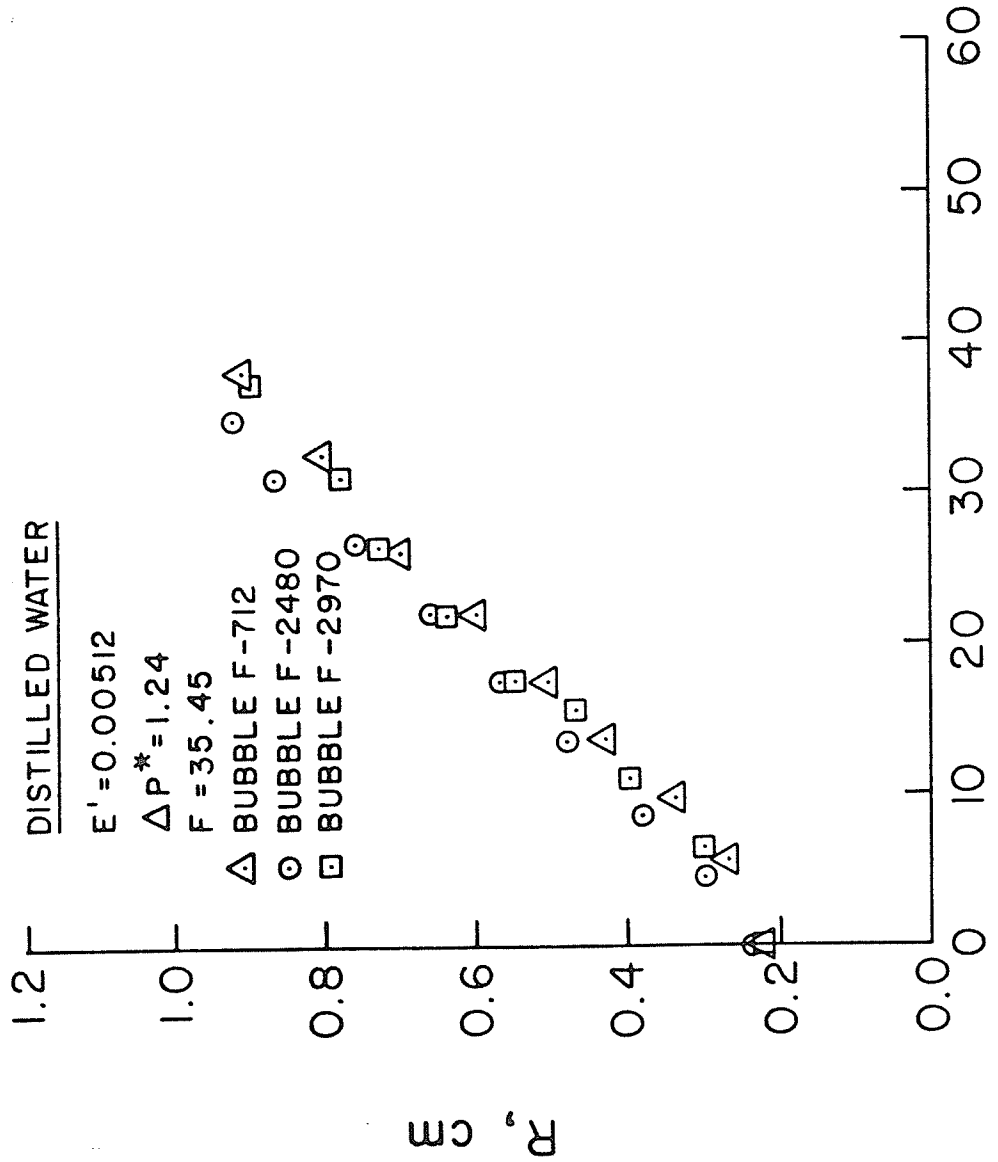

Fig. 6.8 Bubble Growth Data in Distilled Water
(E' = 0.00512, ΔP* = 1.24, F = 35.45)

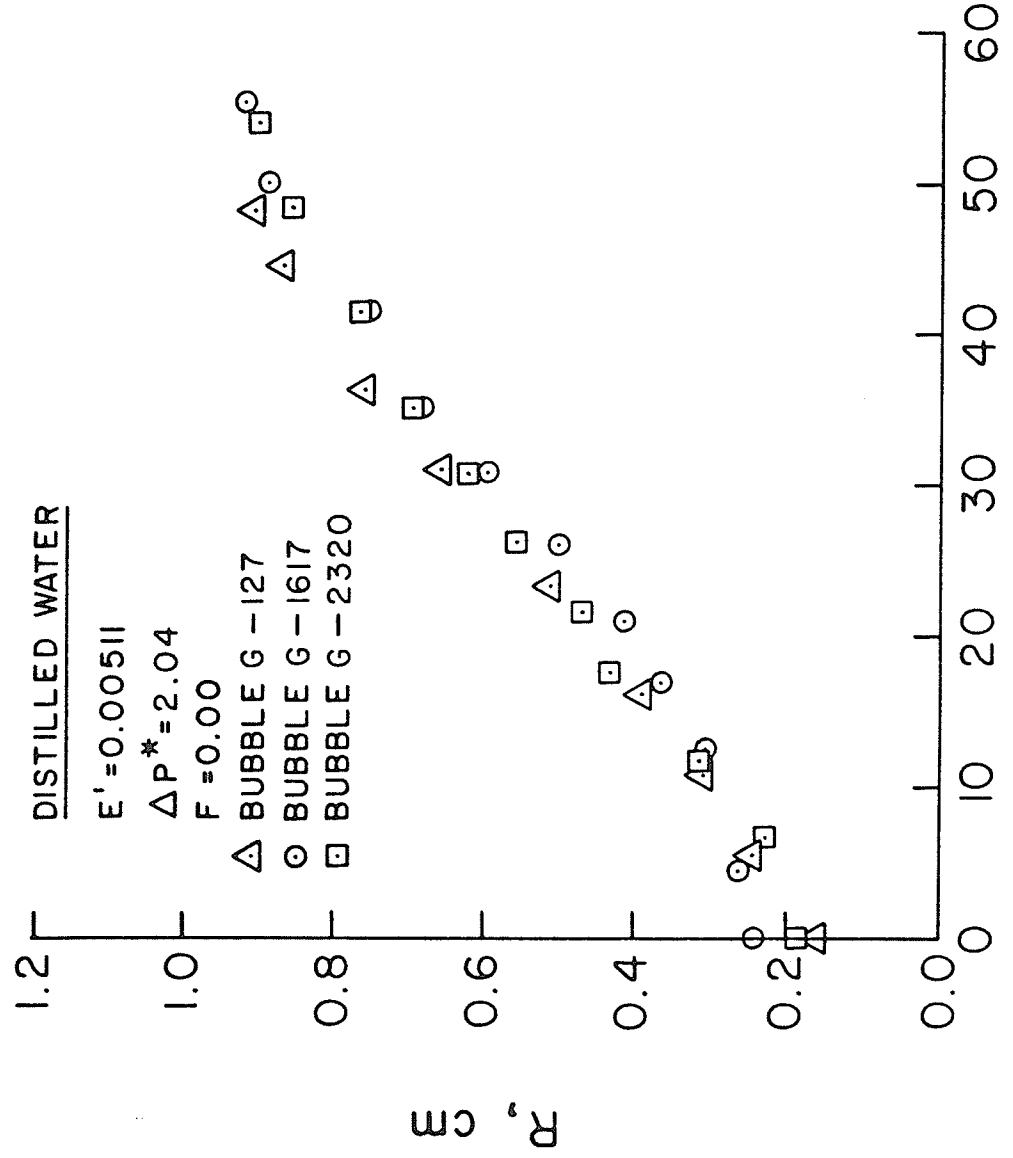

Fig. 6.9 Bubble Growth Data in Distilled Water
(E' = 0.00511, Δp* = 2.04, F = 0.00)

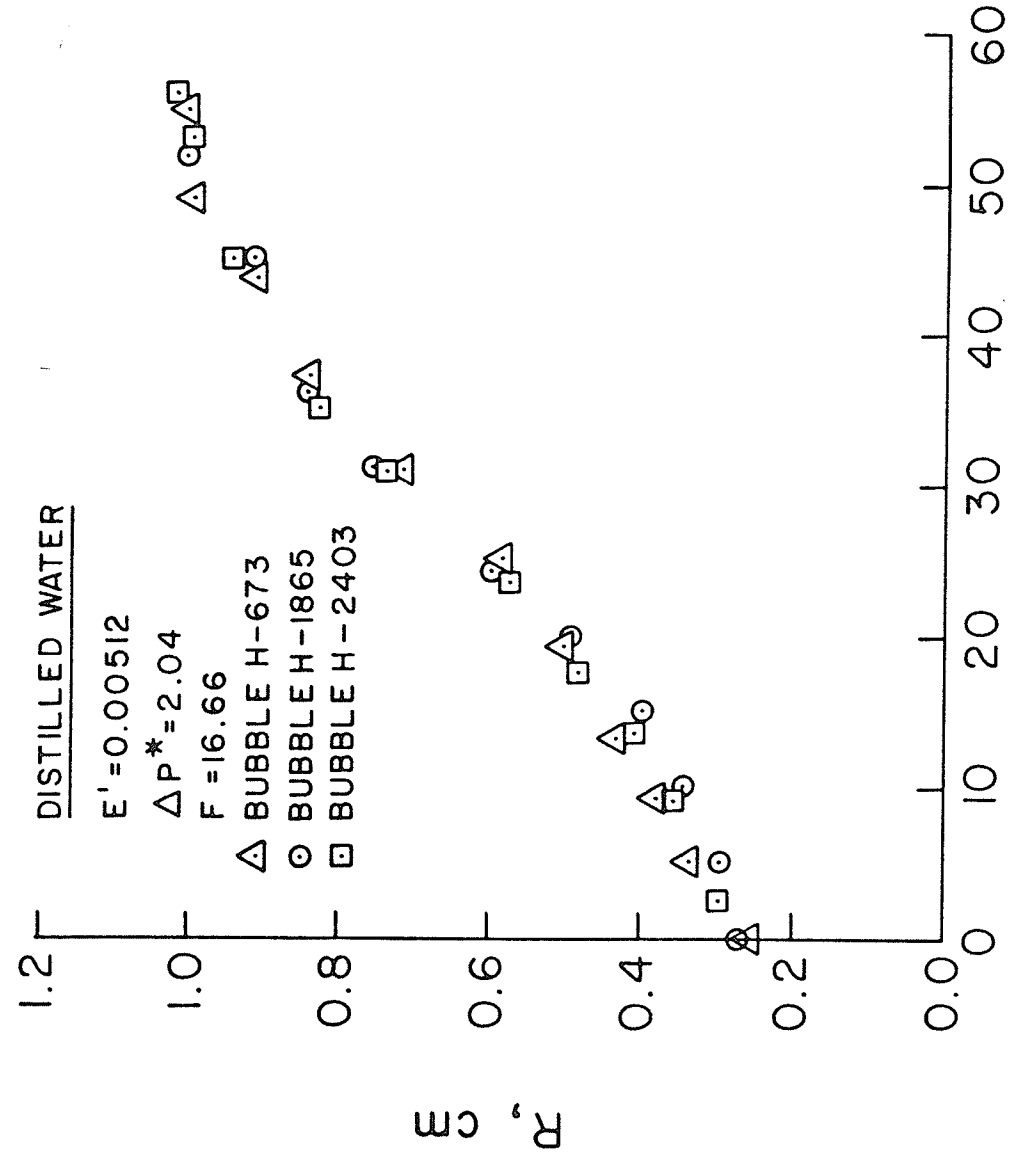

Fig. 6.10 Bubble Growth Data in Distilled Water
(E' = 0.00512, ΔP^* = 2.04, F = 16.66)

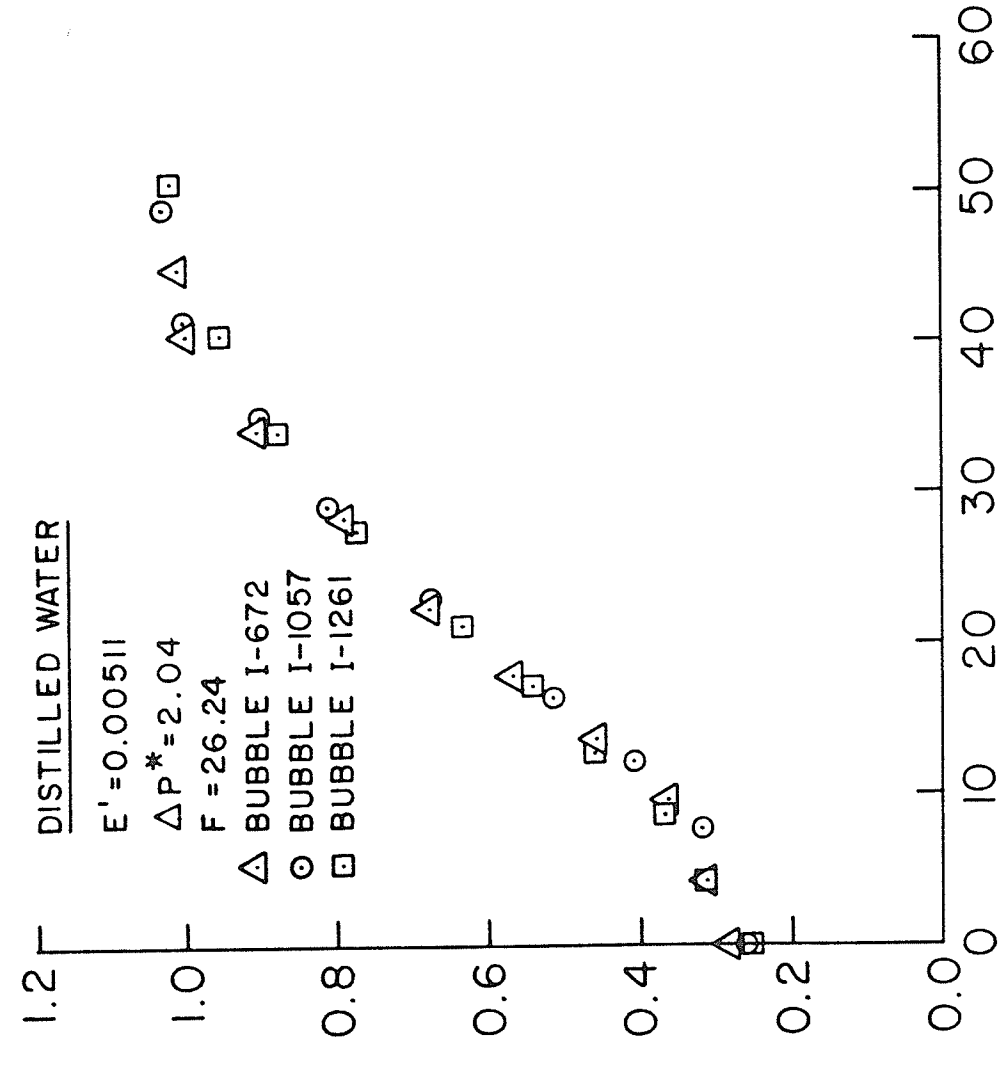

Fig. 6.11 Bubble Growth Data in Distilled Water
(E' = 0.00511, ΔP* = 2.04, F = 26.24)

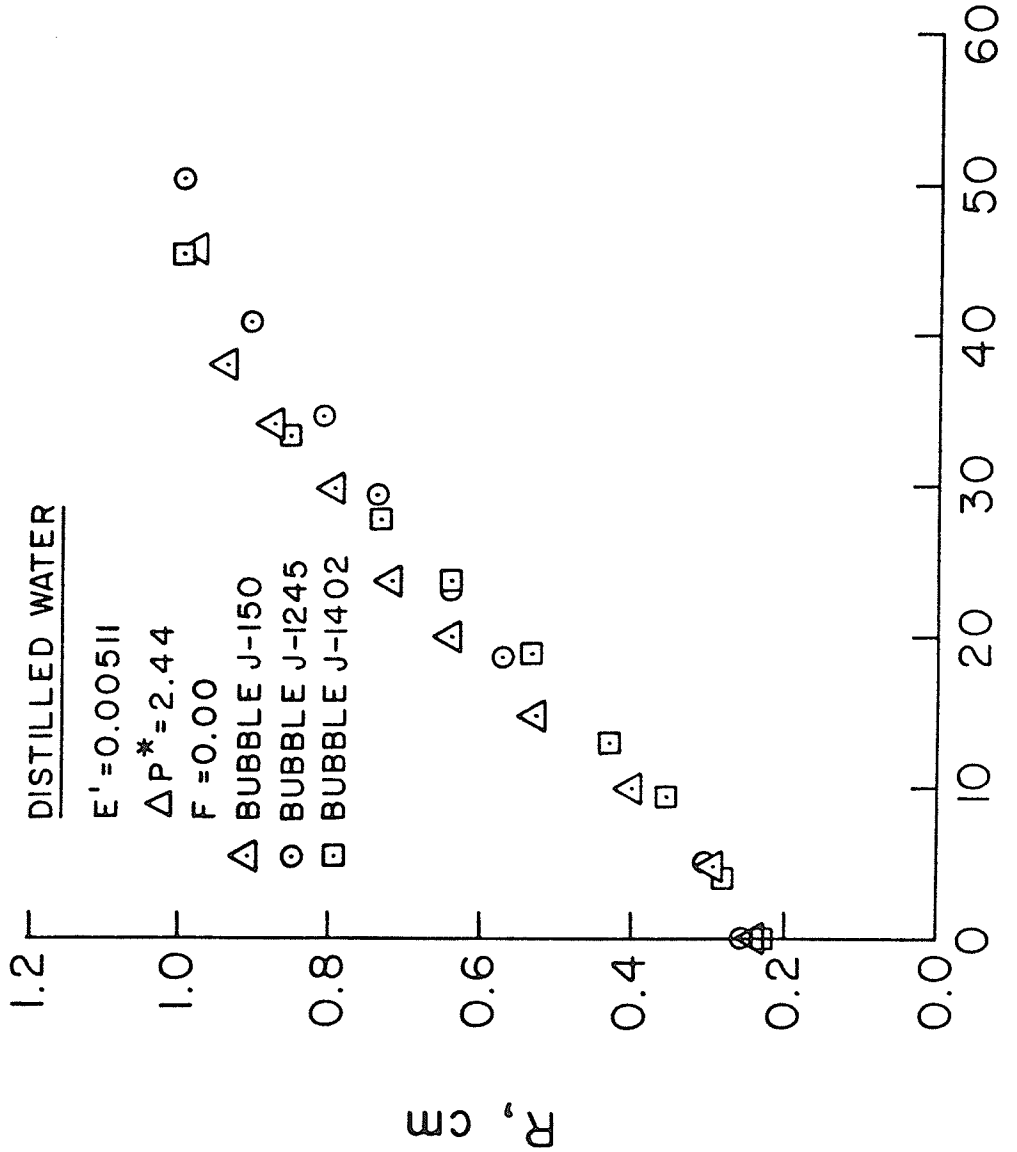

Fig. 6.12 Bubble Growth Data in Distilled Water
(E' = 0.00511, Δp^* = 2.44, F = 0.00)

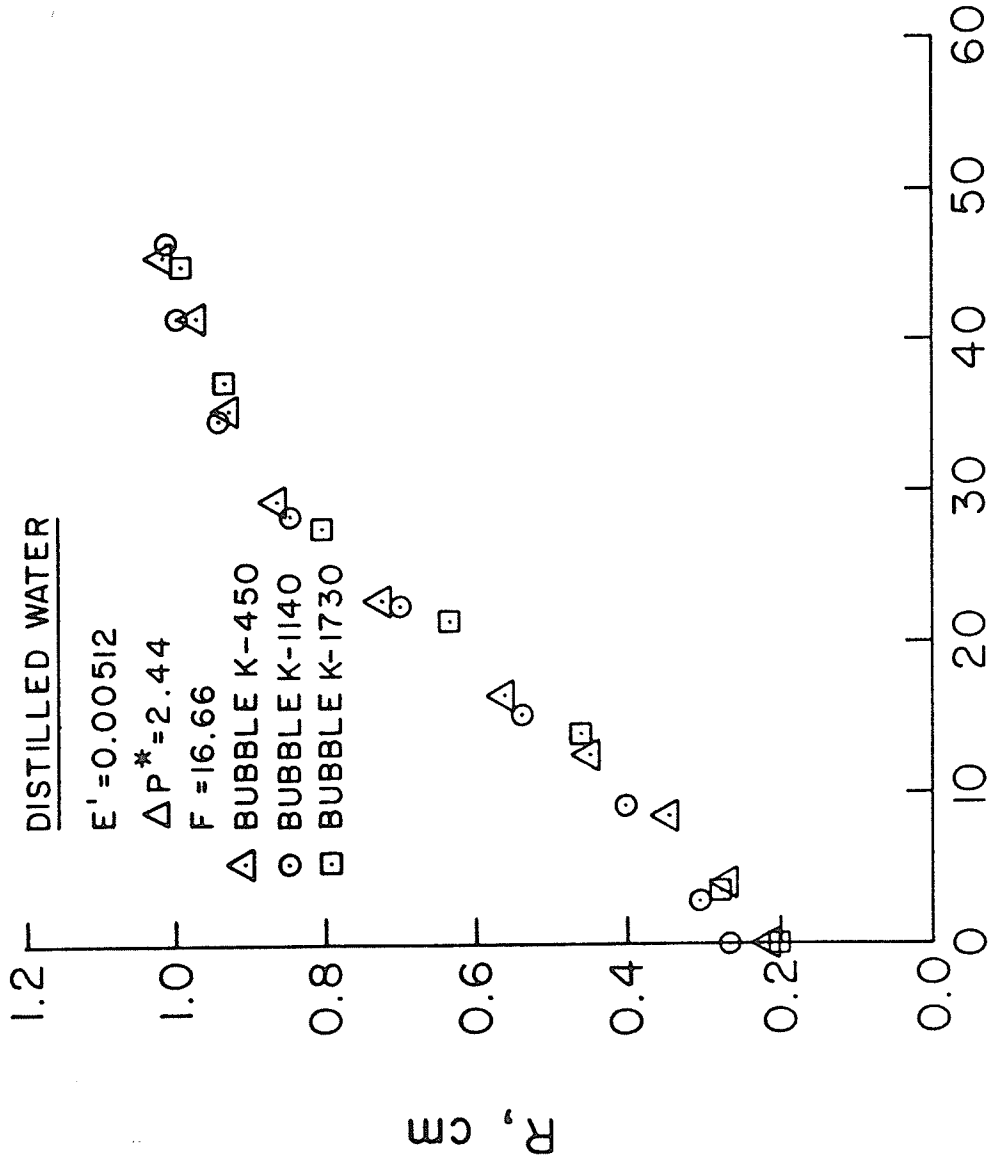

Fig. 6.13 Bubble Growth Data in Distilled Water
(E' = 0.00512, ΔP* = 2.44, F = 16.66)

Comment

As far as the author is aware, this is the first time that barbotage results have been reported with the combined effects of constant pressure and constant flow in parallel and there are, therefore, no results available for direct comparison. It is noted that for the same conditions the three bubbles analyzed fall quite close together; the deviations in the radii among the three bubbles range between zero to a maximum of 0.07 cm, in bubble sizes (radii) ranging from approximately 0.18 - 0.27 cm at zero time to 0.84 - 1.1 cm at maximum radius.

For a given ΔP^* the bubble radius at any time increases with increasing constant-flow rate (or F) in the same fashion as predicted by the theory, in for example, Fig. 5.9. This can be seen by noting the theoretical behaviour (as indicated above) and the agreement between theory and experiment (as discussed below).

6.2.2 Comparison of Experimental and Theoretical Bubble Growth

Figures 6.14 through 6.24 show the present experimental work with corresponding theoretical curves obtained from Eqn. 5.8 in Chapter 5. The parametric conditions corresponding to the curves are given in Table 6.2.

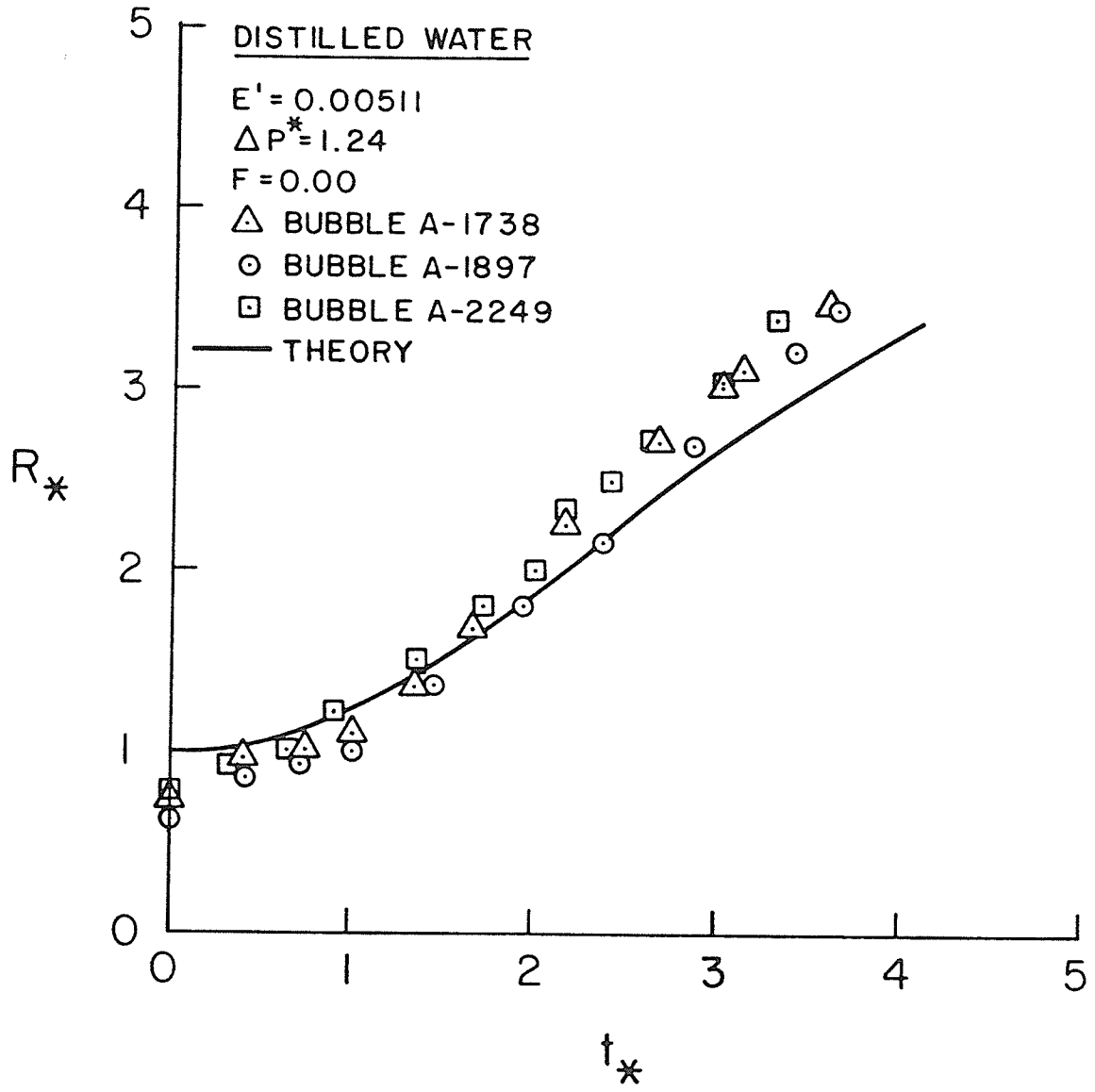

Fig. 6.14 Comparison of Experimental Results and Theoretical Bubble Growth Curve for Distilled Water
($E' = 0.00511$, $\Delta P^* = 1.24$, $F = 0.00$)

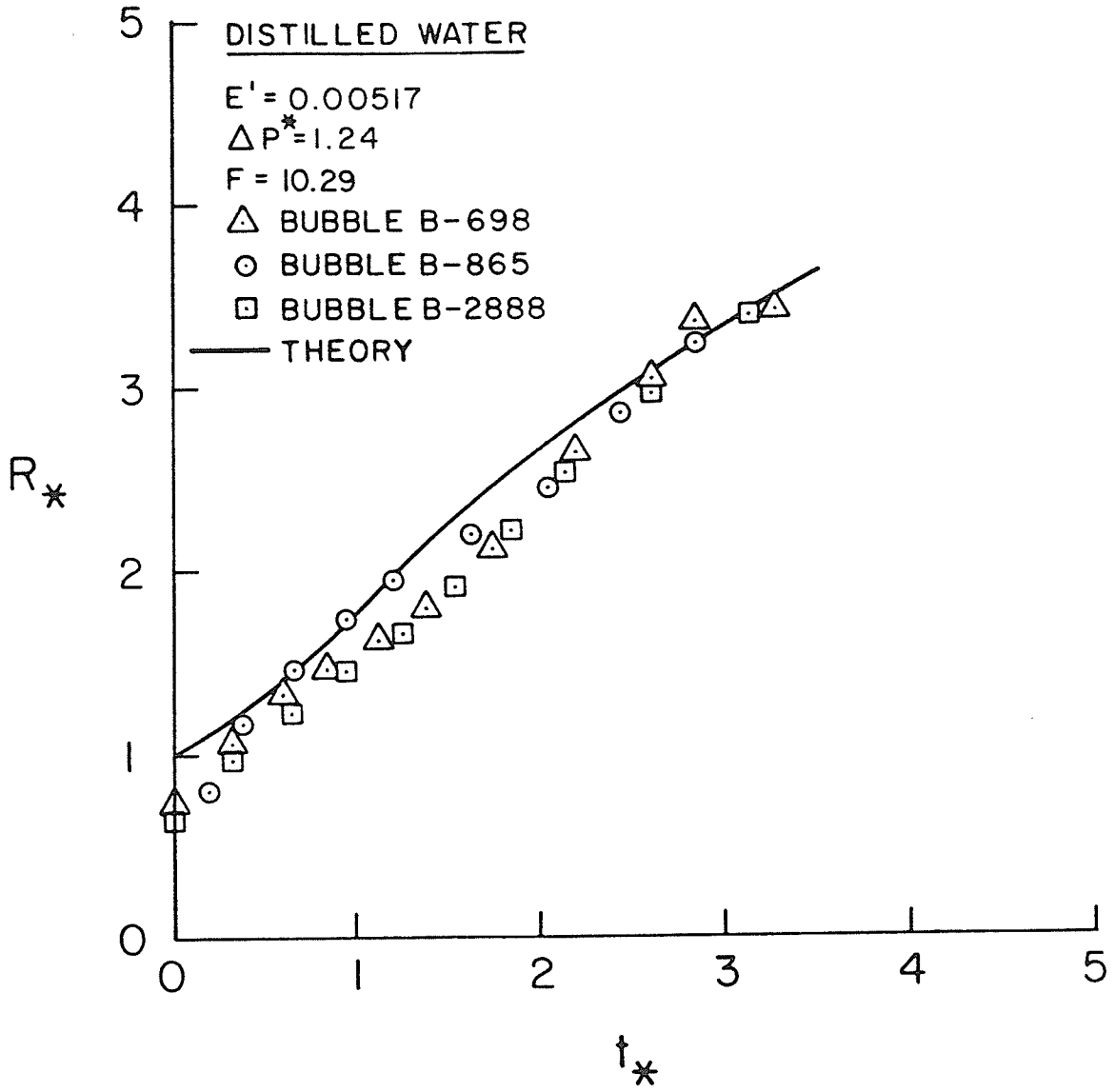

Fig. 6.15 Comparison of Experimental Results and Theoretical Bubble Growth Curve for Distilled Water
(E' = 0.00517, ΔP^* = 1.24, F = 10.29)

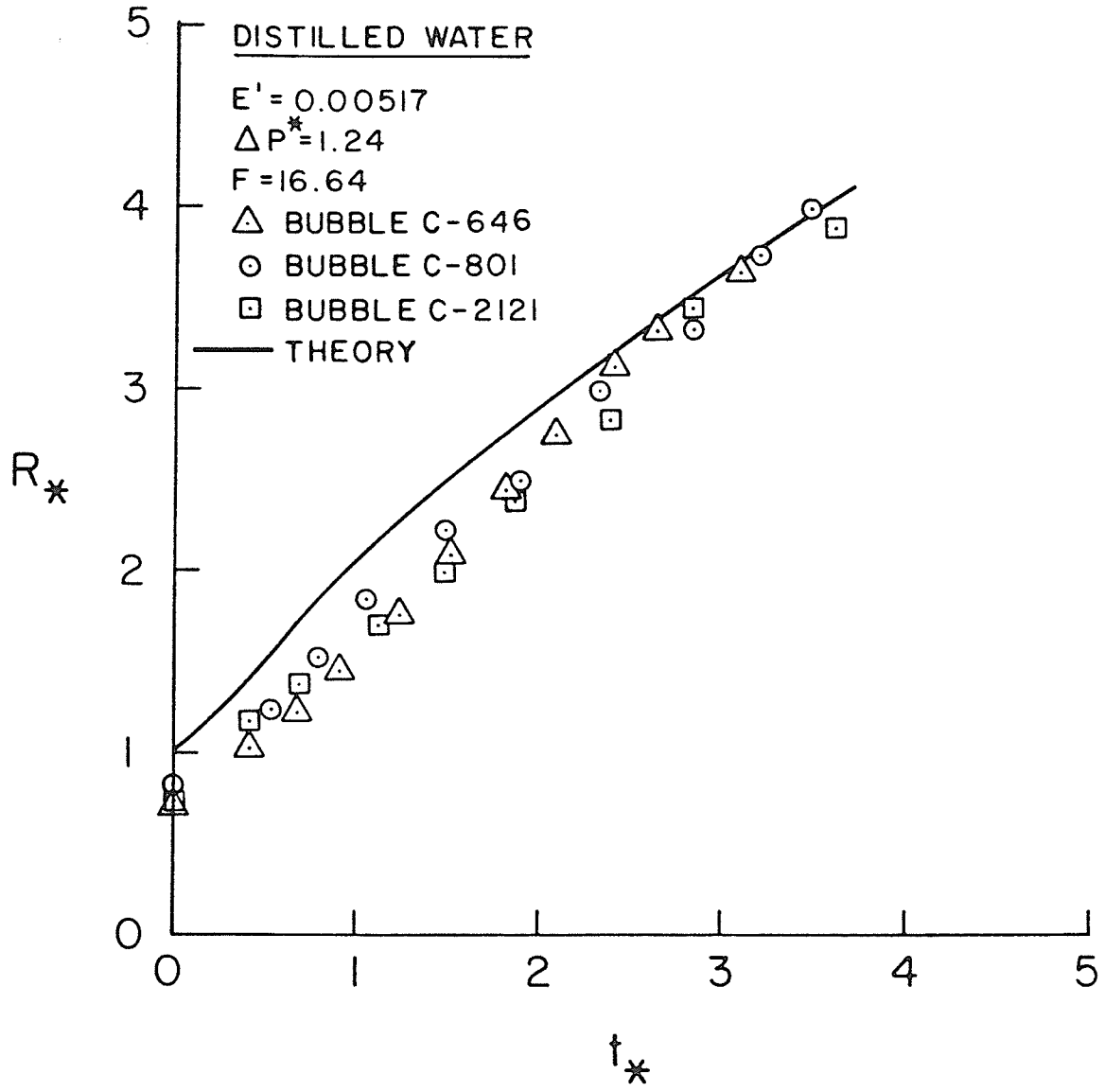

Fig. 6.16 Comparison of Experimental Results and Theoretical Bubble Growth Curve for Distilled Water
(E' = 0.00517, Δ P* = 1.24, F = 16.64)

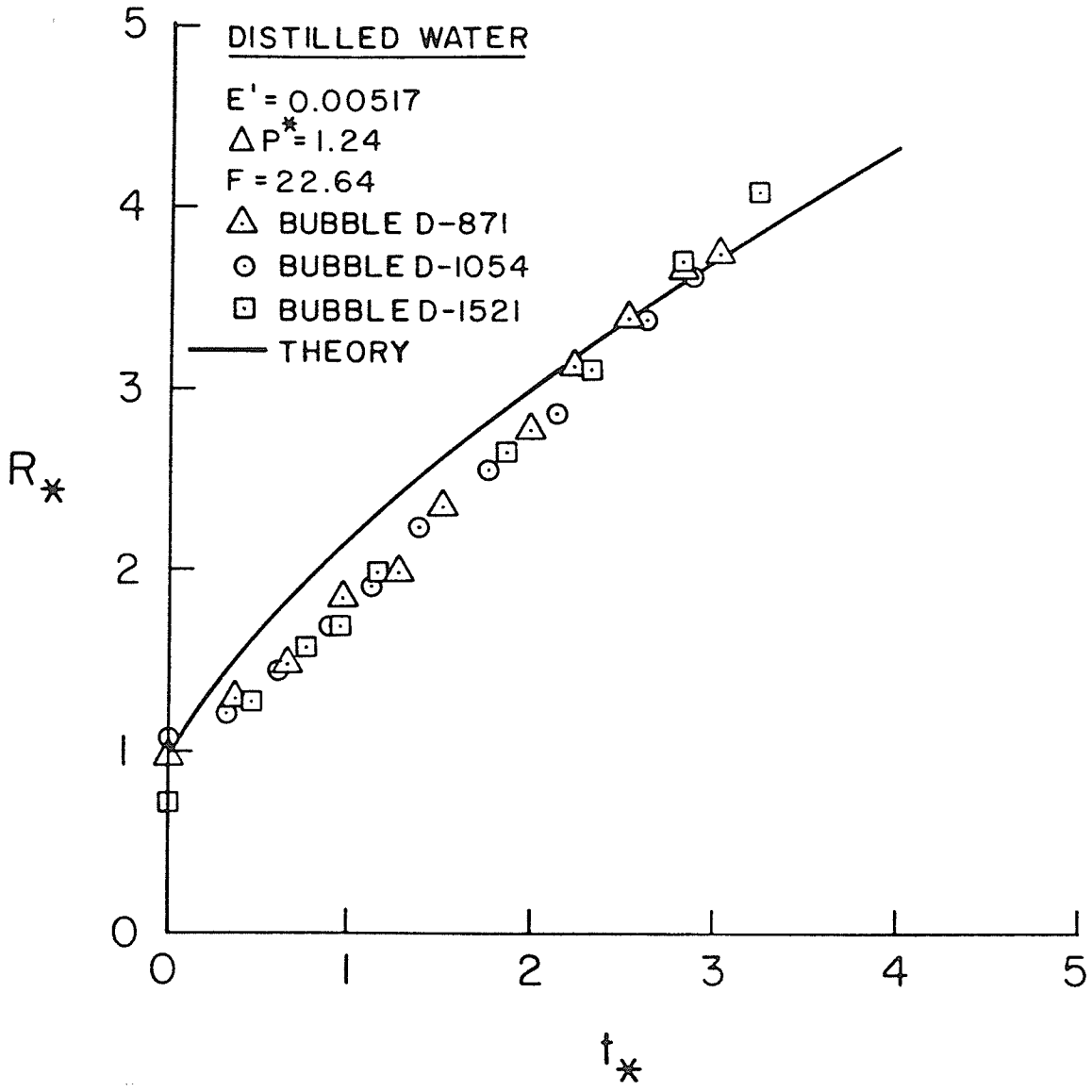

Fig. 6.17 Comparison of Experimental Results and Theoretical Bubble Growth Curve for Distilled Water
(E' = 0.00517, ΔP* = 1.24, F = 22.64)

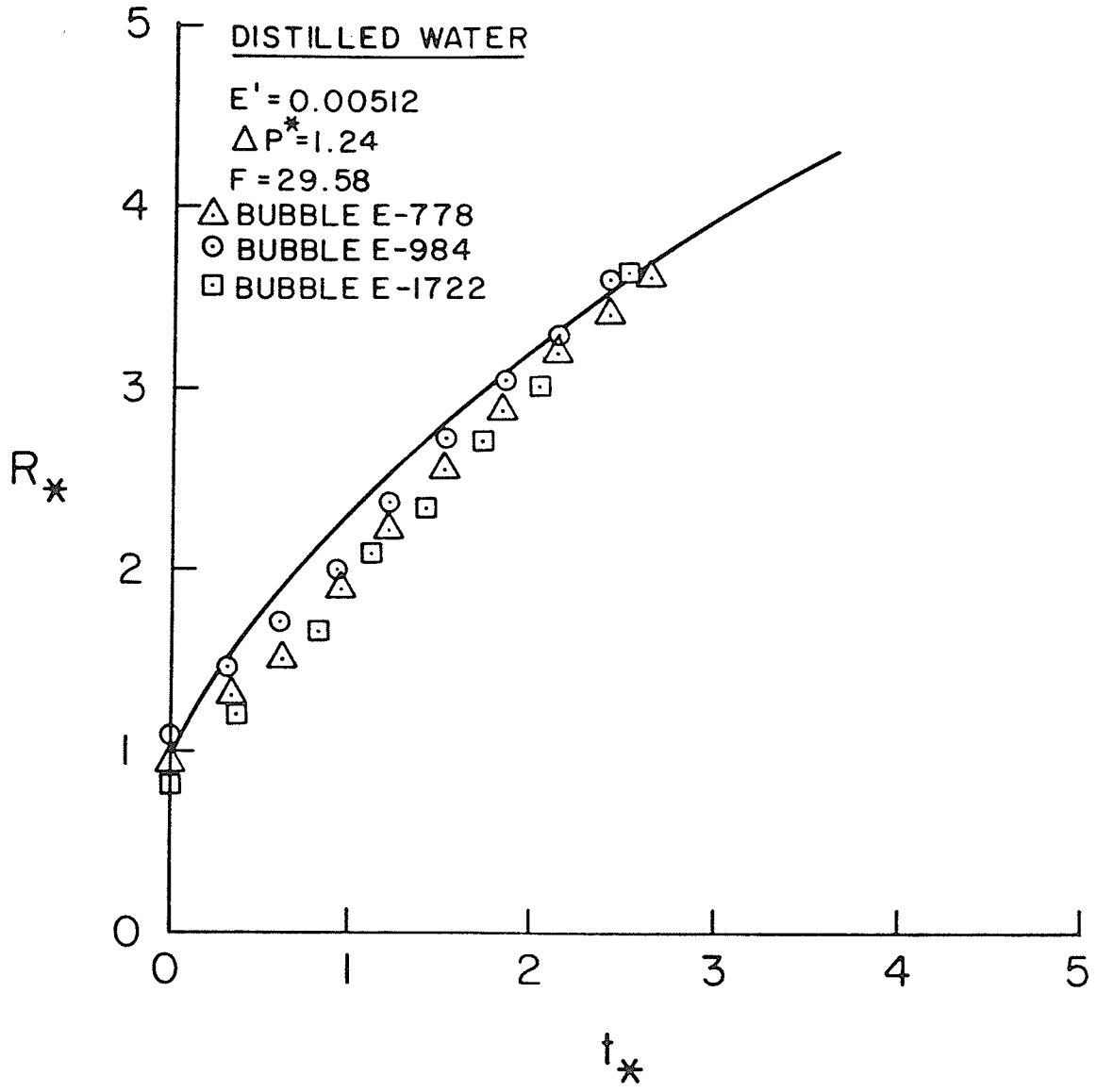

Fig. 6.18 Comparison of Experimental Results and Theoretical Bubble Growth Curve for Distilled Water
(E' = 0.00512, ΔP* = 1.24, F = 29.58)

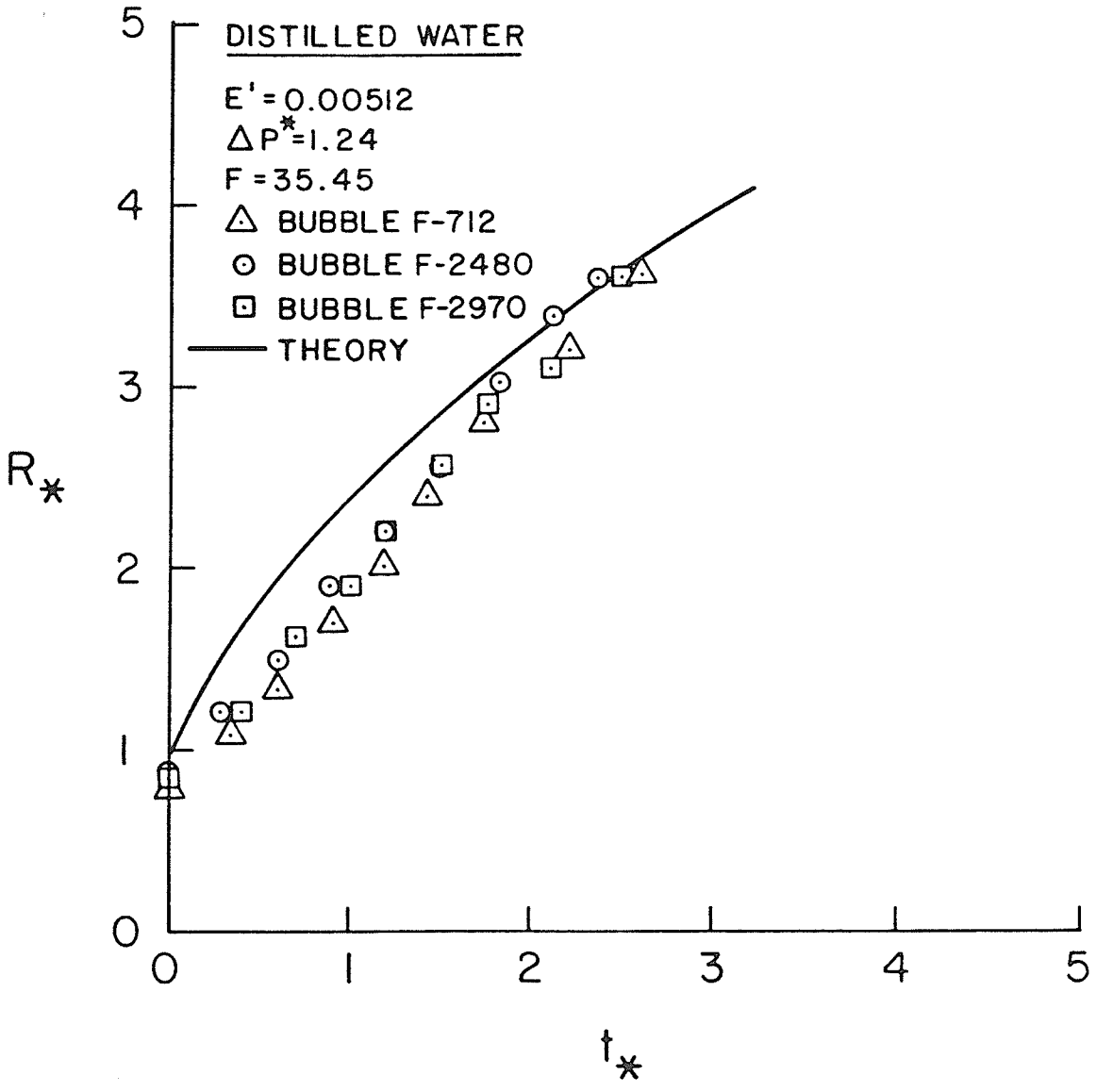

Fig. 6.19 Comparison of Experimental Results and Theoretical Bubble Growth Curve for Distilled Water
(E' = 0.00512, ΔP* = 1.24, F = 35.45)

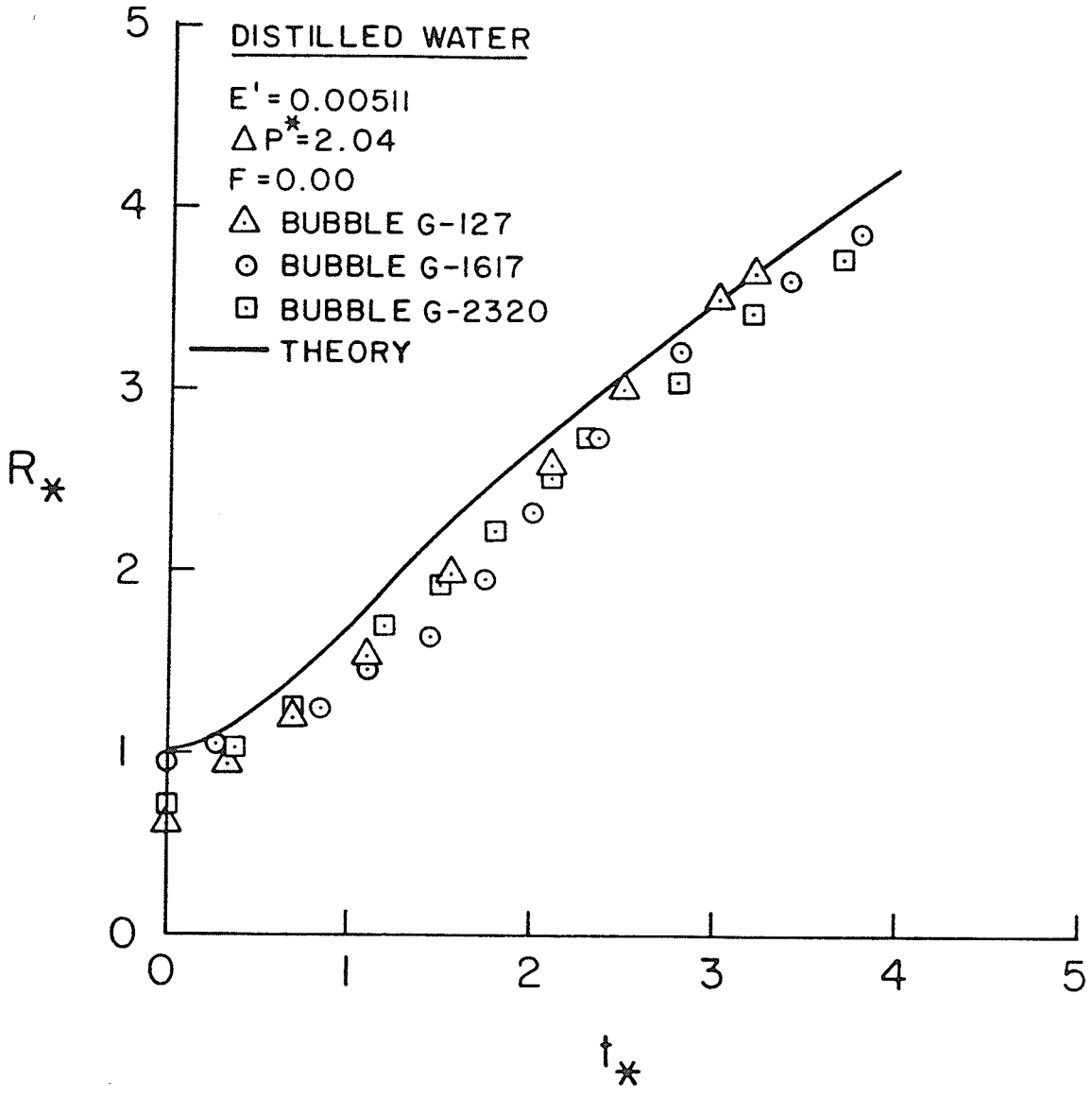

Fig. 6.20 Comparison of Experimental Results and Theoretical Bubble Growth Curve for Distilled Water
(E' = 0.00511, ΔP* = 2.04, F = 0.00)

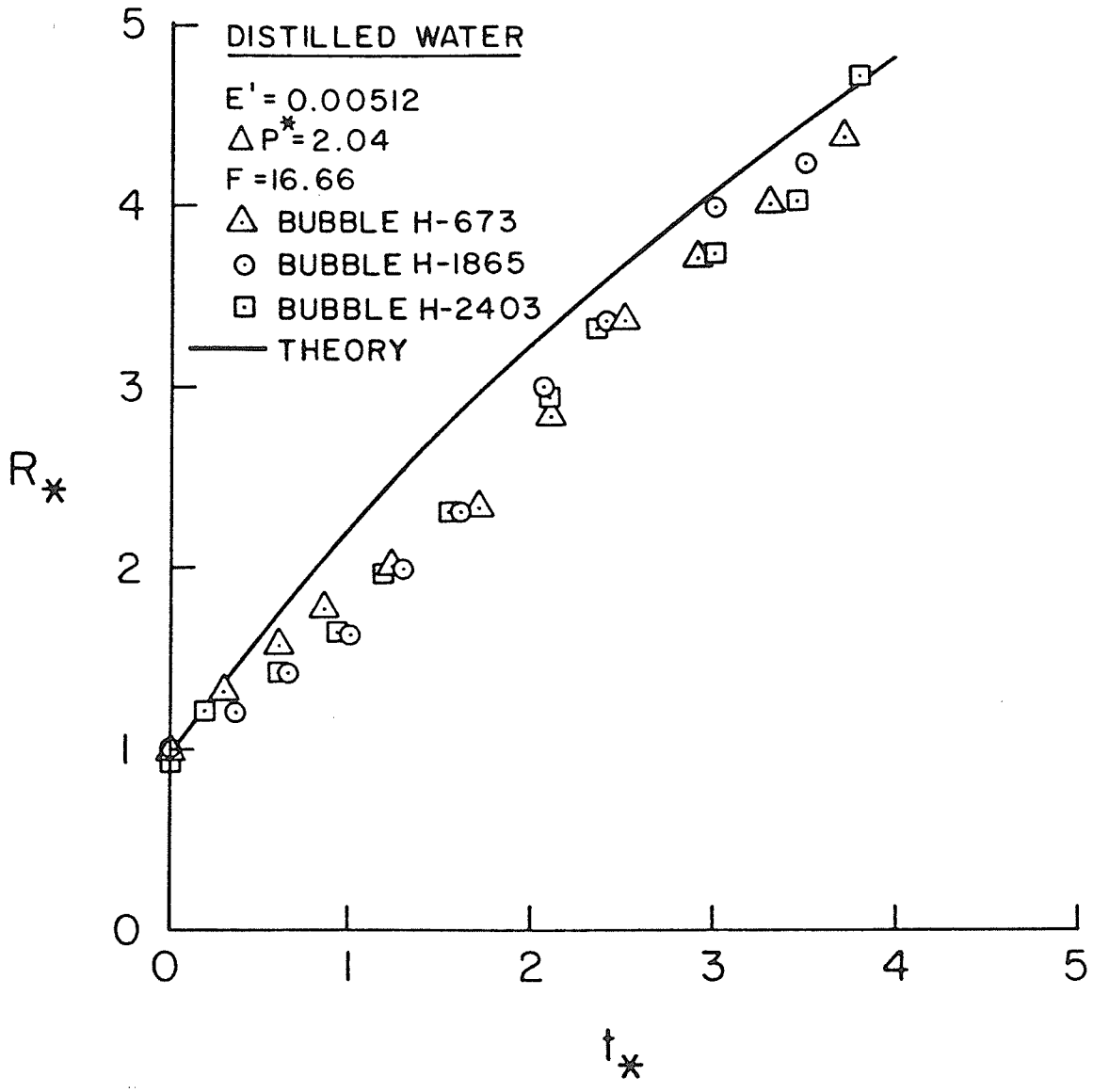

Fig. 6.21 Comparison of Experimental Results and Theoretical Bubble Growth Curve for Distilled Water
(E' = 0.00512, ΔP* = 2.04, F = 16.66)

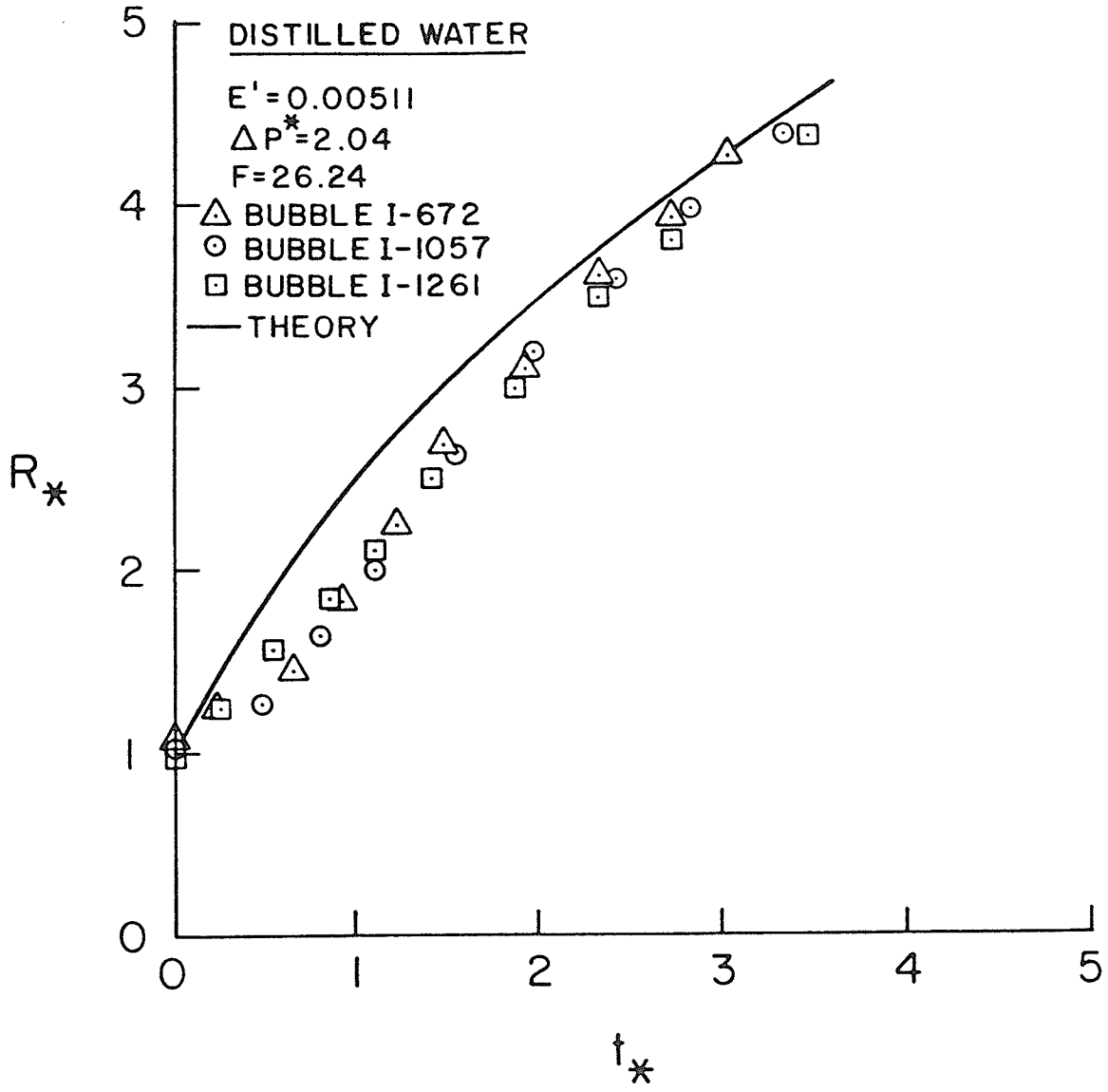

Fig. 6.22 Comparison of Experimental Results and Theoretical Bubble Growth Curve for Distilled Water
(E' = 0.00511, Δ P* = 2.04, F = 26.24)

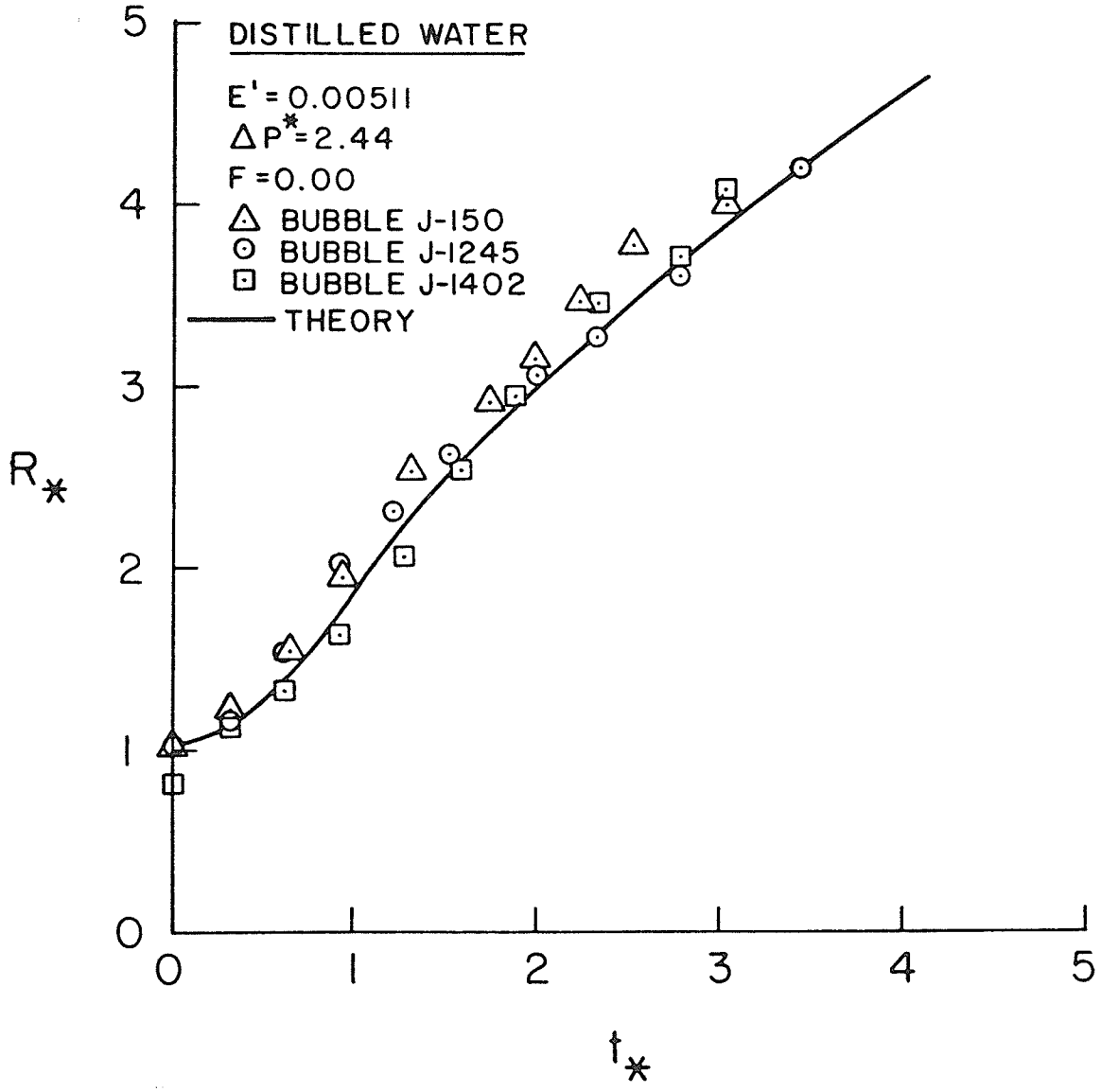

Fig. 6.23 Comparison of Experimental Results and Theoretical Bubble Growth Curve for Distilled Water
(E' = 0.00511, ΔP* = 2.44, F = 0.00)

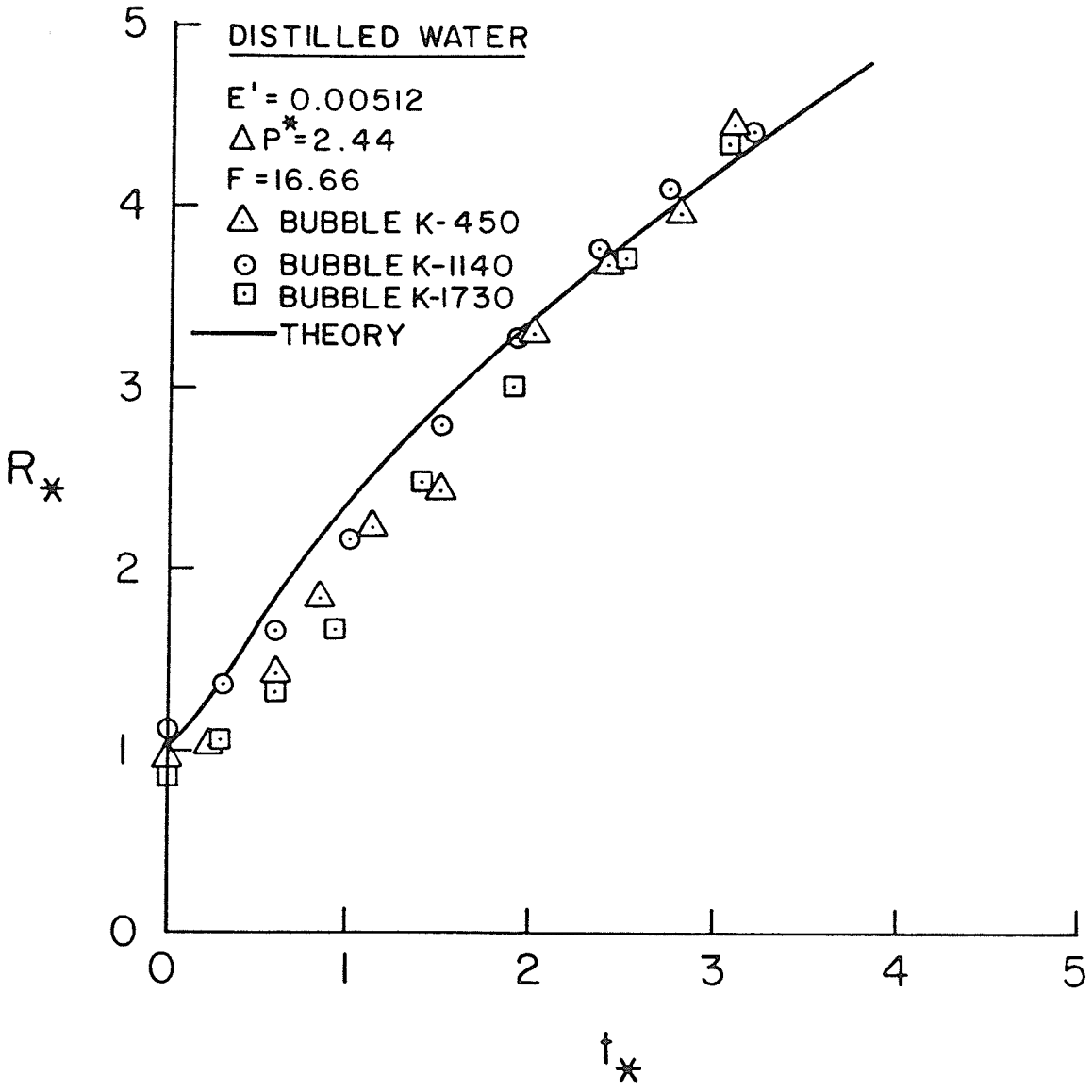

Fig. 6.24 Comparison of Experimental Results and Theoretical Bubble Growth Curve for Distilled Water
(E' = 0.00512, ΔP^* = 2.44, F = 16.66)

K value

The dimensionless parameter E' [$\equiv \frac{\pi^2}{A_a^2} \frac{R_o^4}{K^2} \frac{1}{\rho_l} \frac{\rho_g}{}$] has to be determined in order to compare with the theoretical results. Since the liquid-gas combination and the geometry of the apparatus had been chosen, the only concern is the value of K of the annular orifice. Appendix A outlines the procedure to determine the K value. With some variation within the range, a good representative value would be 0.69. This value is used to calculate the E' value in the experiments.

Comments

It is seen that the agreement between theory and experiment can be considered as good, especially for this rather simple theory. As a quantitative measure, the following can be done. One can draw by eye a best-fit single line to represent the experimental data (a single line for the three bubbles at the same conditions); the deviations between this line and the theoretical curve range on any figure from typically zero to some maximum deviation where this maximum (approximate) is given below.

Film No.	Maximum Deviation
A	25%
B	30%
C	25%
D	17%
E	15%
F	24%
G	25%
H	18%
I	23%
J	5%
K	18%

The deviation is defined as

$$\frac{R_{*exp} - R_{*theor}}{R_{*theor}} \times 100\%$$

where R_{*exp} and R_{*theor} are the experimental and theoretical dimensionless radii respectively at the same t_*.

In general it will be noted that where deviations exist there is a tendency for overprediction. In general too (but not exclusively) there is better agreement near maximum radii. Predictions at $t_* = 0$ will require more work.

Some of the reasons for the deviations between theory

and experiment might be as follows. The shape of the bubbles is not truly spherical as assumed in the theory. The theory does not take into account the effect of the preceding bubble, and the geometry of the orifice plate and pool containment. The accuracy of placement of the centre tubing might affect the results to some extent.

6.3 Discussion of Time Exponent of Present Barbotage

It was indicated in Sec. 2.2 that in the classic boiling theories and much experimental boiling data, the radius varies as the square root of time (other time exponents appear as well). To determine the time exponent in their constant-pressure barbotage experiments Subash and Sim [48] recast their results in the form of the equations

$$R = at^n \tag{6.1}$$

or

$$\overline{R} = \theta^n \tag{6.2}$$

where

$\overline{R} = R/R_d$,

$\theta = t/t_d$,

a = a constant ,

R_d = departure radius ,

t_d = departure time .

They found that n varied from 0.6 to 1.1 for the average of three bubbles for the same conditions. Cheung [7], using constant-flow barbotage, had bubble radii varying as the cube root of time (i.e., $R \propto t^{1/3}$).

It was thought that more control over the exponent might be gained by using constant-flow and constant-pressure conditions in parallel, as in the present case, with the possibility of obtaining an exponent close to $\frac{1}{2}$. As a measure of the possibility, the experimental results of the present work were recalculated in the form of Eqn. 6.1 using the least-squares method to obtain a value of n for each bubble. The values of n were calculated in two ways. The first one (n_1) included all R vs. t data points except the first point at time equal to zero. The second one (n_2) used the last three-quarters of R vs. t data points for each bubble. The exponent n_1 gives a measure of the mean exponent over the life of the bubble while the other (n_2) is based on bubble life excluding times near zero (the three-quarters was chosen arbitrarily). Both n values are presented in Table 6.3. The n_1 value (average of three bubbles for the same conditions) varies from 0.52 to 0.66 while n_2 value (average of three bubbles for the same conditions) varies from 0.61 to 0.96. Generally, the higher values of n_1 are associated with the pure constant-pressure case (F = 0) while finite values of F tend to reduce n_1 (the exception to this is $\Delta P^* = 2.44$, where only

Film Identification	ΔP*	F	n_1		n_2	
			Range	Average	Range	Average
A	1.24	0.00	0.59-0.70	0.66	0.83-0.99	0.96
B		10.29	0.58-0.64	0.61	0.68-0.88	0.77
C		16.64	0.50-0.59	0.54	0.55-0.75	0.67
D		22.64	0.51-0.63	0.57	0.72-0.76	0.74
E		29.58	0.46-0.59	0.53	0.63-0.72	0.66
F		35.45	0.56-0.64	0.61	0.69-0.74	0.70
G	2.04	0.00	0.57-0.63	0.60	0.69-0.84	0.77
H		16.66	0.46-0.60	0.52	0.70-0.78	0.74
I		26.20	0.51-0.55	0.53	0.64-0.73	0.69
J	2.44	0.00	0.49-0.57	0.53	0.54-0.75	0.61
K		16.66	0.54-0.64	0.61	0.67-0.80	0.71

Table 6.3 Growth Exponents for Barbotage Bubble, Obtained in Present Work

one finite F is available). It is seen that at least some of the n_1 values approach $\frac{1}{2}$.

An apparatus of the present type does appear to give additional scope in obtaining some control over the time exponent. Particularly, a simple theory is available for predicting bubble radius against time, which could be very useful.

CHAPTER 7

CONCLUSIONS AND SUGGESTIONS FOR FURTHER RESEARCH

The present work is summarized below, the important conclusions reiterated, and suggestions for further work are made.

(1) Barbotage experiments with the combined effects of constant-flow and constant-pressure conditons were devised and reported for the first time. High-speed photography was employed to record the sequence of bubble formation for distilled water with air as the injected gas under a wide range of ante-chamber pressures and constant-flow rates. The volume of a bubble at any instant during formation was determined frame-by-frame using a motion analyser and the calculation method of L'Ecuyer and Murthy [29].

(2) A simple theoretical analysis of the problem of bubble growth under the combined effects of constant flow and constant pressure was performed; key relations were the Rayleigh equation and orifice equation.

(3) The theoretically predicted bubble growth curves were generally found to be in good agreement with the experimental data.

(4) An apparatus of the present type does appear to give additional scope in obtaining some control over the time

exponent.

(5) Judging from the present study, one can make suggestions about future research.

(a) The present work indicates there are three parameters which can be controlled by the investigator, namely, E', ΔP^* and F. Further investigations can be easily generated by changing the orifice size (orifice plate hole diameter and tubing size), liquid and gas under investigation (E') and controlling ante-chamber pressure (ΔP^*) and constant-flow rate (F).

(b) One should re-examine the initial conditions and shape of the bubble during the early stages of growth, where it is known that there are considerable deviations from the assumed spherical shape. It is expected that the work of L'Ecuyer and Murthy [29] will be helpful here.

REFERENCES AND BIBLIOGRAPHY

1. Akiyama, M., F. Tachibana, and N. Ogawa, Effect of pressure on bubble growth in pool boiling, J.S.M.E. 12, 1121-1128 (1969).

2. Akturk, N.U., Heat transfer from a heated porous surface to a pool of liquid with gas injection at the interface, Proceedings of the Symposium on Two-Phase Flow, Vol. II, Exeter, pp. D501-520 (1965).

3. ASME Power Test Code, Supplement on Instruments and Apparatus Part 5, Chapter 4 - PTC 19,5; - (1959).

4. Barakat, S.A., Flow platterns and heat transfer in pool barbotage, Ph.D. Thesis, University of Manitoba, Winnipeg, Canada (1977).

5. Barakat, S.A. and G.E. Sims, Liquid flow patterns about barbotage bubbles, Int. J. Multiphase Flow 3, 383-397 (1977).

6. Barakat S.A. and G.E. Sims, Heat transfer in pool barbotage, Proceedings of the Sixth International Heat Transfer Conference, Toronto, Canada, Vol. 1, 127-132 (1978).

7. Cheung, M. Bubble dynamics in constant-flow barbotage, M.Sc thesis, University of Manitoba, Canada (1984).

8. Cole, R. and H.L. Shulman, Bubble growth rates at high Jakob numbers, Int. J. Heat Mass Transfer 9, 1377-1390 (1966).

9. Cooper, M.G. and A.J.P. Lloyd, The microlayer in nucleate pool boiling, Int. J. Heat Mass Transfer 12, 895-913 (1969).

10. Datta, R.L., D.H. Napler, and D.M. Hewitt, The properties and behavior of gas bubbles formed at a circular orifice, Trans. Inst. Chem. Engrs. 28, 3 (1950) as reported in Ref. [26].

11. Davidson, L. and E.H. Amick, Formation of gas bubbles at horizontal orifices, A.I.Ch.E.J. 2, 337-342 (1956).

12. Davidson, J.F. and B.O.G. Schüler, Bubble formation at an orifice in a viscous liquid, Trans. Inst. Chem. Engrs. 38, 144-154 (1960).

13. Davidson, J.F. and B.O.G. Schüler, Bubble formation at an orifice in an inviscid liquid, Trans. Inst. Chem. Engrs. 38, 335-341 (1960).

14. Forster, H.K. and N. Zuber, Growth of a vapor bubble in a superheated liquid, J. Appl. Physics, 25, 474-478 (1954) as reported in Refs. [22, 51, 53, 57].

15. Forster, K.E. and R. Greif, Heat transfer to a boiling liquid--Mechanism and correlations, ASME J. of Heat Transfer, 81, 43-53 (1959).

16. Fritz, W. and W. Ende, The vaporization process according to cinematographic pictures of vapor bubbles, Physikalishe Zeitschrift 37, 391-401 (1936) as reported in Refs.[51, 57].

17. Gallant, R.W., PHYSICAL PROPERTIES OF HYDROCARBONS, Vols. 1 and 2, Gulf Publishing Co. (1974).

18. Han, C.Y. and P. Griffith, The mechanism of heat transfer in nucleate boiling - Part I, Int. J. Heat Mass Transfer 8, 887-904 (1965).

19. Hatton, A.P., and I.S. Hall, Photographic study of boiling on prepared surfaces, Proc. 3rd Int. Heat Trans. Conf., Chicago, Vol. IV, pp 24-37 (1966) as reported in Ref. [42].

20. Hospeti, N.B. and R.B. Mesler, Vaporization at the base of bubbles of different shape during nucleate boiling of water, A.I.Ch.E.J. 15, 214-219 (1969).

21. Hsu, Y.Y., On the size range of active nucleation cavities on a heating surface, ASME J.of Heat Transfer, 84, 207-216, (1962).

22. Hsu, Y. and R.W. Graham, TRANSPORT PROCESS IN BOILING TWO-PHASE SYSTEMS, McGraw-Hill (1976).

23. Hughes, R.R., A.E. Handlos, H.D. Evans and R.L. Maycock, The formation of bubbles at simple orifices, Chem. Eng. Prog. 51, 557-563 (1955).

24. Keenan, J.H., F.G. Keyes, P.G. Hill and J.G. Moore, STEAM TABLES, Wiley (1969).

25. Keshock, E.G. and R. Siegel, Effects of reduced gravity on nucleate boiling dynamics in saturated water, A.I.Ch,E.J. 10, 509-516 (1964) as reported in Ref. [48].

26. Kumar, R. and N.R. Kuloor, The formation of bubbles and drops, in ADVANCES IN CHEMICAL ENGINEERING, Vol. 8, pp. 225-368, Academic Press (1970).

27. Kutateladze, S.S. and N.N. Mamontova, The nature of motion of a liquid about a vapour bubble. Heat Transfer - Soviet Research 5, No. 6, 149-153 (1973).

28. Kutateladze, S. and I.G. Malenkov, Heat Transfer in boiling and barbotage, similarity and dissimlarity, Proc. of the Fifth Int. Heat Transfer Conference, Vol. IV, pp. 1-5 Tokyo (1974).

29. L'Ecuyer, M.R. and S.N.B. Murthy, Energy transfer from a liquid to gas bubbles forming at a submerged orifice, NASA Report TND-2547 (1965).

30. Leibson, I., E.G. Holcomb, A.G. Cacoso, and J.J. Jamic, Rate of flow and mechanics of bubble formation from single submerged orifices, A.I.Ch.E.J. 2, 296-300 (1956).

31. McCann, D.J. and R.G.H. Prince, Bubble formation and

weeping at a submerged orifice, Chem. Eng. Sci. 24, 801-814 (1969).

32. Mikic, B.B., W.M. Rohsenow and P. Griffith, On bubble growth rates, Int. J. Heat Mass Transfer 13, 657-666 (1970).

33. Mills, R.D., Numerical solutions of viscous flow through a pipe orifice at low Reynolds numbers, Journal Mechanical Engineering Science, 10, 113-140 (1968).

34. Park, Y., The formation of bubbles from submerged orifices, Ph.D. Thesis, University of Utah (1974) U.S.A.

35. Plesset, M.S. and S.A. Zwick, The growth of vapor bubbles in superheated liquids, J. Appl. Phys. 25, 493-500 (1954).

36. Quigley, C.J., A.I. Johnson and B.L. Harris, Size and mass transfer studies of gas bubbles, Chem. Eng. Prog. Symp. Series 16, 31-45 (1955) as reported in Ref. [26].

37. Rayleigh, L., On the pressure developed in a liquid during the collapse of a spherical cavity, Phil, Mag. 34, 94-98 (1917).

38. Rohsenow W.M., Chapter 8 in DEVELOPMENTS IN HEAT TRANSFER, M.I.T. Press (1964).

39. Rohsenow, W.M. and J.P. Hartnett, Sec. 13, in HANDBOOK OF HEAT TRANSFER, McGraw-Hill (1973).

40. Saddy, M. and G.J. Jameson, Prediction of departure diameter and the bubble frequency in uniformly superheated liquids, Int. J. Heat Mass Transfer 14, 1777-1785 (1971).

41. Satyanarayan, A., R. Kumar and N.R. Kuloor, Studies in bubble formation--II Bubble formation under constant flow conditions, Chem. Eng. Sci. 24, 731-747 (1969).

42. Scriven, L.E., On the dynamics of phase growth, Chem. Eng. Sci. 10, 1-13 (1959).

43. Siemes, W. and J.F. Kauffmann, Die periodishe entstehung von gasblasen an dusen, Chem. Eng. Sci. 5, 127 (1956) as reported in Refs. [26, 34, 54].

44. Silberman, E., Proc. Fifth Midwestern Conference on Fluid Mechanics, Ann Arbor, Michigan, 236 (Apr. 1-2, 1957).

45. Sims, G.E., U. Akturk and K.O. Evans- Lutterodt, Simulation of pool boiling heat transfer by gas injection at the interface, Int. J. Heat Mass Transfer 6, 531-535 (1963).

46. Sims, G.E. and P.L. Duffield, Comparison of heat-transfer coefficients in pool barbotage and saturated pool boiling, Trans. Can. Soc. Mech. Eng. pp. 55-65

(1971). Also Engineering Institute of Canada Trans. 14, No. B-1, published in the Eng. J. 54 (May, 1971).

47. Staniszewski, B.E., Nucleate boiling bubble growth and departure, Report DRS7-7673, Massachusetts Institute of Technology (1959).

48. Subash, N. and G.E. Sims, Bubble dynamics in barbotage and boiling, Dept. of Mech. Eng., Publication No. ER.25.22., University of Manitoba, Winnipeg, Canada (1973).

49. Theofanous, T.G. and P.D. Patel, Universal relations for bubble growth, Int. J. Heat Mass Transfer 19, 425-429 (1976).

50. Timmermans, J., PHYSICO-CHEMICAL CONTENTS OF PURE ORGANIC COMPOUND, Vol. I, Elsevier Publishing Co. Inc. (1950).

51. Tong, T.S., Chapter 2 in BOILING HEAT TRANSFER AND TWO-PHASE FLOW, Wiley (1965).

52. Van Krevelen, D.W. and P.J. Hoftijzer, Studies of gas bubble formation, Chem. Eng. Prog. 46, 29 (1950).

53. Van Stralen, S. and R. Cole, Chapter V in BOILING PHENOMENA, Vol. 1, McGraw-Hill (1979).

54. Wallis, G.B., The analogy between the bubbling of air into water and nucleate boiling at saturation temperature, U.K. Atomic Energy Authority Report

AEEW-R28 (1960).

55. Wallis, G.B., Two-phase flow aspects of pool boiling from a horizontal surface, U.K. Atomic Energy Authority Report AEEW-R103 (1961).

56. Weast, R.C., CRC HANDBOOK OF CHEMISTRY AND PHYSICS, 62nd Edition, CRC Press (1981-1982).

57. Westwater J.W., P.H. Streng and Aluf Orell, Microscopic study of bubble growth during nucleate boiling, A.I.Ch.E.J. 7, 578-583 (1961).

58. Westwater, J.W., Boiling of liquids, Part I, in ADVANCES IN CHEMICAL ENGINEERING, Vol. I, T.B. Drew(Ed.), Academic Press (1956).

59. Yamagata, K., F. Hirano, K. Nishikawa and H. Matsuoka, Nucleate boiling of water on the horizontal heating surface, Memoirs of Faculty of Eng., Kyushu Univ. 15, No. 1, 97-163 (1955).

60. Zuber, N., Hydrodynamic aspects of boiling heat transfer (Thesis), U.S. Atomic Energy Commission Report AECU-4439 (1959).

APPENDIX A

DETERMINATION OF FLOW COEFFICIENT OF AN ANNULAR ORIFICE

The flow coefficient of the present annular orifice was determined. The schematic arrangement of the apparatus is given in Fig. A.1. Before starting the experiment, any joints in the air line and the ante-chamber were checked to make sure there was no air leakage. The compressed air passing through the pressure regulator valve was reduced in pressure to the operating conditions. The air then passed through a filter, gas dryer and rotameter. Finally, the air entered the ante-chamber and was discharged to atmosphere through the annular orifice. The pressure inside the ante-chamber was measured by an E.M.T. manometer (Betz-type, discrimination to approximately 0.05 mm H_2O) with the low-pressure side open to the atmosphere. The room temperature and barometric pressure were also recorded before and after the experiment. The mass flow rate and flow coefficient were determined from the measurements as described below.

It was necessary to correct the indicated air flow rate at the rotameter to obtain finally a mass flow rate. Assuming the friction loss between the rotameter and the ante-chamber was negligible (measurements of the pressure drop were made and the maximum error (at maximum flow rate) on assuming no pressure drop was 0.37% relative to the absolute pressure),

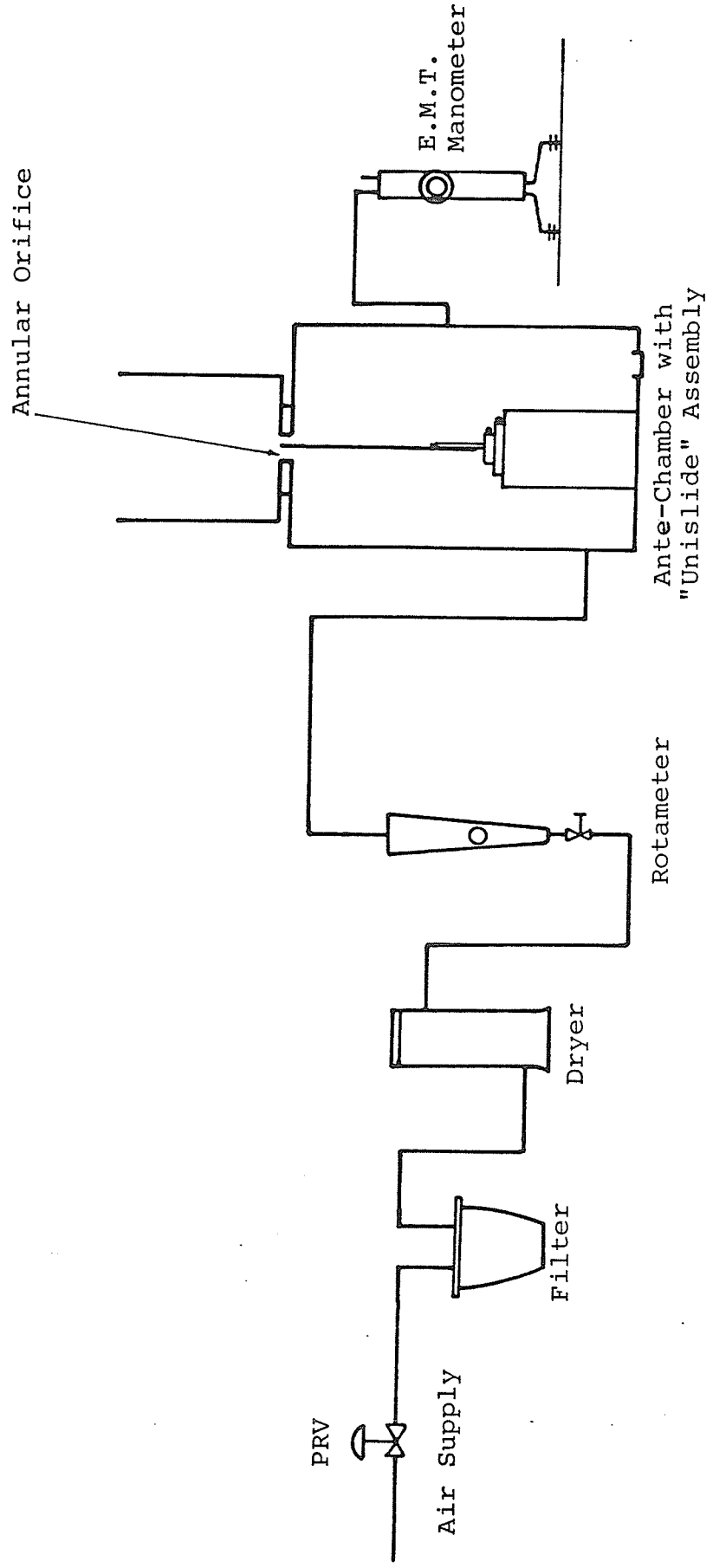

Fig. A.1 Apparatus Arrangement for the Flow Coefficient

it follows that, very closely

$$P_m = P_t \qquad (A.1)$$

where

P_m = absolute pressure at rotameter,

P_t = absolute pressure inside the ante-chamber.

The indicated flow rate obtained from the manufacturer's curve* for standard conditions (14.7 psia and 70°F, or 76 cm Hg and 21.1°C) was corrected to the rotameter conditions by the following equation [A.1].

$$Q_m = Q_I \sqrt{\frac{1.0 \times 76 \times T_m}{S.G \times P_m \times (21.1 + 273.2)}} \qquad (A.2)$$

where

Q_m = volumetric air flow rate at metering conditions,

Q_I = indicated volumetric air flow rate at standard conditions,

T_m = absolute temperature at metering conditions,

S.G = specific gravity of tested gas.

---

*The rotameter was calibrated by Cheung [7] and was found in good agreement with the manufacturer's curve. Therefore, the manufacturer's curve was used in the present experiments.

The mass flow rate under metering conditions and throughout the circuit was found from

$$\dot{m}_{act} = \rho_m Q_m$$

where

$\dot{m}_{act}$ = actual mass flow rate at metering conditions,

ρ_m = density of air at metering conditions.

The density of air at metering conditions was calculated using the ideal gas law.

The ideal mass flow rate is given by Eqn. A3 [A.2]

$$\dot{m}_{ideal} = A_a \sqrt{2 \rho_t (P_t - P_{atm})} \qquad (A.3)$$

where

$\dot{m}_{ideal}$ = ideal mass flow rate

A_a = area of annular orifice

ρ_t = density of air at ante-chamber conditions

(= ρ_m at the metering conditions)

The flow coefficient K is defined through the equation:

$$\dot{m}_{act} = K \dot{m}_{ideal}$$

$$= K A_a \sqrt{2 \rho_t (P_t - P_{atm})}$$

where K, the flow coefficient is the product of discharge coefficient C_d and the velocity of approach factor M. The flow coefficient is essentially equal to the discharge coefficient as the velocity approach factor is approximately equal to one. Table A.1 summarizes the experimental conditions and results in the experiment.

Figure A.2 shows the K value against the orifice Reynolds number (Re_o) which is defined as follows:

$$Re_o = \frac{\dot{m}_{act} (D - d)}{A_a \mu} \qquad (A.4)$$

where

D = diameter of the circular orifice,

d = outside diameter of the capillary tube,

A_a = area of annular orifice,

μ = dynamic viscosity of air.

From the tabulated values and the graph, it is noted that the range of K is 0.68-0.71; in the calculations an average value of 0.69 is used to calculate

$$E' \left(\equiv \frac{\pi^2 R_o^4}{A_a^2} \frac{1}{K^2} \frac{\rho_g}{\rho_l} \right) .$$

Barometric pressure = Start 72.60 cm Hg; End 72.60 cm Hg
Room temperature = Start 22°C; End 22°C

Air flow rate scale (cm)	Indicated Air flow rate at standard conditions (cm^3/sec)	P_t (gauge) mm H_2O	Actual mass flow rate (10^{-5} kg/sec)	Ideal mass flow rate (10^{-5} kg/sec)	K	Re_o
3	13.37	0.15	1.56	2.28	0.68	134
4	18.88	0.30	2.21	3.23	0.68	189
5	23.99	0.47	2.46	4.06	0.69	240
6	29.49	0.70	3.45	4.93	0.70	295
8	39.32	1.25	4.60	6.59	0.70	394
10	49.55	1.90	5.77	8.12	0.71	494
12	59.78	2.80	6.99	9.86	0.71	598
14	69.22	3.95	8.11	11.71	0.69	693
16	79.84	5.30	9.35	13.57	0.69	799
18	90.46	7.00	10.59	15.59	0.68	905

Table A.1 Calculation Results of Flow Coefficients and Corresponding Experimental Conditions

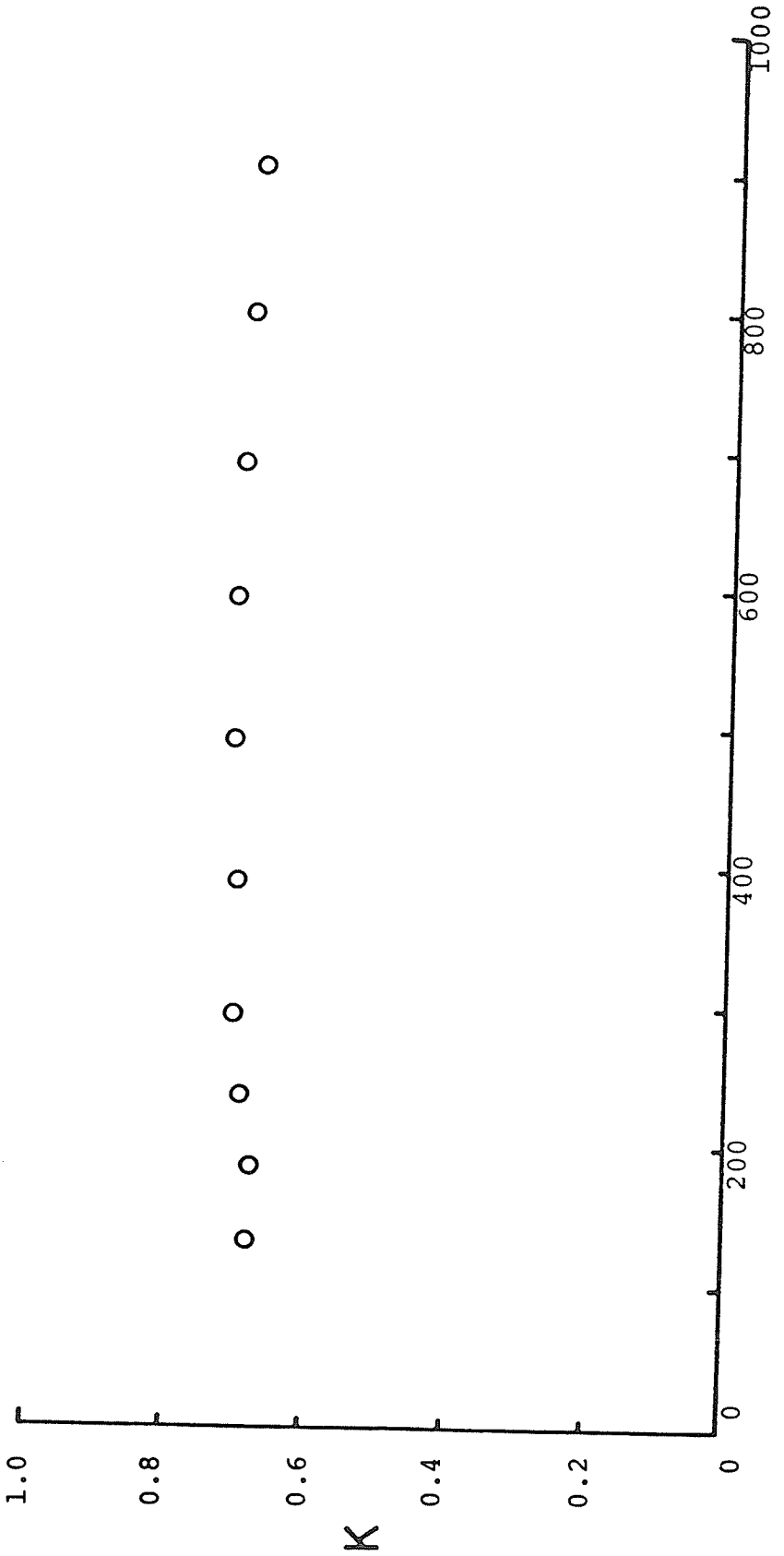

Fig. A.2 K Value as a Function of Orifice Reynolds Number

References for Appendix A

A.1 Brooks Instruments General Catalog
(Identification on back cover 1171-13-5M-13).

A.2 EXPERIMENTAL METHODS FOR ENGINEERS
J.P. Holman, Third Edition, pp. 216-220, McGraw-Hill (1966).

APPENDIX B

CALCULATION OF ACTUAL CONSTANT-FLOW RATE AT ORIFICE

In order to determine the actual constant-flow rate at the orifice, the indicated air flow rate from the calibration curve has to be corrected, i.e. first from standard conditions (14.7 psia and 70°F or 76 cm Hg and 21.1°C) to metering conditions and then from metering conditions to the orifice conditions. The indicated air flow rate at standard conditions can be corrected to metering conditions as follows [B.1, B.2]:

$$Q_m = Q_I \sqrt{\frac{1.0 \times 76.0 \times T_m}{S.G \times P_m \times (21.1 + 273.2)}} \qquad (B.1)$$

where

Q_m = volumetric flow rate at metering conditions, cm^3/sec,

Q_I = indicated volumetric air flow rate at standard conditions of 76 cm Hg and (21.1 + 273.2) K,

T_m = temperature at metering conditions, K,

P_m = absolute pressure at metering condition, cm Hg,

S.G = specific gravity of fluid relative to air.

Assuming air as an ideal gas, the air flow rate at metering conditions is then corrected to the bubbling conditions at the orifice using the ideal gas law which is

given by:

$$\frac{Q_m P_m}{T_m} = \frac{Q_o P_o}{T_o} \qquad (B.2)$$

where

Q_o = volumetric flow rate at the orifice, cm^3/sec,

T_o = temperature at the pool, K,

P_o = pressure in the plane of the orifice (atmospheric pressure and liquid head in pool), cm Hg.

Finally, the volumetric flow rate of liquid vapour has to be determined by Eqn. B.3 which assumes the liquid vapour behaves as an ideal gas

$$\frac{Q_{vap}}{Q_o + Q_{vap}} = \frac{P_{vap}}{P_{tot}} \qquad (B.3)$$

where Q_{vap} and Q_o are the volumetric flow rates of liquid vapour and the air respectively, P_{vap} is the partial pressure of the liquid vapour and P_{tot} is the total pressure of both air and liquid vapour. Then, the actual constant-flow rate is the sum of Q_{vap} and Q_o:

$$Q_c = Q_{vap} + Q_o \qquad (B.4)$$

Example (distilled water)

Indicated rotameter air flow rate (scale) = 16.12 cm^3/sec

Temperature at metering conditions, T_m = 23.9°C

Pressure at metering conditions, P_m (gauge) = 12.4 cm Hg

Temperature of pool liquid, T_o = 23.9°C

Atmospheric pressure = 76.10 cm Hg

P_o at orifice (atmospheric pressure plus head of liquid in pool) = 77.0 cm Hg

P_{vap}, liquid vapour pressure at 23.9°C = 2.25 cm Hg

S.G. of air = 1.0

Substituting the values in Eqn. B.1, we have

$$Q_m = 16.12 \sqrt{\frac{1.0 \times 76.0 \times (273.2 + 23.9)}{1.0 \times (12.4 + 76.10) \times (21.1 + 273.2)}}$$

$$= 15.01 \text{ cm}^3/\text{sec}$$

Then the air flow rate at orifice conditions is calculated from Eqn. B.2. Thus

$$Q_o = 15.01 \times \frac{297.1 \times 88.5}{297.1 \times 77.0}$$

$$= 17.25 \text{ cm}^3/\text{sec}$$

The Q_{vap} is determined from Eqn. B.3

$$\frac{Q_{vap}}{17.3 + Q_{vap}} = \frac{2.25}{77} = 0.02922$$

Therefore

$$Q_{vap} = 0.518 \text{ cm}^3/\text{sec}$$

and

$$Q_c = Q_{vap} + Q_o$$

$$= 17.77 \text{ cm}^3/\text{sec}$$

Table B.1 summarizes the calculation results for the actual constant volumetric flow rates and corresponding experimental conditions. The liquid vapour pressures were obtained from [B3].

References for Appendix B

B.1 Brooks Instruments General Catalog, p. 50, (Identification on back cover 1171-B-5M-B)

B.2 VARIABLE AREA FLOWMETER HANDBOOK: Vol. 1, BASIC ROTAMETER PRINCIPLES, Fisher and Porter Catalog 10A 1021 (1970); Vol. 2, ROTAMETER CALCULATIONS, Fisher and Porter Catalog 10A 1022 (1969).

B.3 FUNDAMENTAL OF CLASSICAL THERMODYNAMICS, SI Version 2^e Wylen G.V., R.E. Sonntag

Film Identification	T_m °C	P_{atm} cm Hg	P_m (gauge) cm Hg	Q_I cm^3/sec	Q_m cm^3/sec	Q_o cm^3/sec	Q_c (vap+air) cm^3/sec	F
A	22.2	75.50					0.00	0.00
B	25.6	77.30	7.7	10.22	9.74	10.64	10.98	10.29
C	25.6	77.30	12.9	16.12	14.90	17.18	17.74	16.64
D	25.6	77.30	25.5	21.63	19.73	23.40	24.16	22.64
E	23.9	76.10	19.6	27.53	24.65	30.64	31.56	29.58
F	23.9	76.10	21.7	32.64	28.91	36.72	37.83	35.45
G	22.2	75.50					0.00	0.00
H	23.9	76.10	12.4	16.12	15.01	17.25	17.77	16.66
I	22.2	75.50	16.0	24.78	22.55	27.17	27.98	26.24
J	22.2	75.50					0.00	0.00
K	23.9	76.10	12.4	16.12	15.01	17.25	17.77	16.66

Table B.1 Experimental Conditions and Calculation Results of the Actual Flow Rate and Constant-Flow Component

APPENDIX C

CALCULATION OF BUBBLE VOLUME

The volume of a bubble (at any instant during formation) was determined from the frames of high-speed motion pictures and was based on the calculation method of L'Ecuyer and Murthy (C.1). A description of the procedures is as follows:

1. One of the picture frames with the rod image whose actual diameter was known was projected on a screen equipped with a digital X-Y reader.

2. A 1:1 ratio of the actual rod diameter to the projected image of the rod was obtained by adjusting the scales of the digital X-Y reader.

3. Bubble images were projected frame by frame allowing for the calculation of instantaneous bubble volume as described below.

4. By means of horizontal lines, the enlarged bubble image was divided into a series of truncated cones. Figure C.1 illustrates one such outline. Generally 7-20 horizontal lines were used depending on the bubble size and shape. The volume of a bubble was then computed from the following equation:

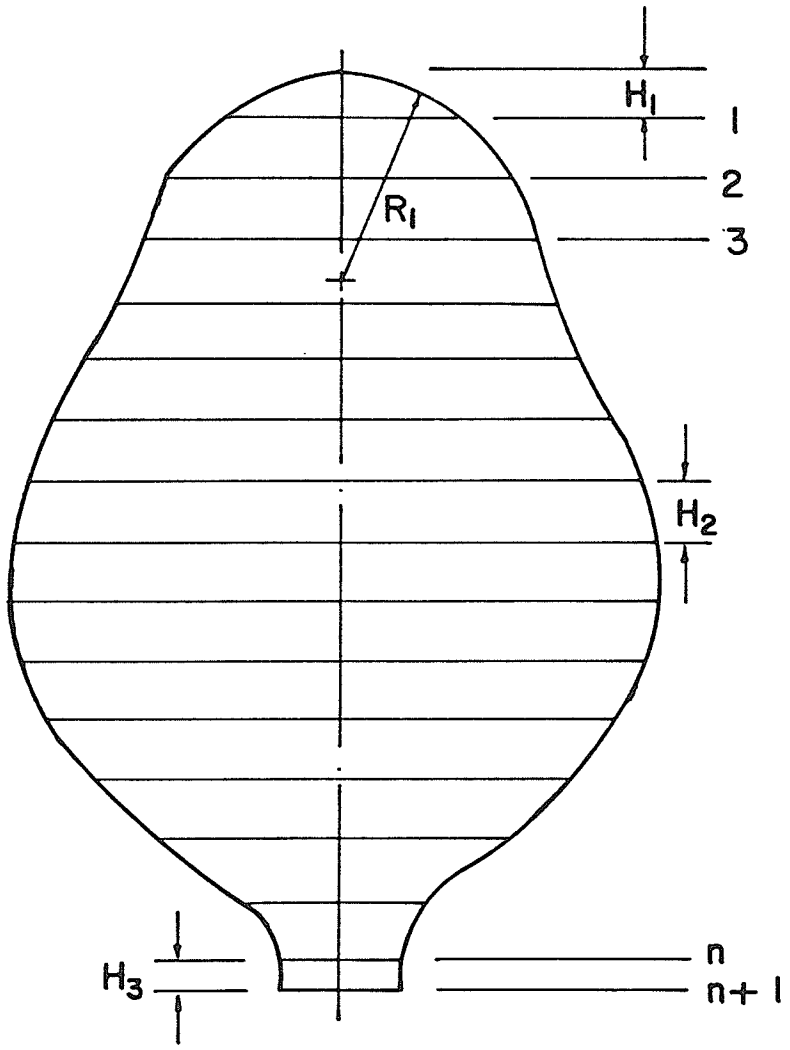

Fig. C.1 Enlarged Bubble Outline for Volume Calculations

$$V = \frac{\pi}{3} H_1^2 \ (3R_1 - H_1) + \sum_{i=1}^{n-1} \frac{\pi}{12} H_2 (d_i^2 + d_{i+1}^2 + d_i d_{i+1}) \qquad (C.1)$$

$$+ \frac{\pi}{12} H_3 (d_n^2 + d_{n+1}^2 + d_n d_{n+1})$$

5. The true bubble volume was calculated directly from the measured values using Eqn. C.1 and an Apple II micro-computer.

Reference for Appendix C

C.1 L'Ecuyer, M.R. and S.N.B. Murthy, Energy transfer from a liquid to gas bubbles forming at a submerged orifice, NASA Report TND-2547 (1965).

APPENDIX D

COMPUTER PROGRAM

This appendix gives the computer program used for calculation of R_* against t_* from Eqn. 5.8. (This program accommodates a number of combinations of ΔP^*, E', and F; a slightly shorter version of the same program was used when only one combination of ΔP^*, E' and F was required, as in the comparison of experimental results with the theory). The various symbols used in the program have meanings described as follows (The symbol in the program appears first and then the symbol used in the rest of this thesis):

$$R = R_*$$

$$R1 = R_*$$

$$E = E'$$

$$P = \Delta P^*$$

$$F = F$$

$$Totaltime = t_*$$

```
WATERLOO PASCAL -- ( OS, VERSION 3.0 ):  UNIVERSITY OF MANITOBA

 1       PROGRAM JOEDATA (INPUT, OUTPUT) ;
 2
 3       CONST
 4          PI = 3.1415926535;
 5
 6    :  VAR
 7    :     L    INTEGER ;
 8    :     N, D : INTEGER ;
 9    :     R, R1 : REAL ;
10    :     V, P, M, S, F : REAL ;
11    :     IR, IR1 : REAL ;
12    :     H, E, TOTALTIME : REAL ;
13    :     KT : ARRAY [1..4] OF REAL ;
14    :     KR : ARRAY [1..4] OF REAL ;
15    :
16    :  PROCEDURE FIVELINES ;
17    :  VAR
18    :     I : INTEGER ;    (* LOOP COUNTER *)
19    :
20    :  BEGIN
21    :  FOR I := 1 TO 5 DO
22    :     WRITELN
23    :  END;
24    :
25    :  PROCEDURE HEADING1(E,P,F:REAL) ;
26    :  BEGIN
27    :  WRITELN;
28    :  WRITELN(' ':38,'E=',E:10:6,' ':10,'P=',P:10:6,' ':10,'F=',F:11:6);
29    :  WRITELN(' ':38,'************',' ':10,'************',' ':10,'************');
30    :  WRITELN
31    :  END ;
32    :
33    :  PROCEDURE HEADING ;
34    :  BEGIN
35    :  WRITELN; WRITELN;
36    :  WRITELN(' ':31,'TOTAL TIME',' ':29,'R',' ':28,'R1');
37    :  WRITELN(' ':31,'**********',' ':27,'******',' ':24,'******');
38    :  WRITELN; WRITELN
39    :  END;    (* HEADING *)
40    :
41    :
42    :
43    :  BEGIN     (* MAIN LINE *)
44    :  PAGE;
45    :  READLN(H);
46    :  READLN(M);
47    :  READLN(V);
48    :  READLN(S);
49    :
50    :
51    :  (* INITIALIZATION *)
52    :  TOTALTIME := 0;
53    :  E :=0.0010;
54    :  P := 1.0000;
55    :  F := S ;
56    :  IR := 1 ;
57    :  IR1 := F/(4*PI*IR*IR);
58    :  R := 1;
59    :  R1 := F/(4*PI*R*R);
60    :
61    :
62    :  WHILE (P <= M) DO
63    :     BEGIN
64    :
```

```
 65  :
 66  :
 67  :      WHILE (F <= V) DO
 68  :         BEGIN
 69  :
 70  :                FIVELINES;
 71  :                HEADING1(E,P,F);
 72  :                HEADING;
 73  :
 74  :            WRITELN (' ':30,
 75  :                     TOTALTIME:10:6,' ':20,R:13:10,' ':20,
 76  :                     R1:13:10);
 77  :                     WRITELN;
 78  :                     WHILE (TOTALTIME <= 8 ) DO
 79  :                     BEGIN
 80  :
 81  :                     TOTALTIME :=TOTALTIME + H;
 82  :                     FOR L := 1 TO 4 DO
 83  :                        BEGIN
 84  :                        KT[L] := H * R1 ;
 85  :                        KR[L] :=H*(4/P)*E*F*R*R1+2*P/R-1.5*(R1*R1)/R-8*E*R*R*R
 86  :                                *R1*R1-2/(R*R)-(E*F*F)/(2*P1*P1*R));
 87  :
 88  :                        IF (L <> 3) THEN
 89  :                           BEGIN
 90  :                           R := IR + 0.5 * KT[L] ;
 91  :                           R1 := IR1 + 0.5 * KR[L]
 92  :                           END   (* IF *)
 93  :                        ELSE
 94  :                           BEGIN
 95  :                           R := IR + KT[L] ;
 96  :                           R1 := IR1 + KR[L]
 97  :                           END ;
 98  :                        END ;    (* FOR *)
 99  :
100  :                     R:=IR+(1/6)*(KT[1]+2*KT[2]+2*KT[3]+KT[4]);
101  :                     R1:=IR1+(1/6)*(KR[1]+2*KR[2]+2*KR[3]+KR[4]);
102  :
103  :                     WRITELN(' ':30,
104  :                             TOTALTIME:10:6,' ':20,R:13:10,' ':20,
105  :                             R1:13:10);
106  :                     WRITELN;
107  :
108  :                     (* UPDATE IR & IR1 *)
109  :                     IR := R ;
110  :                     IR1 := R1 ;
111  :                     END;  (* TOTALTIME *)
112  :                TOTALTIME := 0;
113  :                F := F + 4;
114  :                R := 1;
115  :                R1 := F/(4*PI*R*R);
116  :                IR := 1;
117  :                IR1 := F/(4*PI*IR*IR);
118  :            END;  (* F *)
119  :         P := P + 1.0;
120  :         F := S;
121  :         R1 := F/(4*PI*R*R);
122  :         IR1 := F/(4*PI*R*R)
123  :         END      (* P *)
124  :   END.    (* PROGRAM *)
Execution begins...
```

APPENDIX E

BUBBLE IDENTIFICATION AND TABULATED DATA

Each bubble analyzed is identified by a code* in which the first letter indicates a film number; the experimental conditions for each film are given in Table E.1. Following the letter is a dash and then the picture frame number at which the bubble taken to be analyzed started to form at the orifice. The frame number for each film was set to zero when a completely blank frame was seen on the screen just before the bubble images appeared following the filming of the rod. Should this be required for later review, the frame number in the code serves as a means of locating the analyzed bubble in the film. The following example illustrates the application of the code. Let A-500 be the identification of a bubble analyzed. The first letter (A) refers to the film number with the conditions given in Table E.1, the number (500) refers to the frame number which gives the location of the start of the bubble formation.

The tabulated data for the bubbles analyzed during the experimental investigation are presented in Tables E.2 to E.12.

---

*Earlier the work was described by another code while for the purposes of presentation in the thesis the code appearing throughout the thesis was used. For the sake of completeness, the correspondence between the new and former coding is given in Table E.13.

Liquid: Distilled Water
Gas: Air
Depth of Liquid: 12.7 cm above the orifice
Orifice Dimensions:

Circular orifice diameter = 0.502 cm
Capillary tube I.D. = 0.216 cm
O.D. = 0.277 cm

Film Number	Ante-Chamber pressure (gauge) kPa	ΔP^*	$E' \times 10^3$	Q_c Actual Constant-Flow Rate cm^3/sec	F	Pool Temp. (=Room) Temp) °C	P_{atm} cm Hg
A	1.316	1.24	5.11	0.00	0.00	22.2	75.50
B			5.17	10.98	10.29	25.6	77.30
C			5.17	17.74	16.64	25.6	77.30
D			5.17	24.16	22.64	25.6	77.30
E			5.12	31.56	29.58	23.9	76.10
F			5.12	37.83	35.45	23.9	76.10
G	1.361	2.04	5.11	0.00	0.00	22.2	75.50
H			5.12	17.77	16.66	23.9	76.10
I			5.11	27.98	26.24	22.2	75.50
J	1.385	2.44	5.11	0.00	0.00	22.2	75.50
K			5.12	17.77	16.66	23.9	76.10

Table E.1 Film Identification and Experimental Conditions

Table E.2 Bubble Growth Data for Distilled Water
($E' = 0.00511$, $\Delta P^* = 1.24$
$F = 0.00$)

Liquid temperature: 22.2°C
Room temperature: 22.2°C
Liquid height above the orifice: 12.7 cm

Bubble Identification No. A-1738
(Time/frame, 4.801×10^{-4} sec/frame)

Frame No.	Time, t ms	Bubble Volume 10^{-3} cm^3	Bubble Equiv. Radius cm	R_*	t_*
1738	0.00	32.02	0.197	0.78	0.00
1750	5.76	50.96	0.230	0.92	0.38
1760	10.56	57.90	0.240	0.96	0.71
1770	15.36	91.95	0.280	1.12	1.04
1780	20.20	164.63	0.340	1.35	1.36
1790	24.96	333.04	0.430	1.71	1.68
1805	32.16	775.73	0.570	2.27	2.17
1820	39.40	1418.36	0.697	2.77	2.66
1832	45.00	1767.14	0.750	2.99	3.04
1835	46.56	2144.66	0.800	3.18	3.14
1849	53.30	2664.30	0.860	3.43	3.59

Bubble Identification No. A-1897
(Time/frame, 4.511×10^{-4} sec/frame)

1897	0.00	13.58	0.148	0.60	0.00
1910	5.86	38.79	0.210	0.83	0.39
1920	10.37	50.96	0.230	0.92	0.70
1930	14.80	66.23	0.251	1.00	1.00
1945	21.65	164.63	0.340	1.35	1.46
1960	28.42	381.70	0.450	1.80	1.92
1975	35.18	775.73	0.570	2.27	2.37
1990	41.95	1376.05	0.690	2.75	2.85
2010	50.97	2482.71	0.840	3.30	3.43
2016	53.70	2758.33	0.870	3.47	3.62

Bubble Identification No. A-2249
(Time/frame, 4.511×10^{-4} sec/frame)

2249	0.00	32.54	0.196	0.78	0.00
2260	4.96	57.91	0.240	0.96	0.33
2270	9.47	66.24	0.251	1.00	0.64
2280	13.98	121.20	0.307	1.23	0.95
2295	20.80	233.49	0.382	1.52	1.40
2305	25.30	381.70	0.450	1.79	1.71
2316	30.22	523.59	0.500	2.00	2.02
2320	32.03	804.67	0.577	2.29	2.20
2327	35.10	1047.39	0.630	2.50	2.40
2335	38.80	1317.09	0.680	2.71	2.62
2349	45.11	1987.79	0.780	3.10	3.03
2358	49.17	2482.71	0.840	3.34	3.32

Table E.3 Bubble Growth Data for Distilled Water
($E' = 0.00517, \Delta P^* = 1.24$
$F = 10.29$)

Liquid temperature: 25.6°C
Room temperature: 25.6°C
Liquid height above the orifice: 12.7 cm

Bubble Identification No. B-698
(Time/frame, 4.000×10^{-4} sec/frame)

Frame No.	Time, t ms	Bubble Volume 10^{-3} cm³	Bubble Equiv. Radius cm	R_*	t_*
698	0.00	24.43	0.18	0.72	0.00
710	4.80	72.62	0.26	1.04	0.32
720	8.81	150.53	0.33	1.31	0.59
730	12.80	195.43	0.36	1.42	0.86
740	16.82	229.85	0.38	1.53	1.13
750	20.80	356.82	0.44	1.76	1.40
765	26.81	623.61	0.53	2.13	1.80
780	32.80	1150.35	0.65	2.59	2.21
795	38.80	1838.78	0.76	3.03	2.60
805	42.70	2395.09	0.83	3.29	2.88
820	48.86	2664.31	0.86	3.43	3.29

Bubble Identification No. B-865
(Time/frame, 4.027×10^{-4} sec/frame)

865	0.00	18.47	0.164	0.65	0.00
872	2.82	39.35	0.211	0.84	0.20
880	6.04	115.37	0.302	1.19	0.41
890	10.07	208.75	0.368	1.47	0.68
900	14.09	342.42	0.434	1.73	0.95
910	18.12	489.79	0.489	1.95	1.22
925	24.16	696.91	0.550	2.19	1.64
940	30.36	974.34	0.615	2.45	2.05
955	36.24	1556.95	0.719	2.86	2.45
970	42.28	2193.28	0.806	3.21	2.86

Bubble Identification No. B-2888
(Time/frame, 4.425×10^{-4} sec/frame)

2888	0.00	18.82	0.165	0.67	0.00
2900	5.31	61.60	0.245	0.97	0.36
2910	9.73	113.09	0.300	1.19	0.65
2920	14.16	195.43	0.360	1.43	0.95
2930	18.58	288.69	0.410	1.59	1.25
2940	23.01	448.92	0.475	1.89	1.55
2950	27.43	735.62	0.560	2.23	1.85
2960	31.86	1098.07	0.640	2.55	2.15
2975	38.49	1767.14	0.750	2.99	2.59
2994	46.90	2572.44	0.850	3.39	3.16

Table E.4 Bubble Growth Data for Distilled Water
($E' = 0.00517$, $\Delta P^* = 1.24$
$F = 16.64$)

Liquid Temperature: 25.6°C
Room Temperature: 25.6°C
Liquid height above the orifice: 12.7 cm

Bubble Identification No. C-646
(Time/frame, 4.110×10^{-4} sec/frame)

Frame No.	Time, t ms	Bubble Volume 10^{-3} cm^3	Bubble Equiv. Radius cm	R_*	t_*
646	0.00	22.45	0.175	0.69	0.00
662	6.57	63.89	0.248	0.99	0.44
672	10.68	91.95	0.280	1.12	0.72
682	14.80	179.59	0.350	1.39	0.99
692	18.90	333.04	0.430	1.71	1.27
702	23.02	555.65	0.510	2.03	1.55
712	27.13	904.78	0.600	2.39	1.83
722	31.24	1358.18	0.687	2.74	2.10
732	35.35	1912.32	0.770	3.10	2.38
742	39.47	2527.31	0.845	3.36	2.65
758	46.03	3261.76	0.920	3.67	3.10

Bubble Identification No. C-801
(Time/frame, 4.167×10^{-4} sec/frame)

801	0.00	33.51	0.20	0.79	0.00
820	7.92	113.09	0.30	1.20	0.53
830	12.08	212.17	0.37	1.47	0.81
840	16.25	381.70	0.45	1.80	1.09
855	22.50	696.91	0.55	2.16	1.51
870	28.75	904.78	0.60	2.40	1.93
885	35.00	1697.39	0.74	2.95	2.36
900	41.25	2395.09	0.83	3.30	2.78
915	47.50	3369.28	0.93	3.70	3.20
927	52.50	3942.45	0.98	3.90	3.54

Bubble Identification No. C-2121
(Time/frame, 4.477×10^{-4} sec/frame)

2121	0.00	20.94	0.171	0.68	0.00
2135	6.27	94.94	0.283	1.13	0.42
2145	10.75	164.64	0.340	1.35	0.72
2160	17.46	303.74	0.417	1.67	1.18
2170	21.94	474.92	0.484	1.93	1.48
2185	28.65	882.35	0.595	2.37	1.94
2200	35.37	1436.76	0.700	2.64	2.40
2215	42.10	2572.44	0.850	3.37	2.85
2243	54.62	3705.97	0.960	3.82	3.68

Table E.5 Bubble Growth Data for Distilled Water
(E' = 0.00517, ΔP^* = 1.24
F = 22.64)

Liquid temperature: 25.6°C
Room temperature: 25.6°C
Liquid Height above the orifice: 12.7 cm

Bubble Identification No. D-871
(Time/frame, 4.167 x 10^{-4} sec/frame)

Frame No.	Time, t ms	Bubble Volume 10^{-3} cm^3	Bubble Equiv. Radius cm	R_*	t_*
871	0.00	51.63	0.231	0.92	0.00
883	5.00	113.09	0.300	1.20	0.36
893	9.16	212.17	0.370	1.47	0.62
905	14.16	310.34	0.420	1.70	0.95
915	18.33	454.61	0.477	1.90	1.23
925	22.50	804.67	0.577	2.30	1.51
940	28.75	1376.06	0.690	2.75	1.94
950	32.92	1987.79	0.780	3.11	2.22
960	37.10	2572.44	0.850	3.39	2.50
970	41.25	3261.76	0.920	3.66	2.79
978	44.58	3479.14	0.940	3.75	3.00

Bubble Identification No. D-1054
(Time/frame, 4.274 x 10^{-4} sec/frame)

1054	0.00	77.95	0.265	1.06	0.00
1065	4.70	115.37	0.302	1.20	0.31
1075	8.97	178.06	0.349	1.40	0.62
1085	13.25	288.69	0.410	1.63	0.89
1095	17.52	381.70	0.450	1.79	1.18
1105	21.80	523.59	0.500	2.20	1.47
1115	26.07	735.62	0.560	2.50	1.76
1130	32.50	1563.45	0.720	2.87	2.19
1145	38.90	2572.44	0.850	3.38	2.62
1154	42.74	3261.76	0.920	3.66	2.88

Bubble Identification No. D-1521
(Time/frame 4.651 x 10^{-4} sec/frame)

1521	0.00	25.67	0.183	0.73	0.00
1535	6.51	124.79	0.310	1.24	0.43
1545	11.16	231.67	0.381	1.51	0.74
1555	14.16	290.81	0.411	1.64	0.96
1565	16.86	440.47	0.472	1.97	1.14
1580	27.44	1187.91	0.657	2.61	1.85
1595	34.42	1934.75	0.773	3.08	2.32
1610	41.40	3512.56	0.943	3.76	2.79
1625	48.37	4904.68	1.054	4.20	3.20

Table E.6 Bubble Growth Data for Distilled Water
($E' = 0.00512, \Delta P^* = 1.24$
$F = 29.58$)

Liquid temperature: 23.9°C
Room temperature: 23.9°C
Liquid height above the orifice: 12.7 cm

Bubble Identification No. E-778
(Time/frame, 4.301×10^{-4} sec/frame)

Frame No.	Time, t ms	Bubble Volume 10^{-3} cm³	Bubble Equiv. Radius cm	R_*	t_*
778	0.00	49.65	0.228	0.91	0.00
789	5.16	137.26	0.320	1.30	0.35
799	9.46	237.18	0.384	1.53	0.64
809	13.76	457.48	0.478	1.90	0.93
819	18.06	716.09	0.555	2.21	1.22
829	22.36	1124.00	0.645	2.57	1.55
839	26.67	1616.15	0.728	2.90	1.80
849	30.96	2201.45	0.807	3.22	2.09
859	35.26	2682.94	0.862	3.42	2.38
868	38.71	3156.55	0.910	3.65	2.61

Bubble Identification No. E-984
(Time/frame, 4.494×10^{-4} sec/frame)

984	0.00	104.29	0.292	1.16	0.00
992	4.49	203.69	0.365	1.45	0.30
1002	8.99	323.83	0.426	1.69	0.60
1012	13.48	511.13	0.496	1.97	0.91
1022	17.97	860.29	0.590	2.35	1.21
1032	22.47	1370.08	0.689	2.74	1.52
1042	26.96	1860.64	0.763	3.04	1.82
1052	31.46	2482.71	0.840	3.35	2.12
1062	36.00	3219.40	0.916	3.65	2.43

Bubble Identification No. E-1722
(Time/frame, 4.396×10^{-4} sec/frame)

1722	0.00	43.39	0.218	0.87	0.00
1735	5.71	113.09	0.300	1.20	0.38
1750	12.30	252.32	0.392	1.56	0.83
1760	16.70	613.08	0.527	2.10	1.13
1770	21.10	804.67	0.577	2.29	1.42
1780	25.50	1317.09	0.680	2.71	1.72
1790	29.90	1860.64	0.763	3.03	2.02
1810	38.68	3125.43	0.907	3.61	2.61

Table E.7 Bubble Growth Data for Distilled Water
($E^* = 0.00512, \Delta P^* = 1.24$
$F = 35.45$)

Liquid temperature: 23.9°C
Room temperature: 23.9°C
Liquid height above the orifice: 12.7 cm

Bubble Identification No. F-712
(Time/frame, 4.132×10^{-4} sec/frame)

Frame No.	Time, t ms	Bubble Volume 10^{-3} cm³	Bubble Equiv. Radius cm	R_*	t_*
712	0.00	37.69	0.208	0.81	0.00
725	5.37	82.45	0.270	1.10	0.36
735	9.50	166.09	0.341	1.35	0.64
745	13.64	333.04	0.430	1.71	0.91
755	17.76	539.46	0.505	2.05	1.19
765	21.89	913.86	0.602	2.40	1.48
775	26.03	1449.11	0.702	2.79	1.75
790	32.23	2160.78	0.802	3.19	2.17
806	38.84	3261.76	0.920	3.60	2.62

Bubble Identification No. F-2480
(Time/frame, 4.444×10^{-4} sec/frame)

2480	0.00	50.96	0.230	0.91	0.00
2490	4.44	117.68	0.304	1.21	0.30
2500	8.88	229.85	0.380	1.51	0.60
2510	13.32	466.15	0.481	1.91	0.89
2520	17.76	775.73	0.570	2.27	1.19
2530	22.22	1237.40	0.666	2.65	1.49
2540	26.64	1838.78	0.760	3.03	1.79
2550	31.08	2777.39	0.872	3.47	2.09
2559	35.07	3283.08	0.922	3.67	2.37

Bubble Identification No. F-2970
(Time/frame, 4.444×10^{-4} sec/frame)

2970	0.00	45.83	0.222	0.88	0.00
2985	6.67	113.09	0.300	1.20	0.45
2995	11.11	268.08	0.400	1.59	1.05
3005	15.55	457.48	0.478	1.90	1.20
3010	17.78	696.91	0.550	2.20	1.49
3020	22.22	1098.07	0.640	2.55	1.78
3030	26.66	1616.15	0.728	2.90	2.09
3035	31.00	1957.37	0.776	3.10	2.54
3050	37.66	3125.43	0.907	3.61	0.74

Table E.8 Bubble Growth Data for Distilled Water
($E' = 0.00511, \Delta P^* = 2.04$
$F = 0.00$)

Liquid temperature: 22.2°C
Room temperature: 22.2°C
Liquid height above the orifice: 12.7 cm

Bubble Identification No. G-127
(Time/frame, 5.263×10^{-4} sec/frame)

Frame No.	Time, t ms	Bubble Volume 10^{-3} cm³	Bubble Equiv. Radius cm	R_*	t_*
127	0.00	15.90	0.156	0.62	0.00
137	5.26	62.36	0.246	0.98	0.36
147	10.52	129.68	0.314	1.25	0.72
157	15.79	250.39	0.391	1.56	1.10
170	22.63	568.82	0.514	2.05	1.55
185	30.53	1220.76	0.663	2.64	2.10
195	35.79	1838.78	0.760	3.03	2.46
210	43.68	2758.33	0.870	3.50	3.00
216	46.84	3104.81	0.905	3.60	3.22

Bubble Identification No. G-1617
(Time/frame, 4.487×10^{-4} sec/frame)

1617	0.00	57.91	0.240	0.96	0.00
1627	4.48	71.10	0.257	1.02	0.30
1645	12.56	113.09	0.300	1.19	0.84
1655	17.05	212.17	0.370	1.47	1.15
1665	21.54	288.69	0.410	1.60	1.45
1675	26.02	511.13	0.496	1.97	1.75
1685	30.51	860.29	0.590	2.35	2.06
1695	34.99	1328.74	0.682	2.71	2.35
1710	41.73	2144.66	0.800	3.18	2.81
1730	50.70	3053.63	0.900	3.58	3.42
1742	56.09	3479.14	0.940	3.74	3.78

Bubble Identification No. G-2320
(Time/frame, 4.375×10^{-4} sec/frame)

2320	0.00	28.73	0.190	0.76	0.00
2335	6.56	77.07	0.264	1.05	0.44
2245	10.93	124.79	0.310	1.24	0.74
2360	17.50	333.04	0.430	1.74	1.18
2370	21.87	434.89	0.470	1.90	1.47
2380	26.25	696.91	0.550	2.25	1.77
2390	30.63	998.31	0.620	2.50	2.10
2400	35.00	1376.06	0.690	2.75	2.36
2415	41.56	1838.77	0.760	3.04	2.80
2430	48.13	2545.30	0.847	3.37	3.24
2440	54.70	3156.55	0.910	3.71	3.70

Table E.9 Bubble Growth Data for Distilled Water
($E' = 0.00512, \Delta P^* = 2.04$
$F = 16.66$)

Liquid temperature: 23.9°C
Room temperature: 23.9°C
Liquid height above the orifice: 12.7 cm

Bubble Identification No. H-673
(Time/frame, 4.046×10^{-4} sec/frame)

Frame No.	Time, t ms	Bubble Volume 10^{-3} cm^3	Bubble Equiv. Radius cm	R_*	t_*
673	0.00	74.47	0.261	1.04	0.00
685	4.85	164.64	0.340	3.35	0.32
695	8.90	248.47	0.390	1.55	0.60
705	12.94	356.82	0.440	1.75	0.87
720	19.02	536.26	0.504	2.00	1.28
735	25.10	860.29	0.890	2.35	1.69
750	31.15	1563.46	0.720	2.87	2.09
760	37.20	2482.71	0.840	3.35	2.51
780	43.30	3895.57	0.930	3.70	2.92
795	49.36	4406.07	1.017	4.05	3.33
810	55.43	5575.28	1.100	4.38	3.74

Bubble Identification No. H-1865
(Time/frame, 4.762×10^{-4} sec/frame)

1865	0.00	83.37	0.271	1.07	0.00
1876	5.24	113.09	0.300	1.20	0.36
1886	10.00	179.59	0.350	1.40	0.67
1896	14.76	280.33	0.406	1.62	0.98
1906	19.52	523.59	0.500	2.00	1.31
1916	24.29	950.77	0.610	2.43	1.64
1930	30.95	1838.77	0.760	3.03	2.08
1940	35.72	2482.71	0.840	3.35	2.41
1965	45.20	4113.84	0.994	3.96	3.05
1975	52.38	5031.39	1.063	4.23	3.53

Bubble Identification No. H-2403
(Time/frame, 4.477×10^{-4} sec/frame)

2403	0.00	56.47	0.238	0.95	0.00
2409	2.68	113.09	0.300	1.19	0.17
2423	9.20	195.43	0.360	1.43	0.62
2434	14.00	290.81	0.411	1.64	0.94
2442	17.50	508.04	0.495	1.97	1.18
2454	23.10	825.76	0.582	2.32	1.56
2472	31.10	1732.04	0.745	2.97	2.09
2481	35.00	2395.09	0.830	3.31	2.36
2503	45.01	2618.10	0.920	3.70	3.04
2510	51.02	4188.79	1.000	3.98	3.44
2529	56.40	7238.23	1.200	4.78	3.81

Table E.10 Bubble Growth Data for Distilled Water
($E' = 0.00511, \Delta P^* = 2.04$
$F = 26.24$)

Liquid temperature: 22.2°C
Room temperature: 22.2°C
Liquid height above the orifice: 12.7 cm

Bubble Identification No. I-672
(Time/frame, 4.132×10^{-4} sec/frame)

Frame No.	Time, t ms	Bubble Volume 10^{-3} cm³	Bubble Equiv. Radius cm	R_*	t_*
672	0.00	91.95	0.280	1.11	0.00
682	4.13	137.26	0.320	1.27	0.28
695	9.50	212.17	0.370	1.47	0.64
705	13.64	426.62	0.467	1.86	0.92
715	17.76	775.57	0.570	2.27	1.20
725	21.90	1317.09	0.680	2.71	1.48
740	28.10	2065.23	0.790	3.15	1.89
755	34.29	3156.55	0.910	3.63	2.31
770	40.50	4188.79	1.000	3.98	2.73
782	45.45	5575.28	1.100	4.38	3.07

Bubble Identification No. I-1057
(Time/frame, 4.255×10^{-4} sec/frame)

1057	0.00	73.62	0.260	1.04	0.00
1075	7.66	137.26	0.320	1.27	0.52
1085	11.91	288.69	0.410	1.63	0.80
1095	16.17	555.65	0.510	2.03	1.09
1110	22.55	1259.83	0.670	2.67	1.52
1125	28.94	2234.35	0.811	3.23	1.95
1140	35.32	3084.27	0.903	3.60	2.38
1155	41.70	4188.79	1.000	3.98	2.81
1173	49.36	7238.23	1.200	4.38	3.33

Bubble Identification No. I-1261
(Time/frame, 4.317×10^{-4} sec/frame)

1261	0.00	78.84	0.266	1.06	0.00
1270	3.88	132.17	0.316	1.25	0.26
1280	8.20	240.91	0.386	1.54	0.55
1290	12.52	407.72	0.460	1.83	0.84
1300	16.83	659.58	0.540	2.15	1.13
1310	21.15	1047.39	0.630	2.51	1.43
1325	27.63	1912.32	0.770	3.06	1.86
1340	34.10	2854.54	0.880	3.51	2.30
1355	40.57	3591.36	0.950	3.78	2.74
1380	51.37	5728.72	1.110	4.42	3.46

Table E.11 Bubble Growth Data for Distilled Water
($E' = 0.00511, \Delta P^* = 2.44$
$F = 0.00$)

Liquid temperature: 22.2°C
Room temperature: 22.2°C
Liquid height above the orifice: 12.7 cm

Bubble Identification No. J-150
(Time/frame, 4.762×10^{-4} sec/frame)

Frame No.	Time, t ms	Bubble Volume 10^{-3} cm³	Bubble Equiv. Radius cm	R_*	t_*
150	0.00	58.63	0.241	0.96	0.00
160	4.80	126.00	0.311	1.24	0.32
170	9.52	299.38	0.415	1.65	0.64
180	14.29	670.64	0.542	2.16	0.96
190	19.05	1177.09	0.655	2.61	1.29
200	23.81	1697.39	0.740	2.94	1.61
210	28.57	2242.62	0.812	3.20	1.93
220	33.33	2952.96	0.890	3.55	2.25
230	38.10	3591.36	0.950	3.78	2.57
245	45.24	4577.20	1.030	4.10	3.05

Bubble Identification No. J-1245
(Time/frame, 4.495×10^{-4} sec/frame)

1245	0.00	67.03	0.252	1.00	0.00
1255	4.49	134.70	0.318	1.27	0.30
1265	8.99	310.34	0.420	1.67	0.61
1275	13.49	588.98	0.520	2.07	0.90
1285	17.98	817.28	0.580	2.31	1.21
1295	22.50	1150.34	0.650	2.60	1.52
1310	29.20	1824.30	0.758	3.02	1.97
1320	33.71	2318.02	0.821	3.27	2.30
1335	40.50	3166.96	0.911	3.63	2.73
1357	50.34	5074.11	1.066	4.25	3.40

Bubble Identification No. J-1402
(Time/frame, 4.615×10^{-4} sec/frame)

1402	0.00	55.76	0.237	0.94	0.00
1412	4.62	91.95	0.280	1.12	0.31
1422	9.23	212.17	0.370	1.30	0.62
1432	13.84	359.26	0.441	1.67	0.93
1442	18.46	696.91	0.550	2.07	1.25
1452	23.08	1103.22	0.641	2.55	1.55
1462	27.70	1697.39	0.740	2.95	1.87
1475	33.70	2758.33	0.870	3.50	2.27
1490	40.61	3156.55	0.910	3.63	2.70
1501	45.70	4617.32	1.033	4.11	3.08

Table E.12 Bubble Growth Data for Distilled Water
($E' = 0.00512$, $\Delta P^* = 2.44$
$F = 16.66$)

Liquid temperature: 23.9°C
Room temperature: 23.9°C
Liquid height above the orifice: 12.7 cm

Bubble Identification No. K-450
(Time/frame, 4.110×10^{-4} sec/frame)

Frame No.	Time, t ms	Bubble Volume 10^{-3} cm³	Bubble Equiv. Radius cm	R_*	t_*
450	0.00	48.93	0.227	0.90	0.00
460	4.11	68.64	0.254	1.01	0.27
470	8.22	173.51	0.346	1.38	0.56
480	12.33	391.97	0.454	1.81	0.84
490	16.44	751.49	0.564	2.24	1.11
505	22.60	1602.87	0.726	2.89	1.53
520	28.77	2767.85	0.871	3.47	1.95
535	35.00	3456.98	0.938	3.74	2.37
550	41.10	4039.79	0.988	3.94	2.78
560	45.20	6205.88	1.140	4.54	3.07

Bubble Identification No. K-1140
(Time/frame, 4.286×10^{-4} sec/frame)

1139	0.00	117.68	0.304	1.21	0.00
1150	4.71	190.58	0.357	1.42	0.32
1160	9.00	301.55	0.416	1.66	0.61
1175	15.43	648.65	0.537	2.14	1.05
1190	21.85	1505.56	0.711	2.83	1.48
1205	28.28	2572.44	0.850	3.38	1.92
1220	34.72	3740.82	0.963	3.84	2.36
1235	41.15	4698.24	1.039	4.14	2.78
1250	47.57	5884.95	1.12	4.38	3.22

Bubble Identification No. K-1730
(Time/frame, 4.724×10^{-4} sec/frame)

1730	0.00	36.08	0.205	0.82	0.00
1740	4.72	73.62	0.260	1.04	0.31
1750	9.44	150.53	0.330	1.31	0.63
1760	14.17	310.34	0.420	1.67	0.95
1775	21.25	998.31	0.620	2.50	1.43
1790	28.34	1802.72	0.755	3.00	1.91
1810	37.80	3412.94	0.984	3.72	2.55
1826	45.35	5605.74	1.102	4.29	3.06

New Identification Number	Old Identification Number
A	7W0
B	7W3
C	7W4
D	7W5
E	7W6
F	7W7
G	7.4W0
H	7.4W4
I	7.4W5.5
J	7.6W0
K	7.6W4

Table E.13 The Correspondence Between the New and Old Code System

APPENDIX F

BUBBLE GROWTH DATA FOR 0.3-cm DIAMETER ORIFICE PLATE

F.1 Introductory Remarks

This appendix gives the bubble growth data for the orifice diameter equal to 0.3 cm* and the centre tubing with I.D. = 0.160 cm and O.D. = 0.211 cm. The results are summarized in Section F.2. Section F.3 gives the results for the flow coefficient of the present orifice. The accuracy of placement of centre tubing inside the circular orifice is discussed in Sec. F.4.

For the bubble growth, the experiments were conducted as outlined in the body of the thesis. The flow coefficient was determined exactly the same as in Appendix A. These results appear in an appendix as time did not allow the taking of a more complete of data (similar to those in the body of the thesis) and comparison with theory; further the small orifice dimensions (annular gap $\simeq$ 0.49 mm) made the typical eccentricity larger and errors in calculating A_a larger.

F.2 Experimental Results

The experimental conditions and the corresponding parametric values for the bubble growth experiments are summarized

*The orifice plate has the same dimensions as the 0.5 cm orifice plate except for the orifice diameter.

in Table F.1. The bubble growth data are tabulated in Table F.3 to F.6 and presented in Figs. F.1 through F.5 in R vs. t.

The symbols in this section have the same meaning as the main body of the thesis.

F.3 Determination of the Flow Coefficient for the Present Annular Orifice (Described in Table F.2)

The flow coefficient (K) of the present annular orifice was determined as outlined in Appendix A. The experimental conditions and the results are summarized in Table F.2. Figure F.6 shows the coefficient (K) as a function of orifice Reynolds number (Re_o). A characteristic value of 0.6 is used to calculate the E' value in this appendix.

F.4 Accuracy of Placement of Centre Tubing

The procedure of measuring the error ($\frac{e}{r}$) is mentioned in Section 4.2. Due to the small gap between the circular orifice and the capillary tube, a larger percentage error was expected. The typical error was estimated to be around 7-8% for this orifice.

Liquid: Distilled Water
Gas: Air
Liquid Height: 12.7 cm above orifice
Orifice Dimension:
Orifice diameter = 0.308 cm
Capillary tube
I.D.= 0.160 cm
O.D.= 0.211 cm

Film Number	Pool Temp (= Room Temp) °C	P_{atm} cm Hg	E'	Actual Constant-Flow Rate cm^3/sec	ΔP^*	F
L	21.1	76.58	12.22×10^{-3}	23.34	1.24	45.51
M	25.6	76.16	12.29×10^{-3}	29.79		58.10
N	25.6	77.28	12.31×10^{-3}	23.34	2.04	45.79
O	25.6	77.28	12.31×10^{-3}	11.36	2.64	22.15
P	25.6	77.28	12.31×10^{-3}	18.76		39.04

Table F.1 Experimental Conditions for the Bubble Growth Experiments

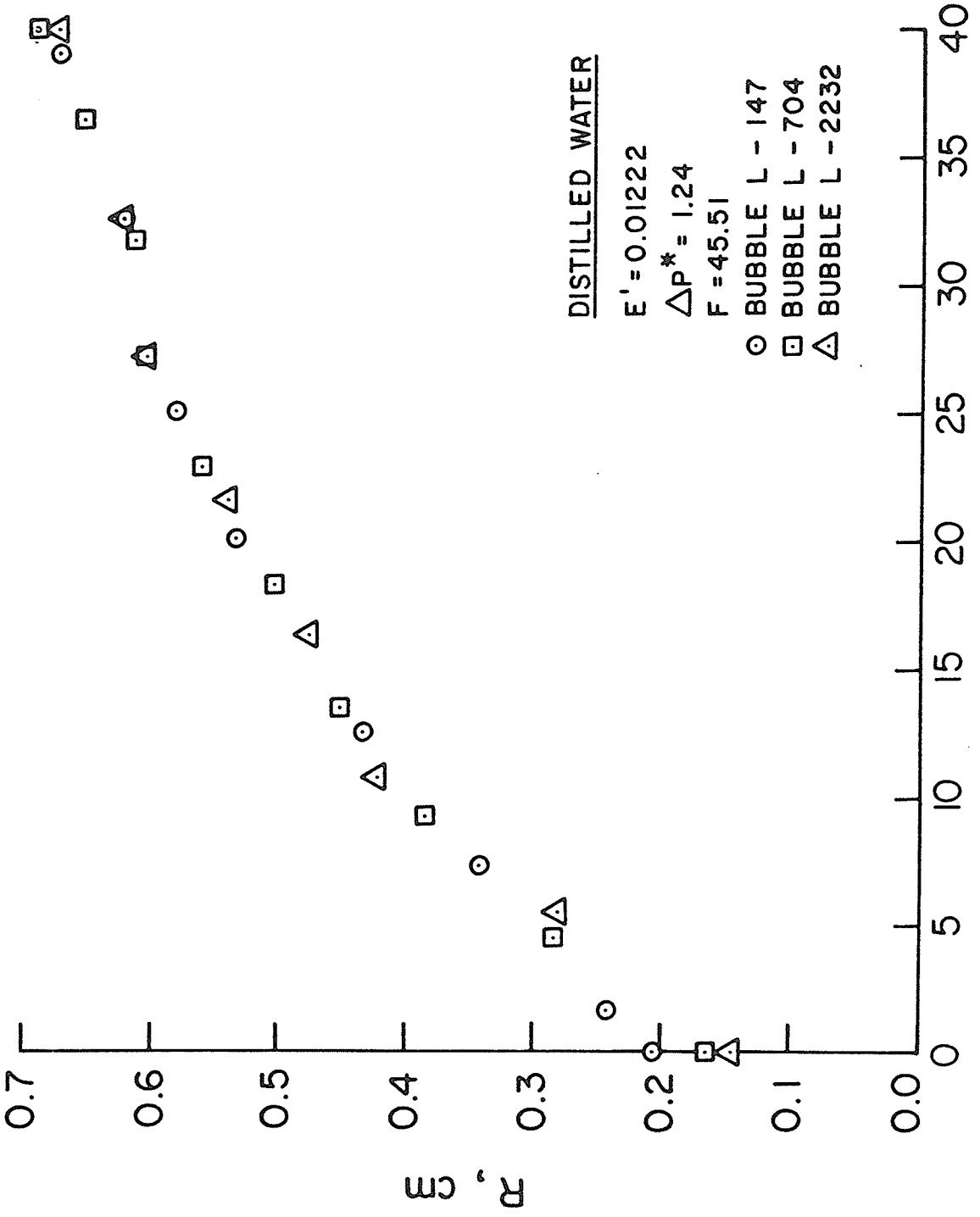

Fig. F.1 Bubble Growth Data in Distilled Water
($E' = 0.01222$, $\Delta P^* = 1.24$, $F = 45.51$)

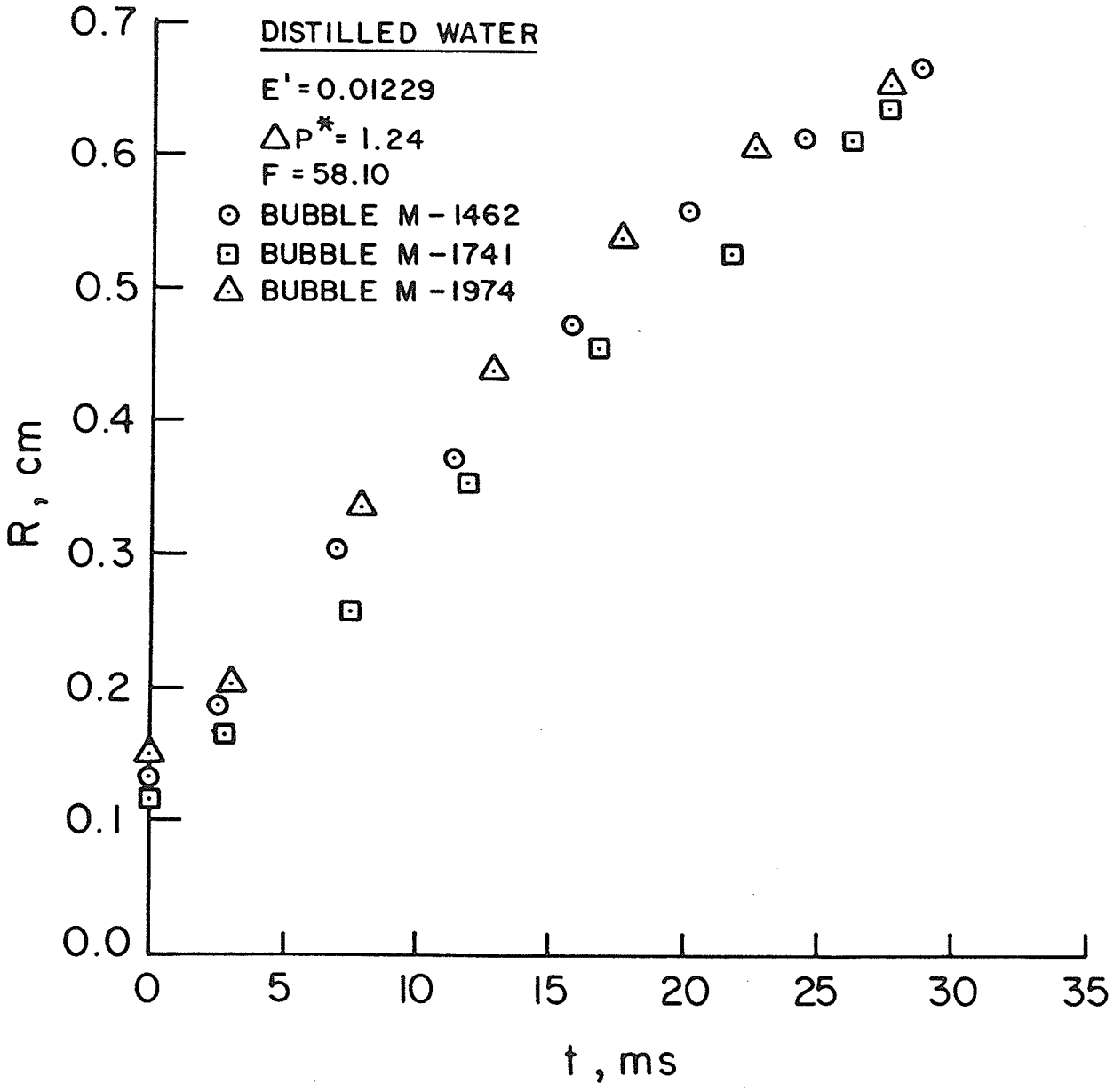

Fig. F.2 Bubble Growth Data in Distilled Water
(E' = 0.01229, Δ P* = 1.24, F = 58.10)

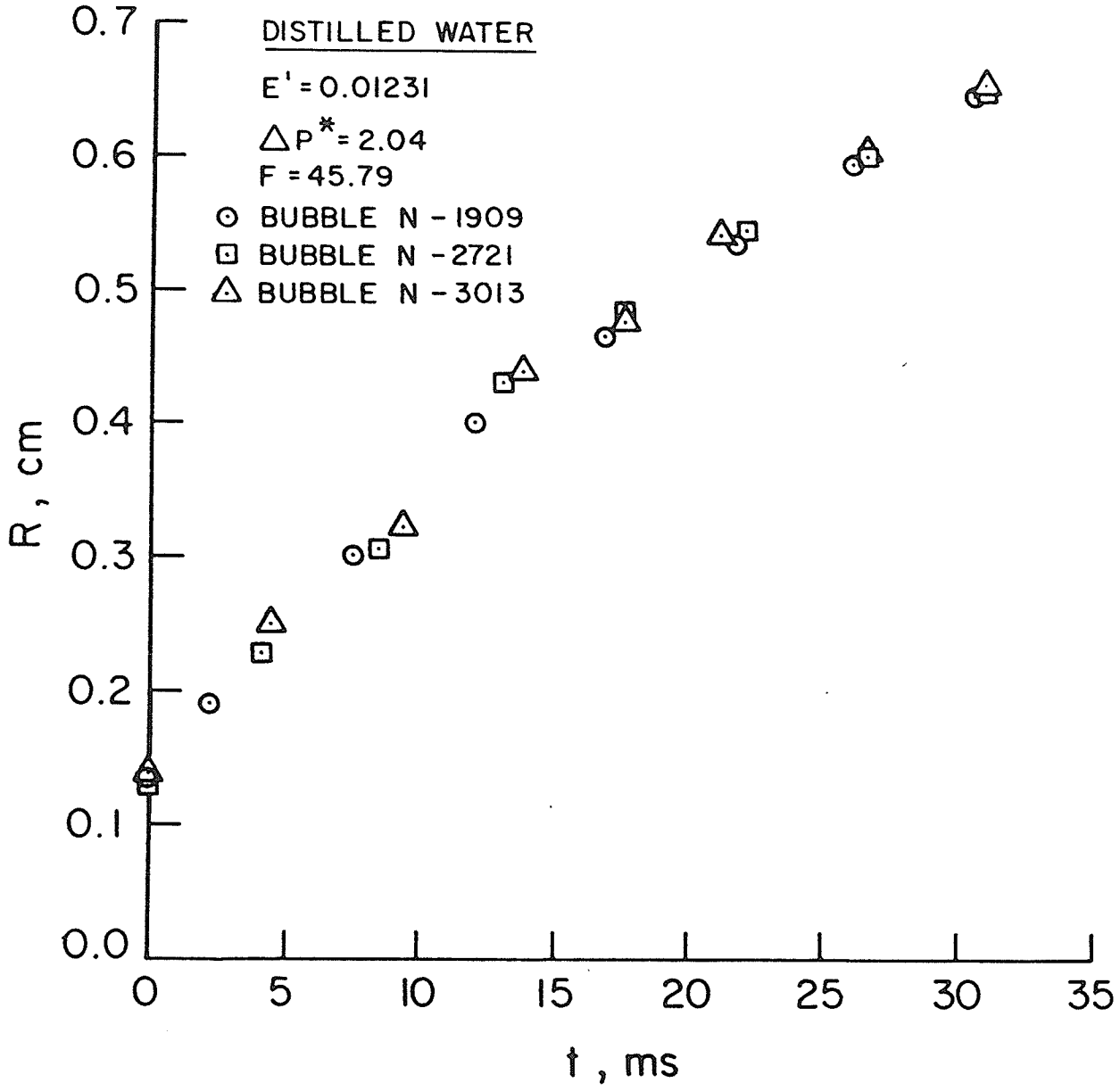

Fig. F.3 Bubble Growth Data in Distilled Water
(E' = 0.01231, Δ P* = 2.04, F = 45.79)

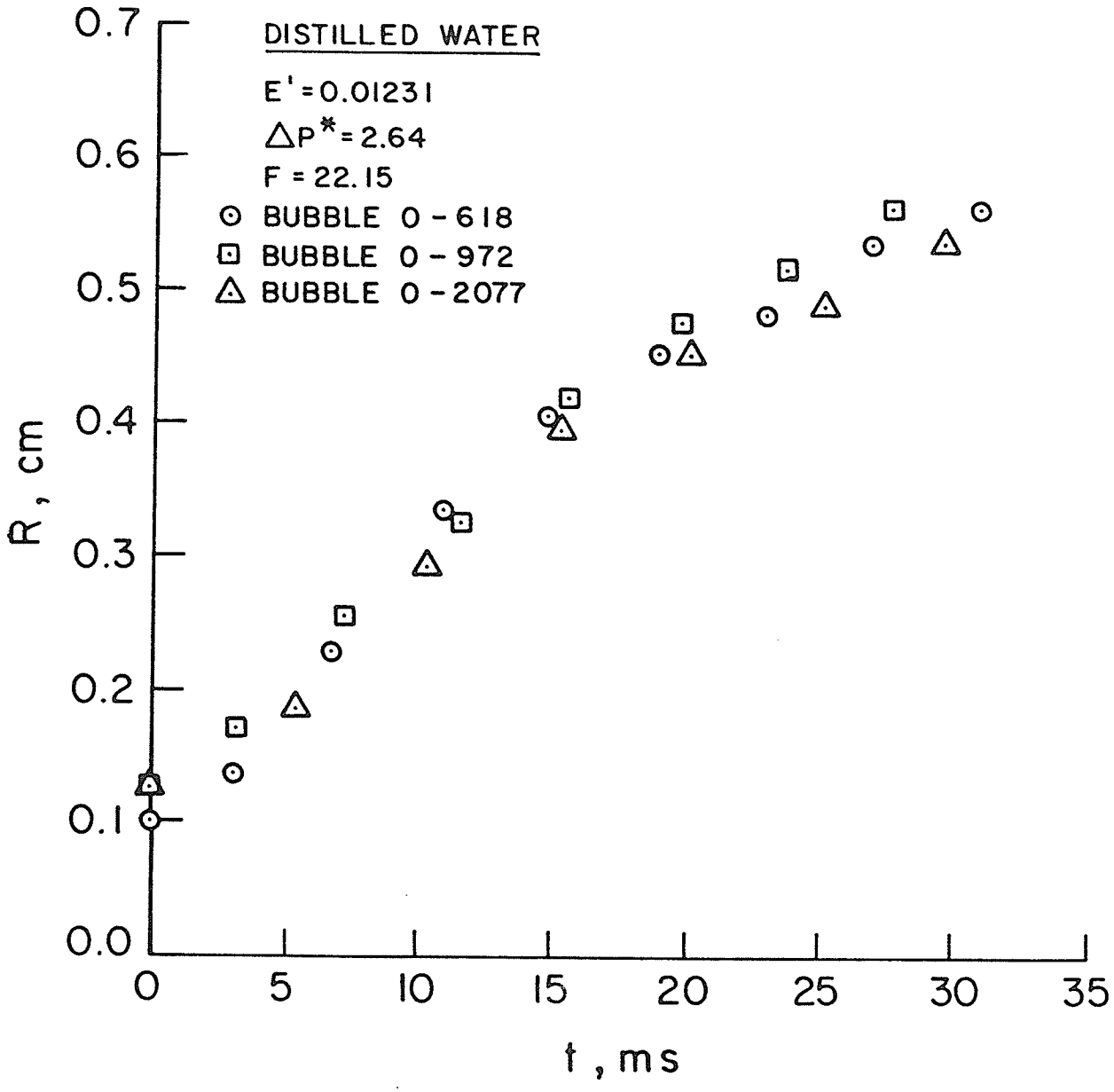

Fig. F.4 Bubble Growth Data in Distilled Water
(E' = 0.01231, Δ P* = 2.64, F = 22.15)

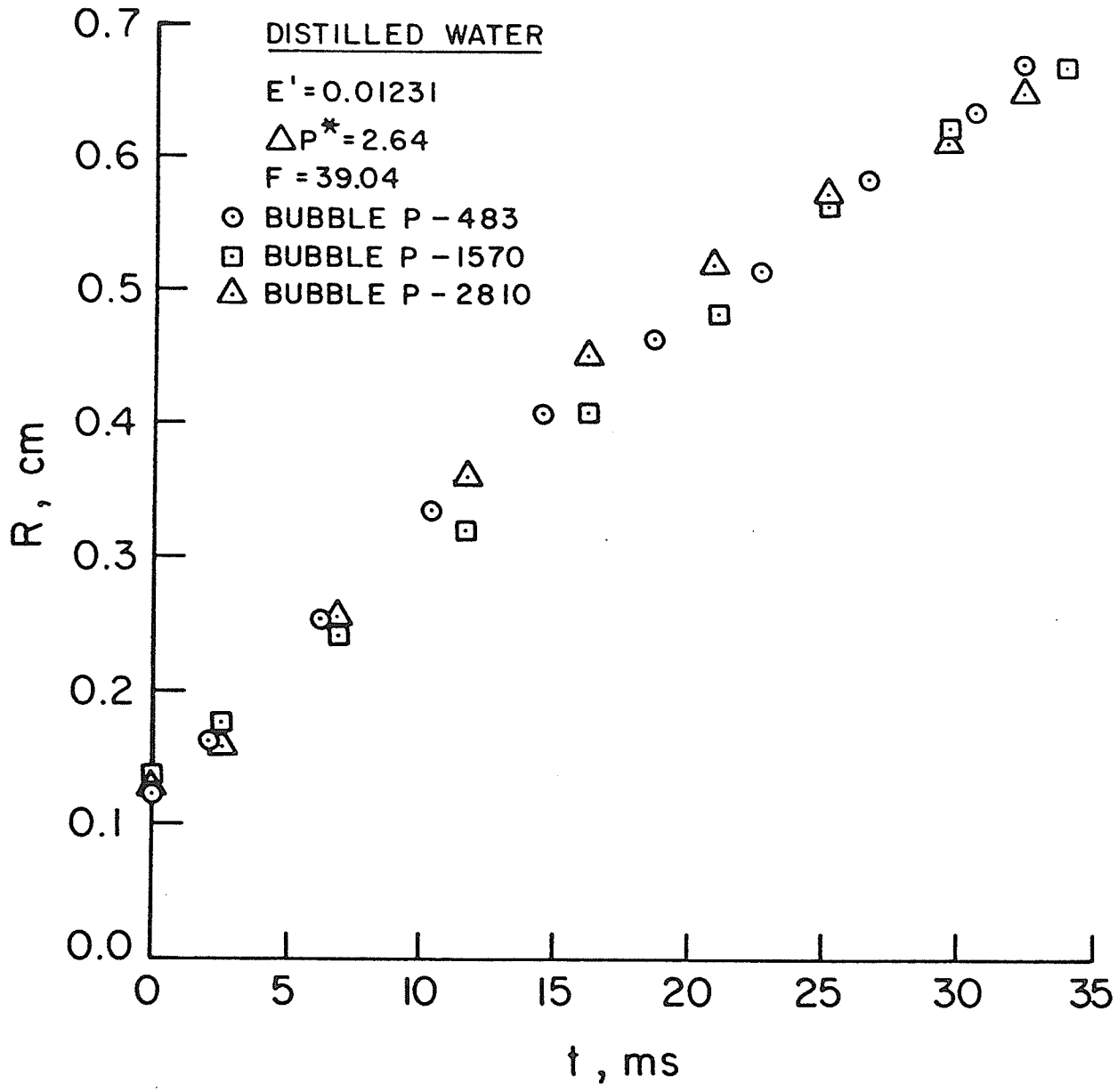

Fig. F.5 Bubble Growth Data in Distilled Water
(E' = 0.01231, ΔP^* = 2.64, F = 39.04)

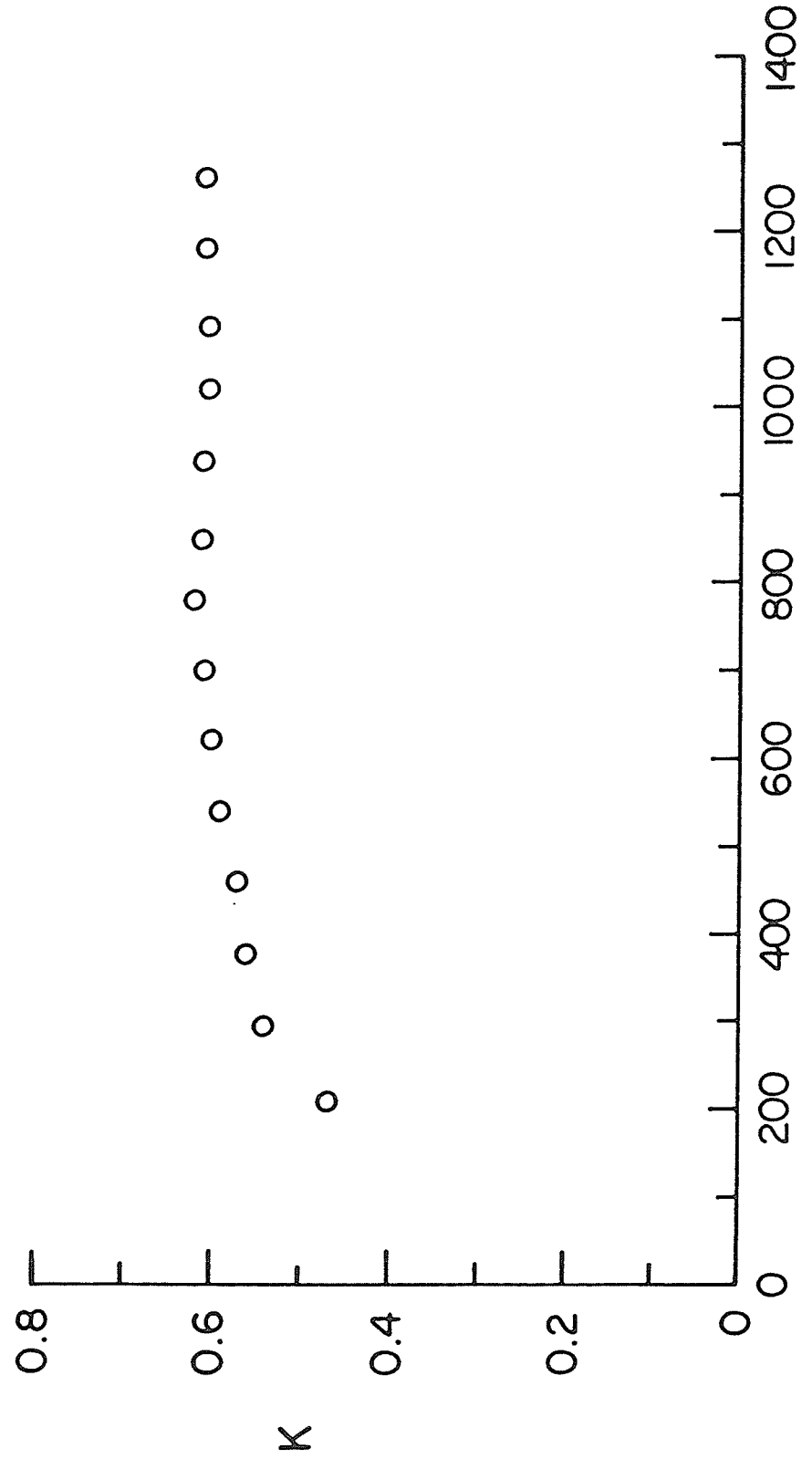

Fig. F.6 K Values as a Function of Orifice Reynolds Number

Barometric Pressure = Start 74.37 cm Hg; End 74.37 cm Hg
Room Temperature = Start 22.2°C; End 22.2°C
Orifice Dimensions :
Orifice Diameter = 0.308 cm
Capillary Tube
I.D.= 0.160 cm
O.D.= 0.211 cm

Air Flow Rate Scale (cm)	Indicated Air Flow Rate at Standard Conditions (cm^3/sec)	P_t (gauge) mm H_2O	Actual Mass Flow Rate ($\times 10^{-5}$ kg/sec)	Ideal Mass Flow Rate ($\times 10^{-5}$ kg/sec)	K	Re_o
3	13.37	3.25	1.58	3.36	0.47	210.7
4	18.88	4.85	2.24	4.11	0.54	297.6
5	23.99	7.30	2.84	5.04	0.56	378.2
6	29.49	10.10	3.49	5.99	0.57	461.4
7	34.22	13.30	4.05	6.81	0.59	539.6
8	39.22	17.10	4.66	7.72	0.60	620.3
9	44.44	21.00	5.26	8.55	0.61	700.9
10	49.55	26.05	5.87	9.53	0.62	782.0
11	54.27	32.20	6.43	10.60	0.61	856.5
12	59.78	39.00	7.09	11.67	0.61	944.0
13	64.50	46.80	7.65	12.78	0.60	1018.0
14	69.22	53.00	8.21	13.61	0.60	1093.0
15	74.72	60.80	8.87	14.58	0.61	1181.0
16	79.84	69.50	9.48	15.60	0.61	1262.0

Table F.2 Calculation Results of Flow Coefficients and Corresponding Experimental Conditions

Table F.3 Bubble Growth Data for Distilled Water
($E' = 0.01222, \Delta P^* = 1.24, F = 45.51$)

Liquid temperature: 21.1°C
Room temperature 21.1°C
Liquid height above the orifice: 12.7 cm

Bubble Identification No. L-147
(Time/frame, 4.762×10^{-4} sec/frame)

Frame No.	Time, ms	Bubble Volume 10^{-3} cm^3	Bubble Equiv. Radius cm
147	0.00	41.086	0.210
152	2.78	57.906	0.240
160	7.16	164.636	0.340
170	12.42	337.707	0.432
185	20.10	623.615	0.530
195	25.10	817.283	0.580
210	32.29	1027.570	0.626
224	38.83	1259.833	0.670

Bubble Identification No. L-704
(Time/frame, 4.545×10^{-4} sec/frame)

704	0.00	20.218	0.169
714	4.54	91.952	0.280
724	9.09	231.667	0.381
734	13.64	381.704	0.450
744	18.18	523.599	0.500
754	22.73	735.618	0.560
764	27.27	904.778	0.600
774	31.82	960.158	0.612
784	36.36	1171.715	0.654
792	40.00	1317.089	0.680

Bubble Identification No. L-2232
(Time/frame, 5.405×10^{-4} sec/frame)

2232	0.00	13.036	0.146
2242	5.40	91.952	0.280
2252	10.81	310.339	0.420
2262	16.22	448.920	0.475
2272	21.62	659.584	0.540
2282	27.03	904.778	0.600
2292	32.43	998.306	0.620
2306	40.00	1259.833	0.670

Table F.4 Bubble Growth Data for Distilled Water
($E' = 0.01229$, $\Delta P^* = 1.24$, $F = 58.10$)

Liquid temperature: 25.6°C
Room temperature: 25.6°C
Liquid height above the orifice: 12.7 cm

Bubble Identification No. M-1462
(Time/frame, 4.348×10^{-4} sec/frame)

Frame No.	Time, ms	Bubble Volume 10^{-3} cm³	Bubble Equiv. Radius cm
1462	0.00	9.634	0.132
1468	2.60	26.522	0.185
1478	6.96	121.200	0.307
1488	11.30	210.459	0.369
1498	15.65	432.123	0.469
1508	20.00	719.967	0.556
1518	24.35	950.775	0.610
1528	28.70	1204.260	0.660
1535	31.74	1346.357	0.685

Bubble Identification No. M-1741
(Time/frame, 4.651×10^{-4} sec/frame)

1741	0.00	6.538	0.116
1747	2.79	18.47	0.164
1757	7.44	68.60	0.254
1767	12.10	179.90	0.350
1777	16.70	381.00	0.450
1787	21.40	597.80	0.523
1797	26.04	951.40	0.609
1800	27.40	1067.472	0.634

Bubble Identification No. M-1974
(Time/frame, 4.878×10^{-4} sec/frame)

1974	0.00	16.210	0.157
1980	2.93	34.015	0.201
1990	7.80	151.905	0.331
2000	12.68	347.175	0.436
2010	17.56	634.264	0.533
2020	22.44	922.995	0.604
2030	27.31	1171.715	0.654

Table F.5 Bubble Growth Data for Distilled Water
($E' = 0.01231, \Delta P^* = 2.04, F = 45.79$)

Liquid temperature: 25.6°C
Room temperature: 25.6°C
Liquid height above the orifice: 12.7 cm

Bubble Identification No. N-1909
(Time/frame, 4.651×10^{-4} sec/frame)

Frame No.	Time, ms	Bubble Volume 10^{-3} cm³	Bubble Equiv. Radius cm
1909	0.00	11.008	0.138
1915	2.30	28.731	0.190
1925	7.44	116.524	0.303
1935	12.09	268.083	0.400
1945	16.74	415.749	0.463
1955	21.39	681.815	0.546
1965	26.04	886.803	0.596
1975	30.70	1098.066	0.640

Bubble Identification No. N-2721
(Time/frame, 4.494×10^{-4} sec/frame)

2721	0.00	9.203	0.130
2730	4.05	52.306	0.232
2740	8.54	123.584	0.309
2750	13.03	335.367	0.431
2760	17.53	454.615	0.477
2770	22.02	678.075	0.545
2780	26.51	909.310	0.601
2790	31.01	1139.760	0.648

Bubble Identification No. N-3013
(Time/frame, 4.396×10^{-4} sec/frame)

3013	0.00	11.249	0.139
3023	4.39	65.449	0.250
3033	8.79	138.549	0.321
3043	13.19	381.703	0.440
3053	17.58	434.893	0.470
3063	21.98	659.584	0.540
3073	26.37	904.778	0.600
3083	30.77	1150.346	0.650

Table F.6 Bubble Growth Data for Distilled Water
($E' = 0.01231$, $\Delta P^* = 2.64$, $F = 22.15$)

Liquid temperature: 25.6°C
Room temperature: 25.6°C
Liquid height above the orifice: 12.7 cm

Bubble Identification No. O-618
(Time/frame, 4.000×10^{-4} sec/frame)

Frame No.	Time, ms	Bubble Volume 10^{-3} cm³	Bubble Equiv. Radius cm
618	0.00	4.189	0.100
625	2.80	10.306	0.135
635	6.80	45.950	0.222
645	10.80	150.000	0.330
655	14.80	270.098	0.401
665	18.80	379.100	0.449
675	22.80	454.990	0.477
685	26.80	624.300	0.530
695	30.80	700.718	0.551

Bubble Identification No. O-972
(Time/frame, 4.040×10^{-4} sec/frame)

972	0.00	8.379	0.126
980	3.23	22.449	0.175
990	7.27	69.456	0.255
1000	11.31	136.802	0.320
1010	15.35	308.701	0.420
1020	19.40	440.401	0.472
1030	23.43	590.270	0.520
1040	27.47	730.703	0.559
1050	31.51	957.504	0.611
1060	35.55	1064.500	0.633

Bubble Identification No. O-2077
(Time/frame, 4.854×10^{-4} sec/frame)

2077	0.00	8.379	0.126
2088	5.34	27.150	0.186
2098	10.20	103.221	0.291
2108	15.05	246.568	0.389
2118	20.00	374.120	0.447
2128	24.76	480.836	0.486
2138	29.61	630.700	0.532
2141	31.07	709.170	0.553

Table F.7 Bubble Growth Data for Distilled Water
($E' = 0.01231$, $\Delta P^* = 2.64$, $F = 39.04$)

Liquid temperature: 25.6°C
Room temperature: 25.6°C
Liquid height above the orifice: 12.7 cm

Bubble Identification No. P-483
(Time/frame, 4.082×10^{-4} sec/frame)

Frame No.	Time, ms	Bubble Volume 10^{-3} cm^3	Bubble Equiv. Radius cm
483	0.00	7.795	0.123
488	2.04	18.141	0.163
498	6.12	65.450	0.250
508	10.21	157.479	0.335
518	14.29	282.405	0.407
528	18.37	410.385	0.461
538	22.45	555.647	0.510
548	26.53	817.283	0.580
558	30.62	1067.470	0.634
568	34.70	1305.502	0.678

Bubble Identification No. P-1570
(Time/frame, 4.545×10^{-4} sec/frame)

1570	0.00	10.771	0.137
1575	2.27	23.624	0.178
1585	6.82	60.105	0.243
1595	11.36	126.000	0.311
1605	15.90	278.262	0.405
1615	20.45	480.836	0.486
1625	25.00	759.518	0.566
1635	29.54	1012.868	0.623
1645	34.08	1226.289	0.664

Bubble Identification No. P-2810
(Time/frame, 4.545×10^{-4} sec/frame)

2810	0.00	10.078	0.134
2815	2.27	18.141	0.163
2825	6.82	70.276	0.256
2835	11.36	193.808	0.359
2845	16.00	374.120	0.447
2855	20.45	575.489	0.516
2865	25.00	771.659	0.569
2875	29.50	950.776	0.610
2881	32.27	1098.662	0.640